UNIVERSITY OF SÃO PAULO
SÃO CARLOS SCHOOL OF ENGINEERING
MECHANICAL ENGINEERING DEPARTMENT

JORGE DAVID AVEIGA GARCIA

A Delamination Propagation Model for Fiber Reinforced Laminated Composite Materials

SÃO CARLOS
2018

UNIVERSIDADE DE SÃO PAULO
ESCOLA DE ENGENHARIA DE SÃO CARLOS
DEPARTAMENTO DE ENGENHARIA MECÂNICA
PROGRAMA DE PÓS-GRADUAÇÃO EM ENGENHARIA MECÂNICA
AERONAVES

JORGE DAVID AVEIGA GARCIA

Modelo de Propagação da Delaminação em Materiais Compósitos Laminados Reforçados com Fibra

Dissertação apresentada à Escola de Engenharia de São Carlos, da Universidade de São Paulo, como requisito parcial para a obtenção do título de Mestre em Engenharia Mecânica.

Área de concentração: Aeronaves.

Orientador: Prof. Marcelo L. Ribeiro

ESTE EXEMPLAR TRATA-SE DA VERSÃO CORRIGIDA.
A VERSÃO ORIGINAL ENCONTRA-SE DISPONÍVEL JUNTO AO DEPARTAMENTO DE ENGENHARIA MECÂNICA DA EESC-USP

SÃO CARLOS
2018

Ficha catalográfica elaborada pela Biblioteca Prof. Dr. Sérgio Rodrigues Fontes da EESC/USP com os dados inseridos pelo(a) autor(a).

Aveiga, David
A249a A Delamination Propagation Model for Fiber Reinforced Laminated Composite Materials / David Aveiga; orientador Marcelo Leite. São Carlos, 2018.

Dissertação (Mestrado) - Programa de Pós-Graduação em Engenharia Mecânica e Área de Concentração em Aeronaves -- Escola de Engenharia de São Carlos da Universidade de São Paulo, 2018.

1. Composite Materials. 2. Delamination. 3. Propagation. 4. Fracture Mechanics. 5. Damage Model. I. Titulo.

Eduardo Graziosi Silva - CRB - 8/8907

FOLHA DE JULGAMENTO

Candidato: Bacharel **JORGE DAVID AVEIGA GARCIA.**

Título da dissertação: "Modelo de propagação da delaminação em materiais compósitos laminados reforçados com fibra".

Data da defesa: 28/05/2018.

Comissão Julgadora:	**Resultado:**
Prof. Dr. **Marcelo Leite Ribeiro** **(Orientador)** (Escola de Engenharia de São Carlos/EESC)	Aprovado
Prof. Dr. **Rodrigo Bresciani Canto** (Universidade Federal de São Carlos/UFSCar)	APROVADO
Prof. Associado **José Ricardo Tarpani** (Escola de Engenharia de São Carlos/EESC)	APROVADO

Coordenador do Programa de Pós-Graduação em Engenharia Mecânica:
Prof. Associado **Gherhardt Ribatski**

Presidente da Comissão de Pós-Graduação:
Prof. Associado **Luís Fernando Costa Alberto**

DEDICATION

This dissertation is a big step in my professional carrier and I dedicate it to my parents Luis and Janeth, my sisters Elaine and Daniela and to my brother Israel for their constant support, love and care.

ACKNOWLEDGMENT

Two years have gone by since I started this research project and a few more time since I arrived in Brazil. During my stay in São Carlos, I have met a lot of people with whom I feel grateful.

I would like to start acknowledging the excellent work done for my advisor Marcelo L. Ribeiro in the task of showing me the path to success. Most of the knowledge that I acquired, along this period, is due to his constant support and guidance.

Thanks to all my friends from the GEA group: Bruno, Denys, Eduardo, Fernando C, Fernando M, Gregório, Humberto, Jailto, Luis, Marcos, Matheus, Murilo and Rafael for their support and for hours of useful and useless discussions about general aspects of life during the coffee breaks.

Thanks to the community of Ecuadorians that resides here in São Carlos for their honest friendship and for bringing a piece of Ecuador to this part of the world, with each of our constant meetings.

And to all the friends that I made here for sharing their time and joy with me.

Finally, I would like to mention that I am grateful with the CAPES founding for their financial support which was fundamental to the development of this research.

ABSTRACT

AVEIGA, D. A Delamination Propagation Model for Glass Fiber Reinforced Laminated Composite Materials. 2018. 103p. Dissertation. São Carlos School of Engineering, University of São Paulo, São Carlos, 2017.

The employment of composite materials in the aerospace industry has been gradually considered due to the fundamental lightweight and strength characteristics that these type of materials offer. The science material and technological progress that has been reached, matches perfectly with the requirements for high-performance materials in aircraft and aerospace structures, thus, the development of primary structure elements applying composite materials became something very convenient. It is extremely important to pay attention to the failure modes that influence composite materials performances, since, these failures lead to a loss of stiffness and strength of the laminate. Delamination is a failure mode present in most of the damaged structures and can be ruinous, considering that, the evolution of interlaminar defects can carry the structure to a total failure followed by its collapse. Different techniques are usually adopted to accurately predict the behavior of damaged structures but, due to the complex nature of failure phenomena, there is not an established pattern. The present research project aims to develop a delamination propagation model to estimate a progressive interlaminar delamination failure in laminated composite materials and to allow the prediction of material's degradation due to the delamination phenomenon. Experimental tests assisted by ASTM Standards were performed to determine material's parameter, like the strain energy release rate, using GFRPs laminated composites. The delamination propagation model proposed was implemented as subroutines in FORTRAN language (UMAT-User Material Subroutine) with formulations based on the Fracture Mechanics. Finally, the model was compiled beside with the commercial Finite Element program $ABAQUS^{TM}$.

Key-words: Composite Materials, Delamination, Fracture Mechanics, Crack Propagation.

Resumo

AVEIGA, D. Modelo de Propagação da Delaminação em Materiais Compósitos Laminados Reforçados com Fibras. 208. 103p. Dissertação. Escola de Engenharia de São Carlos, Universidade de São Paulo, São Carlos, 2018.

O emprego de materiais compósitos na indústria aeroespacial tem sido gradualmente utilizado devido às suas características fundamentais, como peso leve e alta rigidez, que este tipo de material oferece. Tanto a ciência do material como o desenvolvimento tecnológico que se tem logrado, possibilitaram que estes materiais cumprissem com os requisitos de desempenho para aplicações em estruturas aeronáuticas e aeroespaciais, por tanto, o desenvolvimento de elementos de estruturas primárias usando materiais compósitos, passou a ser muito conveniente. É de extrema importância prestar atenção aos modos de falha que comprometem a performance dos materiais compósitos, uma vez que, estas falhas levam a uma perda de resistência e rigidez do laminado. A delaminação é um modo de falha presente na maioria de estruturas danificadas e pode ser desastroso, considerando que, a evolução dos defeitos interlaminares podem levar a estrutura a falhar seguido pelo colapso estructural. Diferentes técnicas são geralmente adotadas para prever, de maneira correta, o comportamento de estruturas danificadas, porém, devido à natureza complexa do fenômeno de falha, não existe um padrão estabelecido. O presente trabalho de pesquisa visa desenvolver um modelo de delaminação e de propagação da delaminação para estimar a evolução da falha interlaminar em materiais compósitos laminados e permitir a predição do comportamento do material com a evolução da delaminação. Ensaios experimentais auxiliados por normas ASTM foram realizados para determinar parâmetros do material, tais como, as taxas de liberação de energia de deformação, usando materiais compósitos laminados de matriz polimérica reforçada com fibra de vidro. O modelo de propagação da delaminação proposto, foi implementado como uma sub-rotina em linguagem FORTRAN (UMAT – User Material) com formulações baseadas na Mecânica da Fratura. Finalmente, o modelo foi compilado com o software comercial de Elementos Finitos, *ABAQUS*^{TM}.

Palavras-chave: Materiais Compósitos, Delaminação, Mecânica da Fratura, Propagação de trincas.

LIST OF FIGURES

LIST OF TABLES

SYMBOLS AND ABBREVIATIONS

ASTM	American Standard Test Method
CC	Compliance Calibration Method
CDM	Continuum Damage Mechanics
CRI	Critical Delamination Length
CZM	Cohesive Zone Model
DCB	Double Cantilever Beam
ENF	End Notched Flexure
FEA	Finite Element Analysis
FEM	Finite Element Method
FM	Fracture Mechanics
FORTRAN	Formula Translation (programming language)
FRC	Fiber Reinforced Composite
FRPs	Fiber Reinforced Plastics
FRPC	Fiber Reinforced Plastic Composite
GFRPs	Glass Fiber Reinforced Plastics
LEFM	Linear Elastic Fracture Mechanics
MBT	Modified Beam Theory
MMB	Mixed-Mode Bending
MVAIP	Modified Vacuum Assisted Infusion Process
PEEK	Polyether Ether Ketone
RVE	Representative Volume Element
SERR	Strain energy released rate
SI	International System
TSL	Traction-Separation Law
UMAT	User Material
VAIP	Vacuum Assisted Infusion Process
VCCT	Virtual Crack Closure Technique
VIS	Visual Delamination Initiation
WWII	World War II
A	Intersection of CC curve
a	Delamination length
a_o	Initial delamination length

α	Mode mixture transformation parameter
b	Specimen width
b_{cal}	Width of calibration specimen
B	ENF specimen with
β	Correction for mode mixture
c	Lever length
C	Experimental compliance curve
C_{cal}	Compliance of calibration specimen
C_{ij}	Stiffness matrix
C_{sys}	System compliance
CV	Coefficient of variation
χ	Crack length correction parameter
d	Damage variable
δ	Displacement
δ_c	Critical separation
δ_o	Ultimate separation
$\lvert\Delta\rvert$	Rotation factor
E_{1f}	Flexural modulus
E_{cal}	Elastic modulus of calibration specimen
E_i	Elastic modulus at direction i
ε_i	Strain at direction i
η	Power for BK law
f	Force
F_{ik}	Bi-univocal relation, transformation tensor
φ	Adjustment coefficient
G	Strain energy release rate
G_C	Critical SERR
G_I	Strain energy release rate at mode I
G_{IC}	Critical SERR at mode I
G_{II}	Strain energy release rate at mode II
G_{IIC}	Critical SERR at mode II
G_{II}/G_T	Mode mixture
G_{III}	Strain energy release rate at mode III

G_{ij}	Shear modulus at ij plane
G_T	Total strain energy released rate
γ	Surface energy
γ_i	Out-of-plane strain
Γ	Transversal modulus correction
h	Specimen thickness
k	Stress intensity factor
K_c	Material toughness
L	Half-span length for ENF and MMB
m	Slope of CC curve
m_{cal}	Slope of L-D curve for calibration test
n	Number of samples
ν_{ij}	Poisson's ratio at ij plane
P	Load
P_{max}	Maximum Load
P_C	Expected critical force
P_j	Peak force
π	Pi
Q_{ij}	Reduced stiffness matrix
S	Surface energy with unit depth
S_D	Damage surface
S_{ij}	Compliance matrix
S_{n-1}	Standard desviation
σ_i	Stress at direction i
σ_C	Nominal stress
σ_f	Critical stress
t	Specimen thickness
T	Traction
$T(\delta)$	TSL function
T_c	Maximum traction
τ_i	Out-of-plane stress
U	Total strain energy released
U^*	Strain energy per unit volume

V	Volume
$\bar{x}$	Average value
x_i	Sample value

SUMMARY

CHAPTER I

1. INTRODUCTION

In the continuous search of sophisticated material during the industrial evolution of humanity, scientists and inventors lead us to the tendency of combining materials in order to improve mechanical properties of all kind of apparatus, tools, and buildings. This took us to develop composite materials which definition by Hashin (1983) says that are the result of mixing two or more different materials firmly bonded together to reach a stiffer and stronger material (Fig. 1). It is possible to classify composite materials in these following categories: mortars or concrete, metal composites, ceramics composites and reinforced plastics such as fiber-reinforced polymers. In a modern technology, this reinforced plastic association usually uses thin fibers and plastic resins so the final product is stiffer, more lightweight than other materials with same properties and cheaper.

Figure 1 - Types of reinforced composites materials.

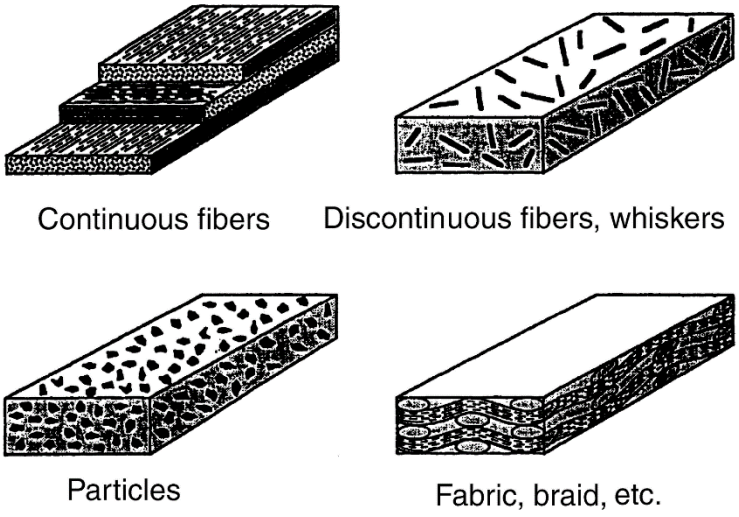

Source - Myer Kutz (2006)

Composites materials have been present in different aspects of life like building or manufacture of more efficient tools and lately uses of composite appear on military equipment, plastic industries, and high-performance materials structures. With the appearance of Fiber Reinforced Polymers (FRPs) in the earliest 1940's, the path for scientists and industrial researchers to take

advantages of the potentialities of this new material was established. The result of several studies in the area begins to emerge, creating a tendency to replace metals in structures of different vehicles and machines, although the first uses of FRPs for aircraft or ships were mainly performed by army's projects around the world during the WWII. The demand for efficient processes to build structural aircraft parts ended up with the improvement of tools and manufacture process that give to composite materials the consideration on structural (Bernadette, 2002)

Few decades after, passing through the end of big wars and the space race, the scenario shown the need for composite materials to improve their properties so they will be able to find civil applications. The automotive industry starts to employ GFRPs and helps with material improvements reaching a new high strength modulus. Regarding aircraft industries, it is possible to note an increasing employment of composite materials, for example in The Boeing Company's aircraft family from the B707 in 1960's until last released B787 Dreamliner (Fig. 2a and 2b), due to finest mechanical properties which evolution of composite materials have reached.

Figure 2 - Evolution of composite employment in aircraft. a) B707 with less than 10% of composite used, John Travolta 2011 ©. b) B787 with almost 50% of composite used.

(a) (b)

Source - Boeing Company ©

With this increase in composite application and experience using them, additional improvements in multiple structural functions were reached. New and better discovers in fibers and matrix, as well as its synthesis, result in a sophisticated composite that could satisfied the demands in stiffness, fracture toughness, fracture strength, ductility, damping and thermal stability, which are important structural functions and the basis for a superior structural performance (Williams, Vaziri, & Poursartip, 2003). Even though the weight is not a variable that has a direct influence on these functions, we cannot discard the advantages of having even more and more lightweight materials (Soutis, 2005).

Especially for aircraft operators, weight saving may be a crucial aspect to decrease the operational expenses since this action is related to combustible consumption. Improvement in fuel efficiency, engine mechanics, aerodynamics and seat distribution may also decrease the fuel consumption but the most critical reduce is achieved by weight saving. Fig. 3 illustrates the reduction of Energy Intensity along the years from 1955 to actual time. The energy intensity is measured by the amount of energy (J) per distance traveled by passengers in kilometers (pkm). It can be also pointed out the increasing employment of composite materials during this evolution, as we know the amount of composite material employed by each aircraft model considered in the figure (Rodrigue, 2012).

Figure 3- Evolution of aircraft fuel consumption.

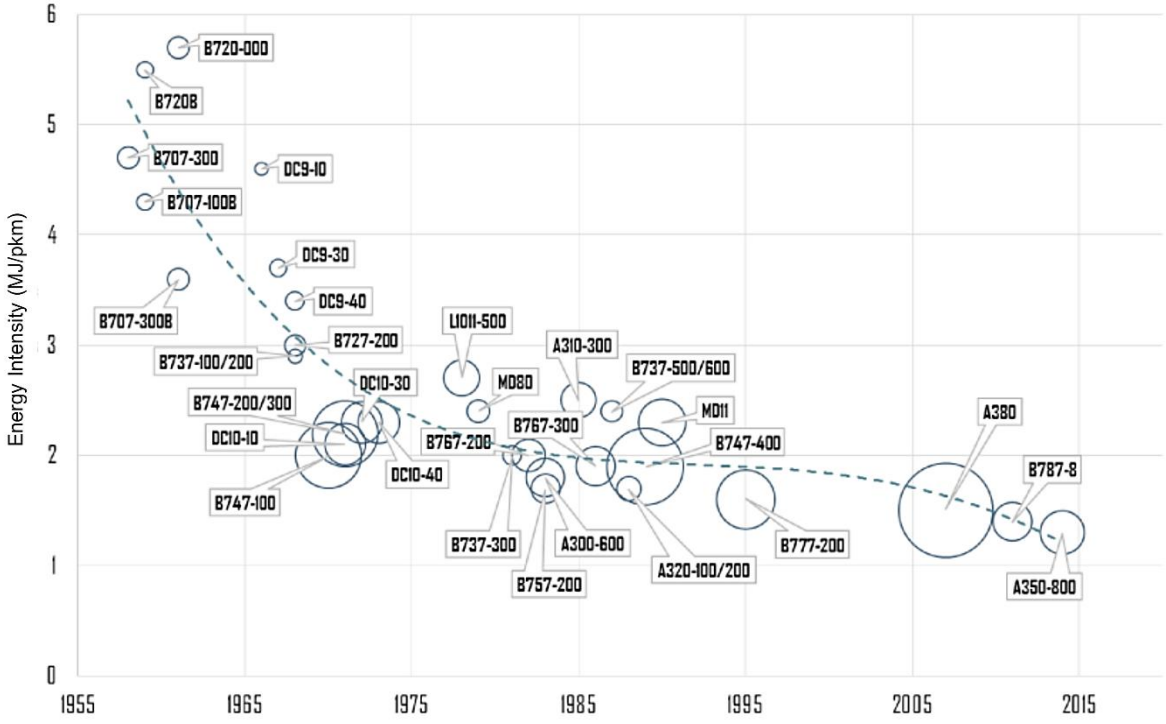

Source – Rodrigue (2012)

Composites afford the unique possibility of designing the material, the manufacturing process and the structure in one unified and concurrent procedure, having a large number of degrees of freedom available enables simultaneous material optimization for several given constraints. The applications of composites tend to become highly desirable in primary and secondary structures, for example, wing stringers, floor beams, fuselage and wing skins surfaces and the empennage.

Being safety one of the mainstays of aviation, all this versatility of composite materials is limited, since failure within primary structures may produce catastrophic accidents. Engineers and structure designers must use large safety factors in order to guarantee an invulnerable performance of a composite part during its life, which leads to an over-weight penalty and compromises the characteristic performance-weight ratio of laminated composite materials. These high-value factors are the product of the inability to correctly predict failure behavior due to the complex damage evolution observed within this material.

Scientists and researchers all over the world are treating this issue, trying to reach even more and more precise predictions of damage behavior, and its influence in structure strength as well, in order to end out with the over-dimensioning of composite structures and, likewise, over-weight of the whole structure. There are good contributions in the literature with different methodologies and assumptions, but despite those hypotheses, the discussion is still open and damage behavior in composite materials has not been successfully solved.

Summarizing the scenario about failure in composite, scientists categorize failures into two groups: Intralaminar and Interlaminar failures. In a loaded structure, when it starts to lose its strength capacity, the intralaminar damage is always observed in the first stages of the failure evolution with the presence of matrix microcracks growing up parallel to the fibers in off-axis plies of the laminate (Kashtalyan & Soutis, 2005). This first damage appearance starts degrading the material stiffness and strength (Singh & Talreja, 2010) and also may have influence in material's coefficients like thermal expansion (Wosu, Hui, & Daniel, 2012), absorption of moisture (Weitsman, 2006) and natural frequencies (Lasn, Echtermeyer, Klauson, Chati, & Decultot, 2015). Initial matrix cracks and degradation of properties usually trigger interlaminar failures, as could be, delamination initiation and growth due to microcracks (Nairn & Hu, 1992), which are more harmful to the whole structure and may compromise its performance. This undesirable delamination is an important concern for designers that have to face an alternative between a vulnerable structure and an over-dimensioned structure, therefore, studies about delamination are convenient since understanding this phenomenon behavior will help to raise the structure efficiency (Garg, 1988).

Finally, the primary aim of this work is to study the delamination phenomenon by the meaning of describing the propagation behavior, the influence in material strength and stiffness degradation as well, in order to create a delamination model for Fiber Reinforced Composites (FRC). Commercial software *ABAQUS*^{TM} was used to model delamination by the employment of a cohesive zone to represent the surfaces involved in the crack propagation, in the region where delamination is supposed to act. Based on Linear Elastic Fracture Mechanics (LEFM),

the Cohesive Zone Model (CZM) was employed to assist the separation modes of elements within the model. Material parameters obtained by separation modes tests, performed using a Mixed-Mode Bending (MMB) Apparatus and a universal testing machine adapted to perform Double Cantilever Beam (DCB) and End Notched Flexure (ENF) tests, will supply the numerical model. Conclusively, development of a UMAT subroutine is considered.

1.1. Objectives and Scope

Aeronautical structures researchers and designers have a main focal point in structural weight saving; this could be achieved considering different strategies like optimizing the structural design, employing alternative materials with low densities, optimizing the aircraft junctions to use fewer fasteners, etc (Kaufmann, 2008).

One primary challenge when optimizing a structure is to not alter its safe operation and usually, this action leads to use high factors-of-safety. Especially when using composite materials, this safety factor can reach values of 2 (Zhu, 1993); and since they are related to materials properties, it is reasonable to study the material behaviors like failure modes in order to reduce those values.

Composite materials failure modes could be several, but interlaminar delamination will be considered in this research project. Thus, the main objective of this work is to introduce a delamination model for the following purposes:

- Measure delamination and describe its propagation within unidirectional fiber reinforced composite laminates. A Fracture Mechanics energy-based criterion will be used.
- Determine the delamination influence in material strength and stiffness degradation. The Continuum Damage Mechanics (CDM) will be employed to find relations between stiffness and damage variables.
- Evaluate the stress-strain response of the material under delamination phenomenon effects.

To accomplish those objectives, a series of steps considered secondary objectives, need to be carried out:

- Perform a literature review of the basis and most recent papers and publication regarding delamination, in order to understand the actual scenario.

- Experimental tests must be carried out with the purpose of collecting materials parameters related to failure mechanism.
- Simulate the experimental tests to computationally validate the partial results.
- Identify critical parameters to describe material performance under failure phenomenon.
- Develop a failure criterion considering different delamination modes.
- Formulate a degradation law.
- Compile this delamination model into a UMAT subroutine so can be linked to ABAQUS software.
- Evaluate the numerical model potentialities and limitation by performing a simulation of a case study.

Therefore, this progressive damage model could support structural designs by improving the design life of structures since it may decrease the values of safety factors, thus, avoiding the structure to become too conservative.

The scope of the study is limited to:

- Unidirectional fiber-reinforced laminated composite materials made from polymer plastics.
- Interlaminar failure by means of delamination phenomenon. Other forms of damage are not considered.
- Quasi-static loading. No fatigue or time-dependent aspects are involved.
- Uniaxial loads.

1.2. Outline

This dissertation is divided into nine chapters organized as follows:

⇒ CHAPTER I: This first chapter contain an introductory review about composite materials and its implementation within aeronautical industries. Potentialities and limitations of the composite are enlisted

⇒ CHAPTER II: Delamination phenomenon theories like Fracture Mechanics and Continuum Damage mechanics were reviewed and are shown in this chapter. Motivations, objectives of the investigation project and its organization are shown here as well.

⇒ CHAPTER III: The third chapter explains the methodology employed in both, material manufacture and testing. In addition, the formulation of a Traction-Separation law (TSL) is explained.

⇒ CHAPTER IV: Subsequent to material testing, experimental results are showed in this chapter. All the curves plots and parameters calculations are present here, with an emphasis on critical material values and unusual observations during testing.

⇒ CHAPTER V: This section provides a delamination propagation criterion to estimate the degradation of the material due to crack growth. A detailed description of damage interpretation is shown. The damage variables are calculated and implemented via UMAT subroutine

⇒ CHAPTER VI: This chapter shows the employment of the subroutine through a finite element simulation. Results of the numerical simulation are presented as well.

⇒ CHAPTER VII: Final conclusions and recommendations for future works are summarized in this chapter.

⇒ CHAPTER VIII: All the publication produced along this study.

⇒ CHAPTER IX: This last chapter lists all the references cited.

CHAPTER II

2. Background and Motivation

Improper lamination and low-quality cure can happen during the manufacturing process, as damage while machining the components for fasteners holes and design cuts, also accidentally drop of tools during maintenance and impact by ground service vehicles, bird strikes, hailstones, etc., can occur during service process. All those injuries are usually a start point for most common failure modes (intra-ply cracking, interlaminar matrix delamination, and fiber failure) (Fig. 4), being delamination the damage mode with major importance whose effect will decrease the material stiffness and create local instability as a product of local stress concentration.

Figure 4 - Microcracks and Delamination.

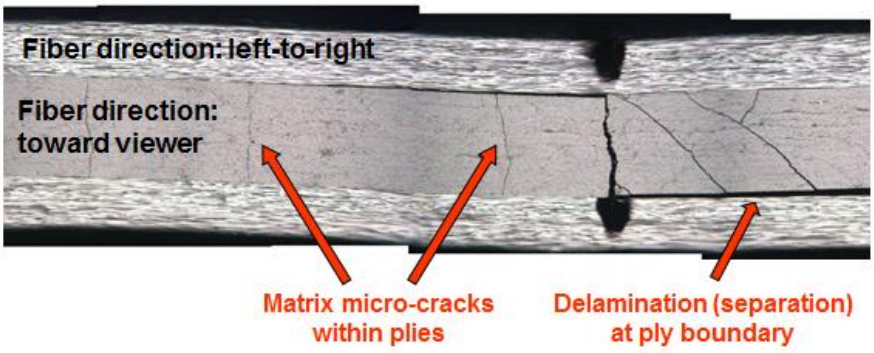

Source – Public Domain

Causes and consequences of delamination could be several, but let us first explore the physics behind this event. The delamination phenomenon is a failure mode not just of composite materials but steels as well, first studies in delamination started by P. Suh (1973) with "*The Delamination Theory of Wear*" in which, the following statements were established:

(1) The contact of two surfaces forming a solid and unique body will implicate an ex-change of normal and shear stresses when summited to loads, and this is possible because of contact points with adhesive actions. Both surfaces will present asperities between them, and a softer surface will appear in which these asperities start to deform until total remove. The initial

contact begins to degrade now since it becomes an asperity-plane contact and each contact point is experiencing a cycling loading.

(2) Plastic shear deformation appears on the softer surface induced by asperities of the harder surface when traction occurs, this deformation has an accumulative constant increase.

(3) While this deformation evolves, cracks begin to nucleate below the contact surface. Compressive stress is now present near the contact regions in a triaxial state.

(4) The cycling loading and related deformation help cracks to evolve and propagate (pre-existing voids too); depth reached by the crack is governed by properties of the material and friction coefficient. When traction is not enough for crack growth, more crack nucleation take place.

(5) Finally, at a certain weak point, a crack will shear to the surface producing "delamination" between contact surfaces. Normal and tangential loads will control the thickness of the crack.

Nam P. Suh (1977) presented a review of his Delamination Theory of Wear in 1977, which was a resume of sequential researches involving each of the statements defined above. Studies about asperities are exposed in L. E. Samuels' book from 1971 (Samuels, 1971), defining the rate of asperities deformation to be dependent on initial roughness, applied load and mechanical properties. In addition, Van Dijck J. A. B. (1977) confirmed that materials remain crystalline near the contact surface, after application of loads, with the presence of smaller grains and big deformations of asperities.

When predicting, analytically, deformation over a surface layer, normal and tangential loads exerted by surface asperities must be defined. Green A. P. (1954) showed that friction coefficient may have an important role over the normal load and it should be lower than materials hardness every time normal and tangential loads are applied to a perfectly plastic solid. As well, plastic deformations will show shear strain component in planes perpendicular to the surface that accumulates incrementally each time a hard asperity passes over the surface (Jahanmir & Suh, 1977).

Researchers give more attention to crack nucleation and propagation rather than other mechanisms related to delamination, thus, there is a bigger and prior investigation record. Regarding studies about crack nucleation and delamination, we have the work done by Jahanmir (1977) whom opened a discussion about crack being nucleated below the contact surface and not at the surface since a large hydrostatic pressure in this region will oppose crack at the surface. He postulated that incremental plastic deformation at the contact surface will favor crack formation and that there is a depth where hydrostatic pressure is not large enough to avoid crack formation.

Teixeira (1977) postulated that with less plastic deformation, the friction coefficient decrease allowing crack nucleation at a shallower depth. The wear of materials produces a poor interface between particles and the matrix which could be equivalent to pre-existing cracks increasing all the rates (wear, crack nucleation, propagation, etc.) and decreasing the distances that cracks must propagate to link up with others (Nam P Suh, Saka, & Jahanmir, 1977). Crack nucleation could still happen even when the mechanism of crack propagation is not operative.

Studying delamination propagation is more challenger since the nature of the phenomenon is notably complex. Linear elastic fracture mechanics is usually the method employed to treat crack propagation. As we can see in the work by Fleming (1977), he uses this method to study crack propagation in sliding contacts and define some statements:

— Significant crack growth is due to the linking up of separated cracks.

— Residual stresses do not affect crack linking up (Merwin & Johnson, 1963).

— There are some cracks that, depending on the loading case, they cannot link up with other cracks.

— At a crack tip, exists a stress state governed by a remote load or a residual load and it could be measured with a stress intensity factor (k).

— Since there are one depth and one effective micro-crack length to produce crack growth at contact, stress intensity factor has distinct maximums at different states of the crack tip, thus, the size of asperities contact is not the same.

— Once the crack tip breaks through contact surface, it takes the path of deformed asperities enable an easy separation of particles.

— Crack propagation rate is the phenomenon of controlling the delamination rate.

These are always some starting assumptions when studying crack propagation and may help to accurately predict crack behavior. Different numerical methods may differ when defining stresses states at different stages of the phenomenon and in how degradation of material properties happens.

All these definitions postulated in the *Delamination Theory of Wear,* that have been reviewed, are applicable to all materials in which surface crack nucleation and propagation are present. Researcher tested these basic behaviors in different types of materials, mostly thermoplastic and thermosetting plastics. For plastics reinforced with fibers, the stress field and the mechanism of crack nucleation and propagation may vary (Nak-Ho & Suh, 1979).

Introducing the "*Delamination Theory of Wear"* into composites resulted in a notorious change in friction and crack behavior. Identifying parameters to understand this alternative behavior have been always very complex because of the presence of secondary phases like filler or reinforcing fibers. Therefore, the starting point for researchers was to develop numerical models to catch these parameters. First attempts could be found in works like Tabor (1974) but with less success in some fiber reinforced composites, especially attention was given to those materials because of their increasing employment. Different types of fibers (mostly Kevlar, carbon and glass fibers) and orientations became the focus of research. Nak-Ho (1979) checked these materials in the normal, transversal and longitudinal direction from the sliding surface, making clear the importance of fiber direction in delamination of composites since this characteristic limits plastic deformation.

Continuing with the sequence of mechanisms involved in delamination phenomenon, we should mention crack nucleation in composites. Nairn (1992) presented a research about matrix microcracks in laminated composites and how they influence the initiation and growth of delamination. Some features are not the same as in metals because of anisotropy of composite materials, and some statements need to be remarked:

— Microcracks nucleate and propagate mostly in the matrix rather than fibers, but fibers distribution may affect the growth and path of the crack.

— The rate of microcracks formed before the onset of delamination decrease with the number of plies composing the laminate.

— Irregularities within interface region are considered as pre-existing microcracks and are more commonly to appear in composites that metals because of material incompatibility.

— Stress levels to produce microcracks into the matrix are much lower than the ultimate strength of the material.

— First instances of crack nucleation show small secondary crack appearance extending a short distance away from primary matrix cracks.

— Microcracks propagation could produce a partial failure of the materials and, in some cases, the failure can be complete.

— When these microcracks evolve until delamination occurs, the path followed by the crack tip is more remarkable since contact surface between plies with different orientation is more vulnerable.

More extent researches about microcracks in composite matrixes can be found in literature, works like (Lim & Hong, 1989), (Varna & Berglund, 1991), and more contemporary

(Kashtalyan & Soutis, 2000) where numerical models are proposed. However, we will focus on delamination propagation phenomenon taking place between fiber plies in FRPs, so microcracks in matrixes are out of the investigation scope.

So far, it is understood that the main mechanism that induces delamination is matrix crack. The redistribution of loads provoked by the cracks concentrates them into a specific region where delamination will show up. Once delamination starts, its propagation is usually abrupt and this supposes a dramatic lost on the laminate stiffness heading to the ultimate failure of the material. This sudden damage is almost limited by angle-ply laminates since fiber direction may difficult or favor the crack propagation (P. Johnson & Chang, 2001).

Once the mechanisms behind delamination phenomenon have been exposed, this leads us to investigate all the tools available to analyze, understand and describe delamination (to meaning analytical and numerical methods). In following sections, theories and well-known researches will be discussed in order to systematize an accurate methodology for our case study.

2.1. State of the Art: Delamination

Analyses of material degradation because of delamination, drawn the attention of researchers since the 1980's. Several methods have been proposed to deal with degradation, which can be categorized into two branches of mechanic science: Fracture Mechanics (FM) and Continuum Damage Mechanics (CDM).

When supported with computer resources, those both theories reach accurate approximations describing delamination behavior or predicting it. The characteristics of delamination damage can be represented as stress/strain functions (CDM) or as the energy released (FM). The aim of most of the studies is to account the stiffness degradation of the material using a number of assumptions suggested by both theories. A brief review is shown below.

2.1.1. Delamination using Fracture Mechanics

For inter-ply delamination prediction, linear elastic fracture mechanics (LEFM) have worked in a proper manner (Kashtalyan & Soutis, 2000), (Davies, Hitchings, & Ankersen, 2006), (Guédra-Degeorges, 2006). If we have a cracked specimen subjected to a tension it will show

a typical asymptotic stress regime near the crack tip with the stresses theoretically reaching infinity (Fig. 5). The elastic stress field within the specimen can be determine describing it as a function of the distance from the crack tip to a reference point.

Figure 5 - (a) Elastic stress distribution and (b) actual stress distribution in a composite.

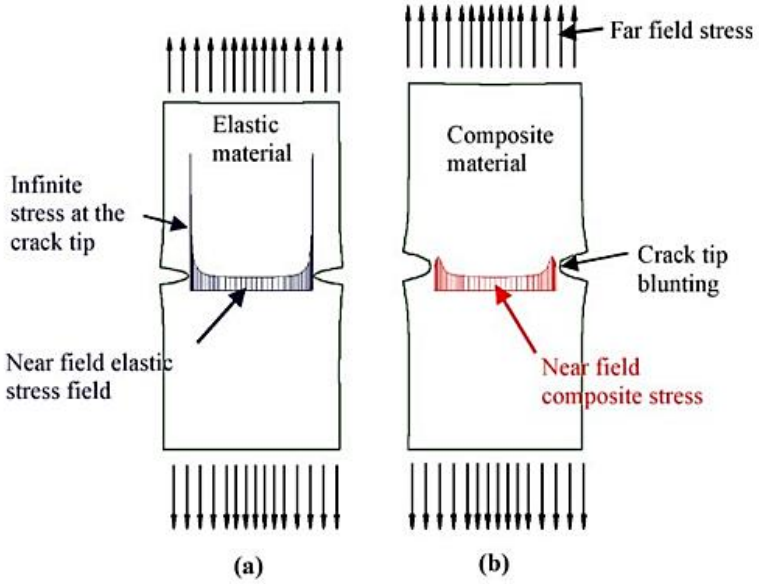

Source - Elder et al. (Elder, Thomson, Nguyen, & Scott, 2004)

There are some variables involved in this theory that need to be explained. The material ability to resist fracture is denominated as "material toughness", K_C, and it is interpreted as the energy required for fracturing the material per unit volume (usually unit in SI: J/m^3). Another variable is the energy that must be supplied to a crack tip to make it grow, balanced with the amount of energy dissipated due to the formation of new surfaces and other processes like plasticity. This variable is known as the "strain energy released rate" (SERR), *G*, and it is interpreted as the energy dissipated during fracture per unit of newly created fracture surface area (usually unit in SI: J/m^2).

To fully characterize a delamination growth, there exit three strain energies that must be calculated; they have a direct relationship with the fracture crack separation modes: the mode I component due to interlaminar tension (G_I), the mode II component due to interlaminar sliding shear (G_{II}) and the mode III component due to interlaminar scissoring shear (G_{III}) (Fig. 6). The literature contributions in experimental information about the mode III fracture, allow us to assume that the energy supply by this mode is insignificant when compared to the total energy released in a multi-axial load case (Ronald Krueger, Cvitkovich, O'Brien, & Minguet, 2000). This evidence is based in the fact that shear deformations at the crack tip do not differ despite

the direction, this is, the shear in any direction, within the crack plane between the fracture surfaces, is the same under subsequent mode II or mode III loading. From now on, this study will consider the energies released rates G_{II} and G_{III} as equivalent.

Once these parameters are determined, the usual procedure is to perform a comparison between the interlaminar fracture toughness and ratios of SERR in order to build a quasi-static Mixed-Mode fracture criterion. Mixed-Mode ratio (G_{II}/G_T) is generated experimentally using pure Mode I $(G_{II}/G_T = 0)$ Double Cantilever Beam (DCB), pure Mode II $(G_{II}/G_T = 1)$ three points End Notched Flexure (ENF), and Mixed-Mode Bending (MMB) tests of varying ratios (R. Krueger & O'Brien, 2001).

Figure 6 - Fracture Modes.

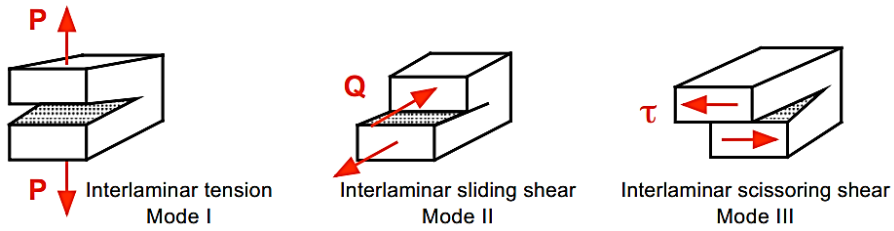

Source - Krueger and O'Brien (2001)

Standard methods to calculate these parameters have been developed for different cases and materials, for FRPC we have ASTM D5528-13 (2013) for pure Mode I, ASTM D7905 (2014) for pure Mode II and ASTM D6671 (2013) for Mixed-Mode interlaminar fracture toughness. Employing LEFM in conjunct with FEM have been widely adopted, however, there are some complicated features that could limit a numerical model (Davidson, Hu, & Schapery, 1995), (Raju & Shivakumar, 1990), (Crisfield, Jelenic, Mi, Zhong, & Fan, 1997):

— In a real case, crack propagation direction is affected by ply orientation adjacent to the crack plane and stress regime at the crack tip. This affection can be complicated to simulate because of the meshing considerations since the mesh shape and size can significantly affect the crack propagation direction.

— Delamination simulations may require a representation of a crack that can be easily accommodated, however, actual delamination may be related to an initial defect such as cracks product of an impact, so delamination become damage and fracture dependent.

— Some results regarding toughness, when simulating, appear to be geometrical dependents. Some cases are predicted to have the same results, thus, to satisfy this condition some relationship between toughness and mix mode should be applied.

— The crack propagation sometimes appears to be led by spontaneous oscillations being developed within the crack geometry.

Diverse approaches have been proposed to take into account those peculiarities, but despite those details, there exist a considerable number of publications regarding delamination characterization by LEFM. There are two approaches commonly used in fracture mechanics: the virtual crack closure technique (VCCT) and the cohesive zone model (CZM), both of them can be easily employed to simulate crack growth. The VCCT formulation is not considered during this research so a review of this subject is not presented, however, results found in the literature were employed in order to compare them with the experimental results.

2.1.1.1. Cohesive Zone Model

In Fracture Mechanics, the Cohesive Zone Model is a criterion relating the separation of two surfaces, a by-product of crack growth within a defined area, with cohesive tractions preventing this phenomenon to happen. First formulations appear in Barenblatt (1962) at the earliest 1960's with calculations of non-linear equilibrium of a solid containing a crack and under certain loads.

Summarizing, a cohesive zone is employed as a layer between two surfaces, which do not represent a physical material but a contact behavior between those surfaces (Fig. 7). This behavior is known as "Cohesive Laws" and is managed by some key parameters related to the energy release rates and the fracture toughness. Sequentially, to reproduce a progressive failure within this layer is needed a traction-separation law shaped by three specific cohesive parameters: critical cohesive strength, initial stiffness and fracture toughness (R. D. Campilho, De Moura, & Domingues, 2008).

Figure 7 - Schematic Cohesive Zone Model.

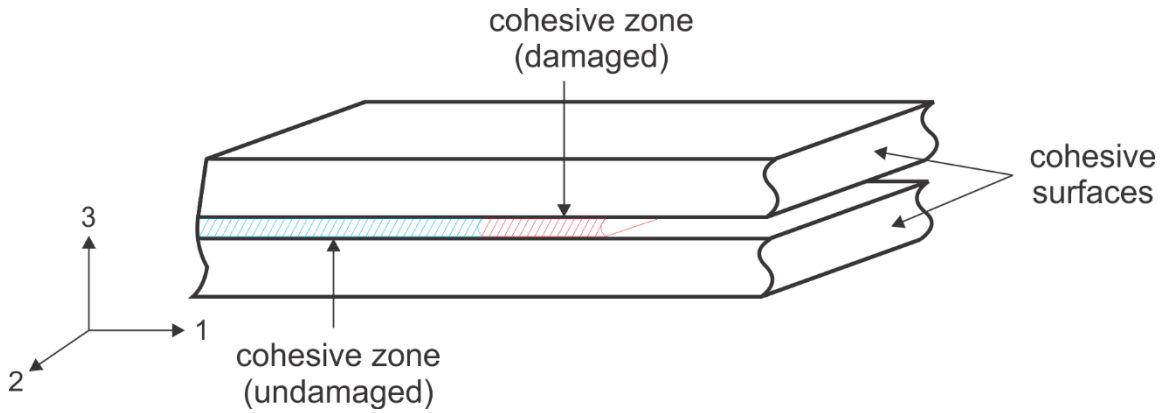

It is possible to calculate the fracture toughness from experiments, but there is not a specific procedure to calculate the critical cohesive strength and initial stiffness, since these parameters may vary according to the case of study (load case, sample geometry, etc.).There exist in the literature some review papers resuming different approaches and procedures to estimate the cohesive parameters (Lee, Cho, Kim, Lee, & Lee, 2010), (CR Chen et al., 2003) and (Cornec, Scheider, & Schwalbe, 2003). In any case, initial data may become from experimental tests to calculate the SERR as described in section 2.1.1.

CZM uses a delamination criterion to define whether a crack should propagate or not, usually, these criteria are developed from mixed-mode to account for both fracture modes influence in the onset of delamination according to the loading case. The literature presents different approaches based on crack opening displacement, stress or strain near the crack tip, stress intensity factor or even strain energy released rate. Nearly all the criteria found in the literature are based in terms of SERR and since delamination in structures is often subjected to mixed-mode loadings, the specific terms employed are the pure-mode toughness G_{Ic} and G_{IIc}.

Most employed criterion is *The Power Law* described in eq. 2.1 (Wu & Reuter, 1965) which is established in terms of an interaction between the energy release rates, and have been demonstrated that handles successfully when predicting failure in thermoplastics PEEK matrix composites with a power $\alpha = 1$.

$$\left(\frac{G_I}{G_{IC}}\right)^{\alpha} + \left(\frac{G_{II}}{G_{IIC}}\right)^{\alpha} = 1 \tag{2.1}$$

When performing a Mixed-Mode delamination, there are different mode ratios configurations that would affect the fracture toughness. The power law does not satisfy this condition and is not able to compute this toughness variation even using both $\alpha = 1$ and $\alpha = 2$. In order to assess the Mixed-Mode fracture toughness variation, by dependence of the mode ratio configuration, the *B-K criterion* (Kenane & Benzeggagh, 1997) is employed. This model presents an interaction between Mode I and Mode II fracture toughness with a parameter η calculated from MMB tests at different mode ratios as seen in eq. 2.2:

$$G_{IC} + (G_{IIC} - G_{IC})\left(\frac{G_{Shear}}{G_T}\right)^{\eta} = G_C, \text{ with } G_T = G_I + G_{Shear} \tag{2.2}$$

Both criteria are considered the most consistent formulation available in literature and are usually implemented in nearly all current FEM software packages. Other formulations that could be mention are the Reeder (1993) with a bilinear failure criterion based on a change in the failure mechanism observed from the delamination surfaces, and Hashemi (1991) whom introduced some correction parameters to asses accurate SERR critical values. A detailed review of delamination criteria can be found in the literature (R., 1992), (Orifici, Herszberg, & Thomson, 2008).

Nowadays, the literature exhibits an innumerous cohesive zone approaches for different structural cases.

2.1.2. Delamination Using Continuum Damage Mechanics (CDM)

The Continuum Damage Mechanics is an attractive tool to describe the progressive degradation of material's mechanical properties. It has been widely improved and used in a variety of cases during these last three decades since it was initially introduced by Kachanov (1958). This theory characterizes damage through the employment of mechanical variables obtained from the mechanisms involved in the degradation of materials submitted to loads. The CDM can use that definition at different scales within the material; at a microscale, the damage is understood as the conception of microsurfaces of discontinuities like the rupture of atomic bonds and the plastic expansion of microcavities. At a mesoscale, the number of this ruptures and the distribution of microcavities can be estimated as well as the identification of weak areas. At a macroscale, all these micro-damages converge and result in a unique failure mechanism which is usually a fracture (Zhang & Cai, 2010).

The literature exhibits diverse examples of the application of CDM with composite materials at any scale. Some primordial researches are (J. L. Chaboche, Lesne, & Maire, 1995), which consider anisotropic brittle composites treated as elastic damageable ones; (Voyiadjis & Deliktas, 2000) using CDM in fiber reinforced metal matrix; defining the damage matrix as a fourth-order damage effect tensor depending on the stress history and describing damage employing kinematic relations; (Ladeveze & Ledantec, 1992) who modeled fibrous composite laminate at an elementary ply scale (mesoscale) and defined the damage variables related with the material stiffness reduction, and others like (Evans & Zok, 1994), (Talreja, 1985), (Varna, Joffe, Akshantala, & Talreja, 1999).

More recent researches are focused on computational simulations; the implementation of FEA in structural software has reduced the time of calculations and allowed the development of more complex damage models. Some review articles can be found, resuming computational mechanics models (Schmauder, 2002), multi-scale computational homogenization (Geers, Kouznetsova, & Brekelmans, 2010), Continuum models for ductile fracture and its computational implementation (Besson, 2010) and exclusively for fiber reinforced laminated composites (Schuecker & Pettermann, 2008) with progressive damage modelling based on failure mechanics. Looking for the most relevant research investigations relating computational implementation, can be mentioned: (Maimi, Camanho, Mayugo, & Davila, 2007), (Donadon, Iannucci, Falzon, Hodgkinson, & de Almeida, 2008), (Lubineau & Ladevèze, 2008), (Tita, de Carvalho, & Vandepitte, 2008), (Pavan, Oliveira, Maghous, & Creus, 2010), (Flatscher & Pettermann, 2011) and (Ribeiro, Tita, & Vandepitte, 2012).

In the case of delamination within composite materials, CDM has been applied in different approaches for delamination onset and propagation. For both cases, there exist models from mesoscale which consist in modeling a laminate as a stacking of homogeneous layers connected by interfaces where is studied the tendency of different stacking sequence to delaminate by the analysis of the stresses at the interface between layers (Herakovich, 1989). The delamination onset is studied at the mesoscale since, to correctly predict this initiation, the stress distribution needs to be known at each layer and the interface between them too (Bordeu, Boucard, & Lubineau, 2010), (Noijen, vd Sluis, Timmermans, & Zhang, 2010). Macroscale models are the most typical in literature, the damage variables determined at this scale are derived usually from strain energy released measures at crack growth. These models are commonly supported by Fracture Mechanic, specifically by a Traction-Separation law, which allows deriving damage variables from relations between the strain energy released rates of critical and damaged states while the delamination crack grows. Some remarkable works about damage mechanics to describe delamination can be mention: (Allix & Ladeveze, 1992), (Point & Sacco, 1996) and (Zou, Reid, & Li, 2003) where the relation between Fracture Mechanics (FM) and Continuum Damage Mechanics (CDM) is clear; models for delamination due to fatigue loads have been developed as well (Turon, Costa, Camanho, & Davila, 2007); mixed-mode crack propagation (Camanho, Davila, & de Moura, 2003) and (Turon, Camanho, Costa, & Renart, 2010); models for thin-walled structures (Zerbst, Heinimann, Donne, & Steglich, 2009) and finally, delamination due to impact (A. F. Johnson, Pickett, & Rozycki, 2001), (Iannucci & Willows, 2006), (Shi, Swait, & Soutis, 2012).

CHAPTER III

3. Materials and Method

Advances in technology generally go hand in hand with advances in material science. The development and application of composite materials represented a huge progress in most of the industrial fields and, without doubts, the aeronautic industry could not be an exception. The clearest example is the case of the Boeing's 787, where the main technological advance is based on widespread incorporation of composites representing almost the 50% of the total material employed.

While the utilization of composite materials is increasing, the requirement for more and more engineers able to design and fabricate composite structures also increases. As a result, academic and industrial researchers are equally interested in expanding the knowledge. Traditional manufacturing and mechanical tests have been formulated and established; each of them with different complexity during the procedure and requiring more or fewer resources.

The sections of this chapter will give the details about the material considered during the research like its mechanical properties and other mechanical aspects. The methodology will be explained as well, which include manufacture procedure, test methods and the formulation of the model by traction-separation law and damage variables definitions.

3.1. Materials

The material considered in this research belongs to a composite material family known as *fiber-reinforced plastic* using glass fibers. The fibers have a unidirectional arrangement woven into a fabric. The plastic matrix is a thermoset polymer matrix named *epoxy*, so the final product is actually a fiberglass-epoxy laminated composite. Further sections will describe more details about the fibers, matrix, mechanical properties of the laminate and a slight review of the classical laminate theory.

3.1.1. Glass Fibers

Figure 8 -Glass Fiber.

One of the most versatile industrial materials known today are the *glass fibers*, which modern method invention is attributed to Games Slayter from Owens-Illinois Glass Co patented in 1933; consisting on numerous extremely fine fiber of glass obtained by melting glass composed by silica and minerals. The glass fibers are produced by a direct draw process and shaped by forcing the glass through a platinum alloy bushing that has thousands and thousands of orifices. The final fiber diameters range from 3 to 20 μm and are usually continuum fibers that can be produced as low-cost general-purpose fibers or premium special-purpose fibers. The most known low-cost general-purpose fiber is the one designated as E-Glass (E stands for low electrical conductivity) which represent over 90% of the total fiber produced; the remaining 10% consists in special types of fiber with high strength, high chemical durability, high stiffness, high alkali composition and low dielectric constant. Typical E-Glass fiber has Young's modulus between 70-78 GPa, Tensile Stress of 3100-3800 MPa and a elongation after the break between 4.5-4.9 % (Wallenberger, Watson, & Li, 2001).

The glass fibers employed to manufacture the specimens for this research was an E-Glass supplied by *Texiglass*. The mechanical properties, informed by the manufacturer, are listed in tab. 1.

Table 1 - E-Glass mechanical properties.

Young's Modulus (GPa)	**Tensile Stress (MPa)**	**Density g/cm^3**	**Elongation %**
72.4	3200	1.5	4.8

3.1.2. Epoxy Resin

Within composite materials, epoxy resins are considered the most employed thermoset polymer to work as a matrix. Firstly patented by Dr. Pierre Castan licensed by Ciba Ltd in 1938 but also claimed by S.O. Greenlee who was parallel studying the production of epoxy and patented a resin in 1946 while working for Devoe-Reynolds.

Epoxies are the product of the condensation of pre-polymer or polymer epoxides and co-reactants amines often known as hardeners or curatives. This resin has extensive applications including coating, adhesive and composite materials like carbon or fiberglass reinforced laminates. The principal properties of epoxy resins are high strength, low shrinkage, good adhesion, effective electrical insulation, chemical and solvent resistance, low cost and low toxicity. The large range of cure time, low viscosity and tendency to wet surfaces easily, allows employing the epoxy resin in several complex manufacture processes from simple plates until more geometrically complex structures. The mechanical properties of this resin, at room temperature, can vary mostly depending on the manufacturing process from a simple manual wet layup cured resin to a high-performance aerospace resin; the tensile strength is between 50-58.3 MPa, Young's Modulus 2.2-3.72 GPa and tensile elongation 2.8-1.8 % (Boyle, Martin, & Neuner, 2001).

The curatives or hardeners that react with epoxy can be several; the most commonly used are amines, amine derivatives, and anhydrides. The choice of resin-curative combination can affect the final product characteristics such as system stability, cure kinetics, physical form, glass transition temperature, mechanical performance and chemical resistance.

Figure 9 - Epoxy resin and hardener.

Epoxy resin employed to manufacture the specimens in this study was supply by epHoxaL, which properties of the cured resin are listed in tab. 2. This resin is a polymer epoxide and, as curative, an amine is employed; with commercial names EPHOXAL RAL 120 and EPHOXAL HAL 115 respectively fig.9.

Table 2 - Mechanical properties of cured epoxy epHoxaL RAL 120/ epHoxaL HAL 115.

	Young's Modulus (GPa)	**Tensile Strength (MPa)**	**Poisson' Ratio**
Cured Epoxy	2.4	50	0.22

3.1.3. Laminated Composites: Structural Analysis

To carry out a structural analysis, we must start by reviewing the classical laminate theory. A lamina is considered the basic unit of a structured laminate, thus, the exploration of the mechanical behavior of a lamina becomes crucial when designing any composite laminate. A lamina is defined as a planar or curved ply reinforced by continuous filaments that could have one or two directions depending on if the fibers are a unidirectional or bidirectional fabric, these fibers must have a defined orientation with respect to the orthotropic axis 1 and 2 as seen in fig. 10:

Figure 10 - Fiber reinforced lamina.

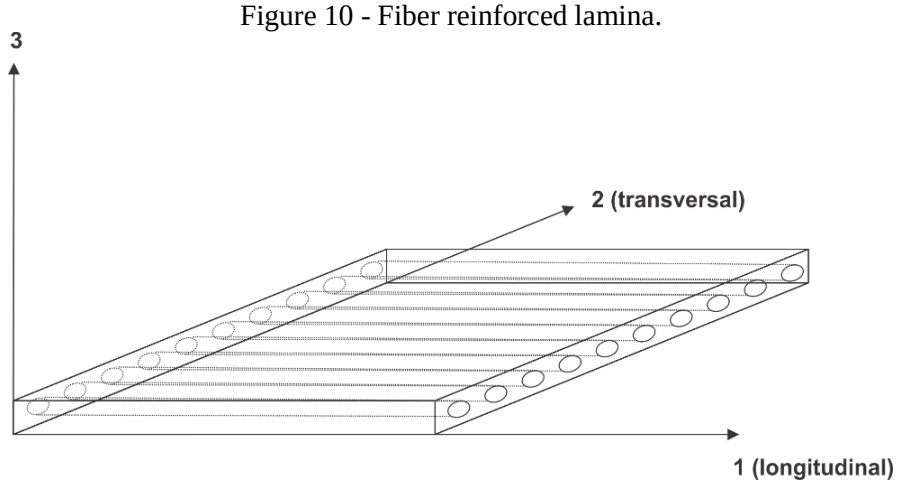

A composite laminate is considered anisotropic and a lamina has three orthotropic planes, thus, for a structural analysis, a laminate is considered an orthotropic material. In continuum

mechanics, an anisotropic material has a general constitutive relation as defined in eq. 3.1. It is also observed that there are three symmetry cases within an orthotropic material: the presence of three perpendicular symmetric planes (orthotropy), the existence of a plane where the mechanical properties are the same in all directions (transversely isotropic material) and infinite planes of symmetry (Isotropic material). By this, the elements of the constitutive matrix of eq. 3.1 are reduced and showed for each case in eq. 3.2, eq. 3.3 and eq. 3.4:

Constitutive Equation

$$\begin{Bmatrix}\sigma_1\\ \sigma_2\\ \sigma_3\\ \tau_4\\ \tau_5\\ \tau_6\end{Bmatrix}=\begin{bmatrix}C_{11} & C_{12} & C_{13} & C_{14} & C_{15} & C_{16}\\ C_{21} & C_{22} & C_{23} & C_{24} & C_{25} & C_{26}\\ C_{31} & C_{32} & C_{33} & C_{34} & C_{35} & C_{36}\\ C_{41} & C_{42} & C_{43} & C_{44} & C_{45} & C_{46}\\ C_{51} & C_{52} & C_{53} & C_{54} & C_{55} & C_{56}\\ C_{61} & C_{62} & C_{63} & C_{64} & C_{65} & C_{66}\end{bmatrix}\begin{Bmatrix}\varepsilon_1\\ \varepsilon_2\\ \varepsilon_3\\ \gamma_4\\ \gamma_5\\ \gamma_6\end{Bmatrix} \qquad 3.1$$

Orthotropy

$$\begin{Bmatrix}\sigma_1\\ \sigma_2\\ \sigma_3\\ \tau_4\\ \tau_5\\ \tau_6\end{Bmatrix}=\begin{bmatrix}C_{11} & C_{12} & C_{13} & 0 & 0 & 0\\ C_{21} & C_{22} & C_{23} & 0 & 0 & 0\\ C_{31} & C_{32} & C_{33} & 0 & 0 & 0\\ 0 & 0 & 0 & C_{44} & 0 & 0\\ 0 & 0 & 0 & 0 & C_{55} & 0\\ 0 & 0 & 0 & 0 & 0 & C_{66}\end{bmatrix}\begin{Bmatrix}\varepsilon_1\\ \varepsilon_2\\ \varepsilon_3\\ \gamma_4\\ \gamma_5\\ \gamma_6\end{Bmatrix} \qquad 3.2$$

Transversely Isotropic Material

$$\begin{Bmatrix}\sigma_1\\ \sigma_2\\ \sigma_3\\ \tau_4\\ \tau_5\\ \tau_6\end{Bmatrix}=\begin{bmatrix}C_{11} & C_{12} & C_{12} & 0 & 0 & 0\\ C_{12} & C_{22} & C_{23} & 0 & 0 & 0\\ C_{12} & C_{23} & C_{22} & 0 & 0 & 0\\ 0 & 0 & 0 & \frac{C_{22}-C_{23}}{2} & 0 & 0\\ 0 & 0 & 0 & 0 & C_{55} & 0\\ 0 & 0 & 0 & 0 & 0 & C_{55}\end{bmatrix}\begin{Bmatrix}\varepsilon_1\\ \varepsilon_2\\ \varepsilon_3\\ \gamma_4\\ \gamma_5\\ \gamma_6\end{Bmatrix} \qquad 3.3$$

Isotropic Material

$$\begin{Bmatrix}\sigma_1\\ \sigma_2\\ \sigma_3\\ \tau_4\\ \tau_5\\ \tau_6\end{Bmatrix}=\begin{bmatrix}C_{11} & C_{12} & C_{12} & 0 & 0 & 0\\ C_{12} & C_{11} & C_{12} & 0 & 0 & 0\\ C_{12} & C_{12} & C_{11} & 0 & 0 & 0\\ 0 & 0 & 0 & \frac{C_{11}-C_{12}}{2} & 0 & 0\\ 0 & 0 & 0 & 0 & \frac{C_{11}-C_{12}}{2} & 0\\ 0 & 0 & 0 & 0 & 0 & \frac{C_{11}-C_{12}}{2}\end{bmatrix}\begin{Bmatrix}\varepsilon_1\\ \varepsilon_2\\ \varepsilon_3\\ \gamma_4\\ \gamma_5\\ \gamma_6\end{Bmatrix} \quad 3.4$$

Where,

$\{\sigma\}_{6x1}$= Stress vector;

$[C]_{6x6}$= Stiffness matrix of the material; and

$\{\varepsilon\}_{6x1}$= Strain vector.

The nomenclature assumed for the directions within the tensors is explained in fig. 11.

The indicial notation would be:

$$\sigma_i = C_{ij}\varepsilon_j \quad 3.5$$

$$\varepsilon_j = S_{ij}\sigma_i \quad 3.6$$

Where,

$S_{ij} = C_{ij}^{-1}$ = Compliance matrix (Inverse of the stiffness matrix C_{ij}).

A lamina is assumed to be under plane stress state since the thickness of the lamina is insignificant when comparing it with its length and width. This means that the stresses that act perpendicularly to the lamina plane can be assumed as zero, thus, $\sigma_3 = \tau_4 = \tau_5 = 0$. Therefore, the plane stress reduces the number of elements composing the constitutive matrix as seen in eq. 3.7:

$$\begin{Bmatrix}\sigma_1\\ \sigma_2\\ \tau_6\end{Bmatrix}=\begin{bmatrix}Q_{11} & Q_{12} & 0\\ Q_{12} & Q_{22} & 0\\ 0 & 0 & Q_{66}\end{bmatrix}\begin{Bmatrix}\varepsilon_1\\ \varepsilon_2\\ \gamma_6\end{Bmatrix} \quad 3.7$$

Where,

$[Q]_{3x3}$= Reduced stiffness matrix under plane stress.

To calculate the elements of this new matrix, the mechanical properties of the lamina are employed according to the orthotropic directions: 1 for fiber direction and 2 for the direction perpendicular to the fibers:

$$Q_{11}=\frac{E_1}{1-\nu_{12}\nu_{21}} \tag{3.8}$$

$$Q_{22}=\frac{E_2}{1-\nu_{12}\nu_{21}} \tag{3.9}$$

$$Q_{12}=\frac{\nu_{12}E_1}{1-\nu_{12}\nu_{21}} \tag{3.10}$$

$$Q_{33}=G_{12} \tag{3.11}$$

Where,

E_i= Young's modulus at *i* direction;

ν_{ij}= Poisson's ratio related to *ij* plane; and

G_{ij}= Shear modulus at *ij* plane.

3.1.4. Laminated Composite: Mechanical Properties

The stress-strain relations reviewed in the previous section can be expressed in terms of engineering constants, i.e., Young's modulus and Poisson's ratios. These expressions are obtained for each normal stress loading case and shear stress loading case illustrated in fig. 11:

Figure 11 - Normal and shear stress loading cases.

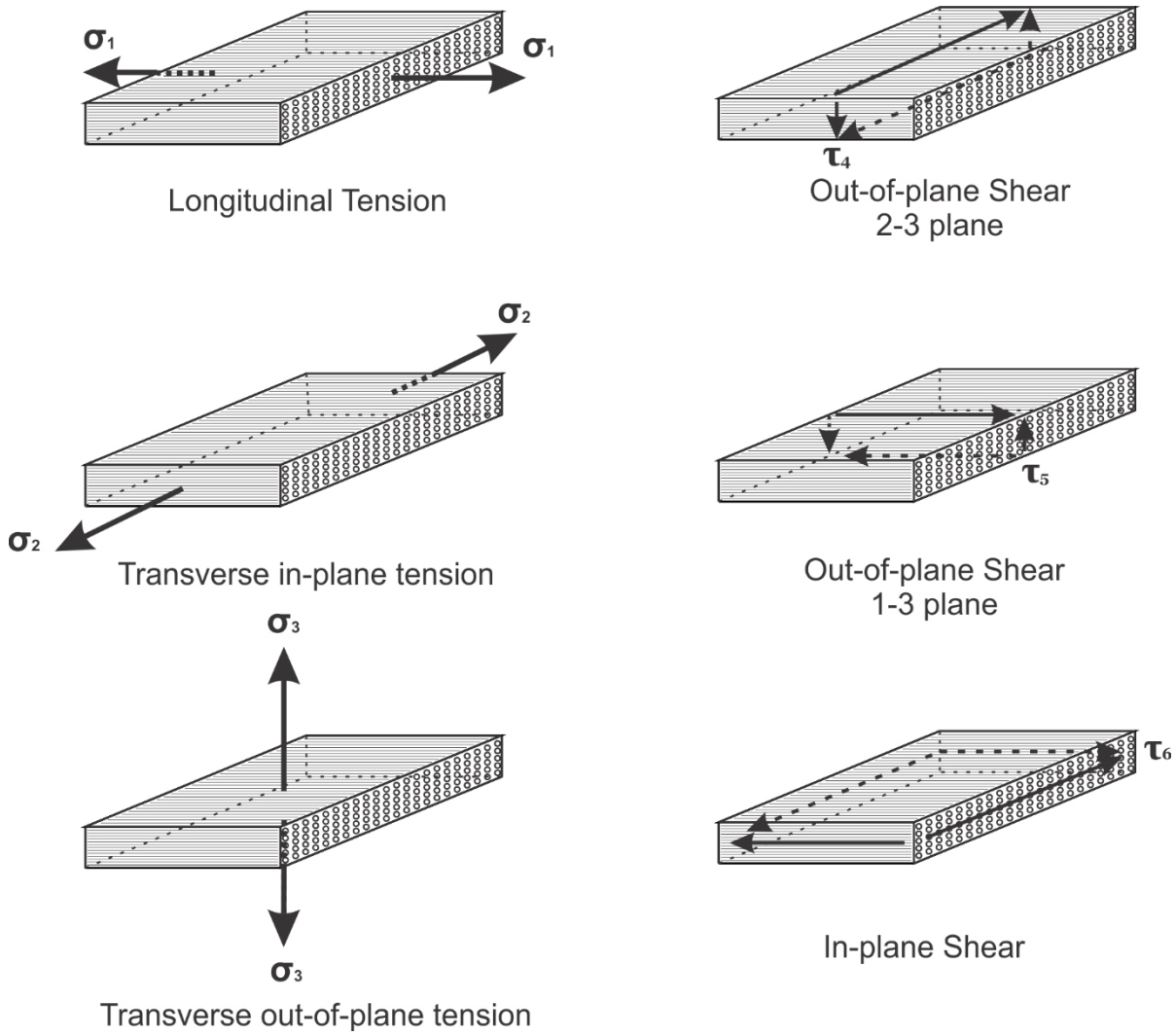

If we consider an orthotropic material element subjected to those loading cases, we can find different expression for eq. 3.6 related to the mechanical properties. For a tensile loading in the longitudinal direction (longitudinal tension), σ_1, we have:

$$\begin{aligned} \varepsilon_1 &= S_{11}\sigma_1 \\ \varepsilon_2 &= S_{12}\sigma_1 \\ \varepsilon_3 &= S_{13}\sigma_1 \\ \gamma_4 = \gamma_5 = \gamma_6 &= 0 \end{aligned} \qquad 3.12$$

From the mechanical behavior of materials, we know that:

$$\varepsilon_1 = \frac{\sigma_1}{E_1}$$

$$\varepsilon_2 = -\frac{\nu_{12}}{E_1}\sigma_1$$

$$\varepsilon_3 = -\frac{\nu_{13}}{E_1}\sigma_1 \qquad 3.13$$

$$\gamma_4 = \gamma_5 = \gamma_6 = 0$$

Then, substituting eq. 3.13 in eq. 3.12, we relate eq. 3.6 with engineering constants:

$$S_{11} = \frac{1}{E_1}, S_{12} = -\frac{\nu_{12}}{E_1}, S_{13} = -\frac{\nu_{13}}{E_1} \qquad 3.14$$

If the lamina is subjected to a tensile loading in the in-plane transverse direction (transverse in-plane tension), σ_2, we have:

$$\varepsilon_1 = S_{12}\sigma_2 = -\frac{\nu_{21}}{E_2}\sigma_2$$

$$\varepsilon_2 = S_{22}\sigma_2 = \frac{\sigma_2}{E_2}$$

$$\varepsilon_3 = S_{23}\sigma_2 = -\frac{\nu_{23}}{E_2}\sigma_2 \qquad 3.15$$

$$\gamma_4 = \gamma_5 = \gamma_6 = 0$$

Then, we obtain the following expressions:

$$S_{12} = -\frac{\nu_{21}}{E_2}, S_{22} = \frac{1}{E_2}, S_{23} = -\frac{\nu_{23}}{E_2} \qquad 3.16$$

The last normal loading in the out-of-plane transverse direction (transverse out-of-plane tension), σ_3, gives the following expressions:

$$\varepsilon_1 = S_{13}\sigma_3 = -\frac{\nu_{31}}{E_3}\sigma_3$$

$$\varepsilon_2 = S_{23}\sigma_3 = -\frac{\nu_{32}}{E_3}\sigma_3 \tag{3.17}$$

$$\varepsilon_3 = S_{33}\sigma_3 = \frac{\sigma_3}{E_3}$$

Thus,

$$S_{13} = -\frac{\nu_{31}}{E_3}, S_{23} = -\frac{\nu_{32}}{E_3}, S_{33} = \frac{1}{E_3} \tag{3.18}$$

Now, for shear loadings, in-plane pure shear loading, τ_6, yields:

$$\varepsilon_1 = \varepsilon_2 = \varepsilon_3 = \gamma_4 = \gamma_5 = 0$$

$$\gamma_6 = S_{66}\tau_6 = \frac{\tau_6}{G_{12}} \tag{3.19}$$

And the following expression is obtained:

$$S_{66} = \frac{1}{G_{12}} \tag{3.20}$$

Out-of-plane shear loading in the 2-3 plane, τ_4, we have:

$$\varepsilon_1 = \varepsilon_2 = \varepsilon_3 = \gamma_5 = \gamma_6 = 0$$

$$\gamma_4 = S_{44}\tau_4 = \frac{\tau_4}{G_{23}} \tag{3.21}$$

Then we obtain:

$$S_{44} = \frac{1}{G_{23}} \tag{3.22}$$

Finally, out-of-plane shear loading in the 1-3 plane, τ_5 , we have:

$$\varepsilon_1 = \varepsilon_2 = \varepsilon_3 = \gamma_4 = \gamma_6 = 0$$

$$\gamma_5 = S_{55}\tau_5 = \frac{\tau_5}{G_{13}} \qquad 3.23$$

Where is possible to obtain:

$$S_{55} = \frac{1}{G_{13}} \qquad 3.24$$

Now, the stress-strain relations showed in eq. 3.6 can be expressed in terms of mechanical properties of the laminate as is shown in eq. 3.25:

$$\begin{Bmatrix} \varepsilon_1 \\ \varepsilon_2 \\ \varepsilon_3 \\ \gamma_4 \\ \gamma_5 \\ \gamma_6 \end{Bmatrix} = \begin{bmatrix} \frac{1}{E_1} & -\frac{\nu_{21}}{E_2} & -\frac{\nu_{31}}{E_3} & 0 & 0 & 0 \\ -\frac{\nu_{12}}{E_1} & \frac{1}{E_2} & -\frac{\nu_{32}}{E_3} & 0 & 0 & 0 \\ -\frac{\nu_{13}}{E_1} & -\frac{\nu_{23}}{E_2} & \frac{1}{E_3} & 0 & 0 & 0 \\ 0 & 0 & 0 & \frac{1}{G_{23}} & 0 & 0 \\ 0 & 0 & 0 & 0 & \frac{1}{G_{13}} & 0 \\ 0 & 0 & 0 & 0 & 0 & \frac{1}{G_{12}} \end{bmatrix} \begin{Bmatrix} \sigma_1 \\ \sigma_2 \\ \sigma_3 \\ \tau_4 \\ \tau_5 \\ \tau_6 \end{Bmatrix} \qquad 3.25$$

Knowing the symmetry present in the stiffness matrix for an isotropic material, we can have the following conclusion:

$$\frac{\nu_{ij}}{E_i} = \frac{\nu_{ji}}{E_j} \qquad (i, j = 1,2,3)$$

Since the laminate is considered a transversely isotropic material with the 2-3 plane as the plane of isotropy, we can define:

$$E_2 = E_3$$
$$G_{12} = G_{13} \qquad 3.26$$
$$\nu_{12} = \nu_{13}$$

After all these definitions, we can now specify the necessary parameters to mechanically characterize a composite unidirectional laminate manufactured with continuous glass fibers and employing epoxy resin as a matrix. Tab. 3 shows the mechanical properties of the material considered for this research:

Table 3 - E-Glass/epoxy mechanical properties.

	E_{11} (GPa)	E_{22} (GPa)	ν_{12}	G_{12} (GPa)	G_{23} (GPa)
E-Glass/Epoxy	32.20	13.77	0.28	8.99	2.75

These properties were calculated at the laboratory of the Group of Aeronautical Structures (GEA) of the University of São Paulo localized in São Carlos City, excepting the value for out-of-plane shear modulus at the 2-3 plane (G_{23}), which correspond to 20% of E_2 (Pandit, Sheikh, & Singh, 2010).

3.2. Methodology

Delamination within composite can be a complex failure mode due to its almost unpredictable onset and propagation. This research is focused on describing and characterizing the delamination propagation; the indicator parameter employed will be the Strain Energy Released Rate (SERR), which will be measured as the crack grows within the laminate. At different relevant crack lengths, the SERR measured will be used to calculate nominal stresses that represent the precise instants before a significant material degradation.

This section describes the methodology carried out during this research, which includes three stages:

(1) Specimen manufacture: At this stage, specimens are manufactured employing the materials described in the previous section and regarding the geometry specifications of the standard test methods considered for this research.

(2) Experimental tests: In this second stage, once the specimens are correctly manufactured, the necessary tests will be carried out. A Double Cantilever Beam (DCB) test will be performed in order to calculate the Mode I interlaminar SERR (G_1) following the ASTM D5528 (2013) standard test method. To calculate the Mode II interlaminar SERR (G_2), an End Notched Flexure (ENF) test will be performed following the ASTM D7905 (2014) standard test method. Since delamination within aeronautical structures may happen by the influence of both, Mode I and Mode II interlaminar fracture, different cases of Mixed-Mode Bending (MMB) will be tested in order to determine the critical SERRs during crack propagation with different Mode I – Mode II rates following the specification of ASTM D6671 (2013) standard test method.

(3) Traction-Separation Law: Finally, after calculating all the SERR values at each critical point, a Traction- Separation Law (TSL) will be derived. This will be achieved by calculating nominal stresses for each SERR value and founding a mathematical function that can represent the degradation and shape the TSL.

Figure 12 - Research Methodology.

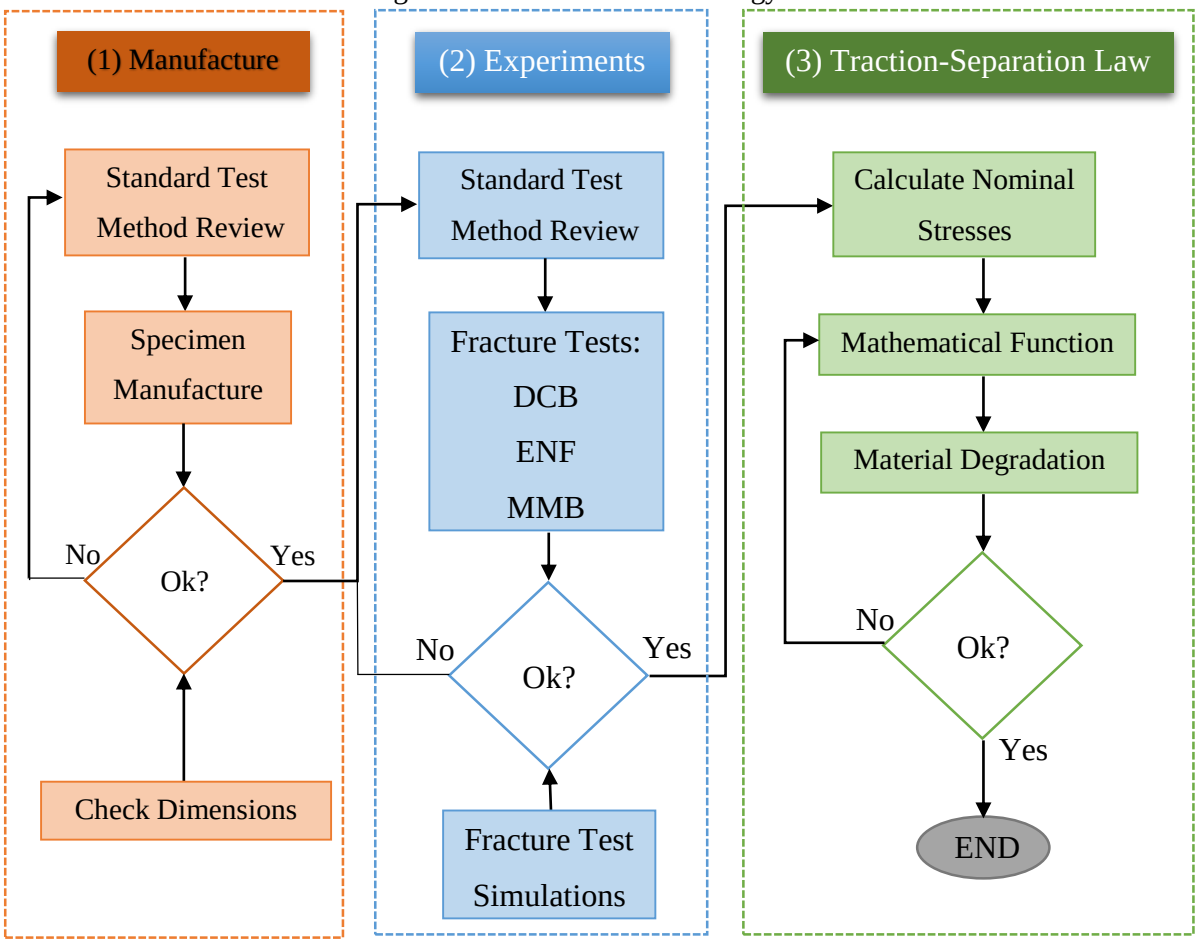

3.2.1. Modified Vacuum Assisted Infusion Process (MVAIP)

The MVAIP is a composite manufacture process that does not require an industrial autoclave pressure vessel. This process is a cost-effective method to manufacture high quality and high strength composite pieces. The quality is similar to the one obtained using an autoclave but it cannot replace it since the production of composite pieces is poor, thus, the MVAIP is usually worth considering for applications requiring low production rates.

It consists of a closed system that is within the void between a sealed bag and a mold. Inside are placed the fiber fabrics with a specific stacking sequence and the amount of resin needed to impregnate the fibers; this is the distinction from classical VAIP, since the resin is placed over the mold and the layup inside the vacuum bag, and not admitted from an external container. The key part of the process is to induce the materials to vacuum by the employment of a vacuum pump; this will evacuate the air inside the system and start a resin flow through the fiber layup. Once the impregnation is completed, the composite laminate can be cured at room temperature or assisted by an industrial curing oven.

This section will detail and illustrate the step followed in order to manufacture the specimens required to perform the experimental tests:

(1) The first step is to examine the standard test methods in order to be aware of the specimens' details. Tab. 4 gives the geometric values of the specimens for the three tests considered; note that these specimens need to be pre-cracked and this is achieved by introducing a TEFLON insert at the midplane of the laminate (Fig. 13).

Figure 13 - Specimen geometry.

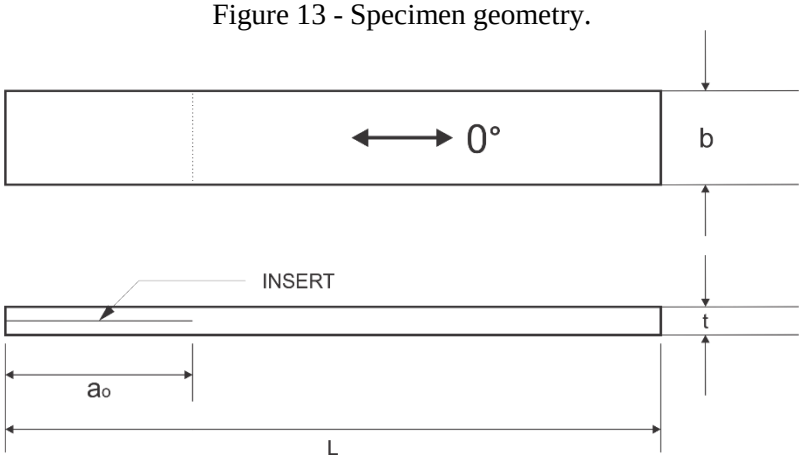

Table 4 - Dimensions of specimens.

	L (mm)	b (mm)	t (mm)	a_o (mm)
Mode I	140	25	3.2	50
Mode II	160	25	3.2	45
Mixed-Mode	140	25	3.2	50

Where,

L = Length of the specimen;

b = Width of the specimen;

t = Thickness of the specimen; and

a_o= Initial delamination length.

(2) We proceed by cutting the fiber fabrics with a dimension limited by the mold employed. For our case, each fabric ply will have a dimension of 350x400 mm for mode I and mixed-mode specimens (Fig. 14) and 380x400 mm for mode II specimens.

Figure 14 - Plate dimensions.

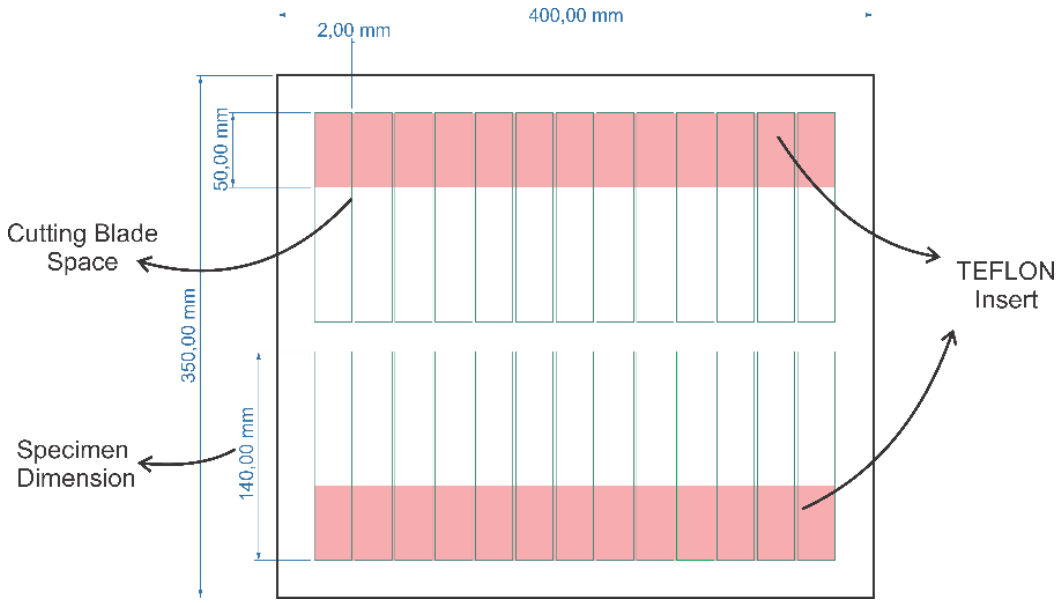

To achieve the required thickness, 32 unidirectional plies were employed with a stacking sequence of $[0^o]_{32}$ for all the cases. A 400x50 mm TEFLON insert is cut and placed at the midplane of the whole stack. This insert impedes the resin to flow through it in order to avoid the bond of the surfaces above and below it and creates an initial crack. The TEFLON insert has a thickness of 13 µm.

Figure 15 - Glass fiber plies.

(3) The amount of resin employed is calculated by a proportion of 1:2.5, this is 2.5 grams of resin per each gram of fiber. According to the dimensions of the plates to be manufactured, they have a volume of 448 cm^3 for Mode I and Mixed-Mode and 486.4 cm^3 for Mode II. Knowing the density of the fibers from tab. 1, we can estimate the amount of resin needed:

$$Amount\ of\ resin = density_{fiber} \times volume_{plate} \times 2.5$$

$$Amount\ of\ resin = 0.15\ \frac{g}{cm^3} \times 448 cm^3 \times 2.5 \cong 168\ g \qquad 3.27$$

This value actually represents the amount of resin plus hardener, which proportion is 85:15. This is, per every 85 grams of epoxy resin, 15 grams of hardener are needed.

(4) Before impregnation starts, the mold needs to be prepared. A glass plate will be employed as a base, where a thin layer of a release agent is spread over the surface in order to ease the disassembly. Others materials like a peel-ply fabric, thin plastic industrial netting, and absorbing cloth ply are employed respectively to avoid undesired bonds, improve the resin flow and to absorb any resin excess. Finally, a plastic bag covers all the assembly and an escape vessel is placed at one of the corners, where the air is extracted to provoke vacuum by using a vacuum pump (Fig. 16).

Figure 16 - (a) Materials to perform a cure (b) Vacuum pump and release agent.

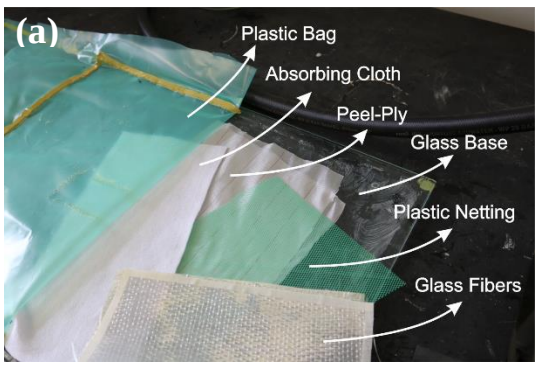

(5) The curing process for this case was carried out by employing an industrial curing oven (Fig.17) with a specific temperature cure cycle described in fig. 18:

Figure 17 - Industrial curing oven.

Figure 18 - Temperature cure cycle.

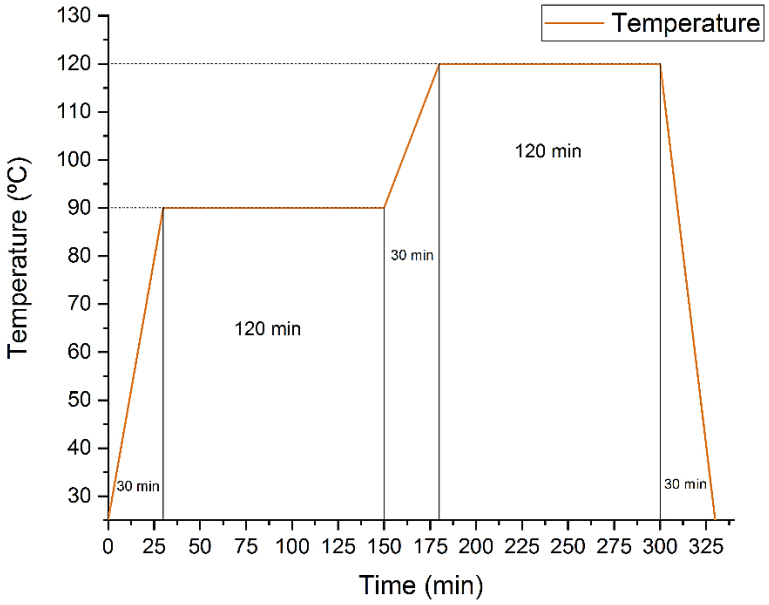

(6) Once the cure has finished its cycle, the specimens plan is sketched over the plate surface following the design in fig. 14. A table saw machine is employed to cut the plates and obtain the specimens, using a continuous rim diamond blade with 1.8 mm of thickness (Fig. 19).

Figure 19 - Table saw machine.

(7) The final step is to refine the surfaces using a polishing machine (fig. 20). For Mode I and Mixed-Mode, piano hinges need to be bonded at the upper and lower surface of the edge where the insert was placed (fig. 21). A surface finishing process needs to be performed before bonding, using polishing papers (grits: 400 and 600) and a cleaner agent; an epoxy adhesive was employed to bond the hinges. The function of these piano hinges is to allow fasting the specimens to the testing machine grips using bolts. For both cases, the piano hinges have an adherent surface of 20 mm.

Figure 20 - Polishing machine.

Figure 21 - Specimens ready for testing.

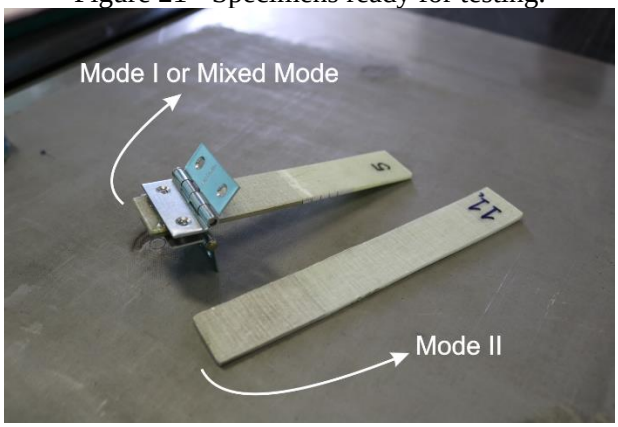

3.2.2. Experimental Tests

To characterize the interlaminar fracture or delamination, the strain energy released rates (G) need to be calculated; three different tests were carried out for Mode I, Mode II and Mixed-Mode fracture. The American Standard Test Methods (ASTM) were considered to go along with most of the researchers worldwide and be able to compare the results. Each test method has its own difficulties and a brief explanation is given in this section.

3.2.2.1. Double Cantilever Beam Test

This test is performed to obtain the SERR for Mode I interlaminar fracture (G_{IC}). For unidirectional continuous fiber-reinforced composite materials with a polymer matrix, the ASTM D5528 (2013) is employed.

As described before, the specimens have a delamination initiator. The initial crack needs to be propagated in order to capture the energy released during the crack growth. Opening forces are applied at the hinges bonded to one end of the specimen with controlled opening displacement (fig. 22); the load and delamination length are recorded. An INSTRON universal testing machine was employed with an adaptation at the grips to allow fastening the specimen with bolts and a camera with a magnifier lens was positioned at the front of the experiment to record the crack growth. A force-displacement plot is expected where the maximum load before degradation is taken to calculate the critical SERR; linear-elastic behavior is assumed in this

test method and this is valid while the zone of damage at the delamination front is small relative to the thickness of the specimen.

Figure 22 - DCB test.

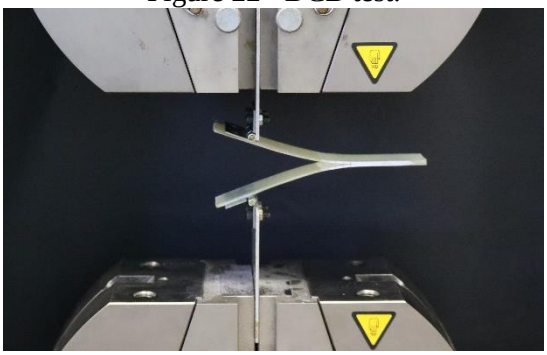

Once the DCB specimens are correctly manufactured and with the dimensions according to tab. 4, the following procedure can be carried out:

(1) The average values of width and thickness are calculated for all the specimens. For this test, at least five specimens need to be tested.

(2) Just ahead of the delamination tip, a coat of white paint is applied to improve the visual detection. The first 5 mm from the insert front are marked with a vertical line at each 1 mm and the forward 20 mm are marked at each 5 mm (Fig. 23).

Figure 23 – Marks.

(3) Measure the initial delamination length (a_o), which is the distance from the loading line (end of the hinge) to the crack tip (Fig. 24).

Figure 24 - Geometry of DCB specimens.

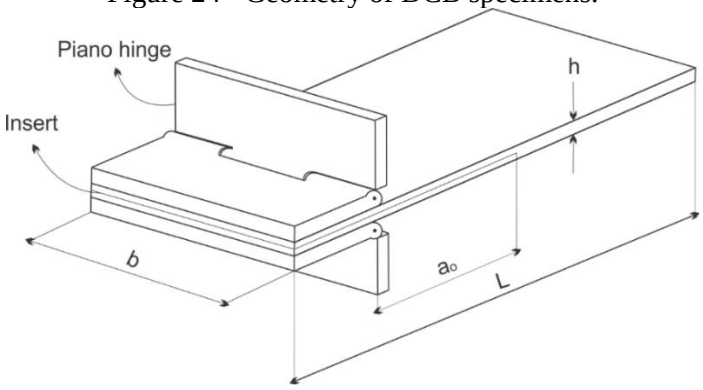

Where,

L = Length of the specimen;

b = Width of the specimen;

h = Thickness of the specimen; and

a_o = Initial delamination length.

(4) Attach the specimen to the grips of the INSTRON and make sure that is perfectly aligned and centered.

(5) Set the camera pointing to the crack tip in order to record the growth while the specimen is loaded. Make sure that the image is magnified enough to observe the crack reaching the vertical lines (fig. 25).

Figure 25 - Magnified image.

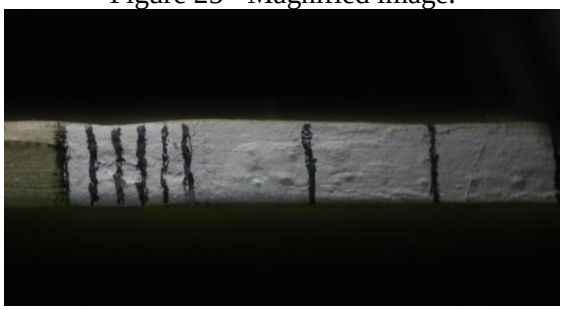

(6) Now the load is applied with a constant controlled displacement rate of 1 mm/min. Since the delamination onset is not of our interest, we are not going to discuss the different suggestions for the visual onset of delamination and we are just going to mark the onset at the load-displacement data at the first advance of the crack observed with the magnifier. Our first point of interest is the maximum load at the exact moment before the degradation starts, and for each point marked as explained in step (2).

(7) After the delamination has reached the last mark, unload the specimen.

Once this procedure is completed, a load-displacement data is obtained for each of the five specimens tested. At each load-displacement data, the maximum load and the load at each mark are identified, and, their respective displacements as well.

To calculate the critical Mode I SERR (G_1), three different methods are available: the modified beam theory (MBT), compliance calibration method (CC) and the modified compliance calibration method (MCC). For our case study, the MBT was employed since is the more conservative method and the most employed as is evident in the literature. The beam theory expression to calculate the strain energy released rate of a double cantilever beam test is as follows:

$$G_{1C} = \frac{3P\delta}{2b\left(a + |\Delta|\right)} \tag{3.28}$$

Where,

P = load;

δ = load point displacement;

b = specimen width;

a = delamination length; and

Δ = rotation factor.

At the delamination front, a rotation may occur. To take into account this rotation, a rotation factor (Δ) is considered, which represent an increment of the delamination length ($a + \Delta$). To calculate this rotation factor, we need to generate a least square plot of the cube root of compliance, $C^{1/3}$, as a function of the delamination length (a) using the values of each propagation point (Fig. 26).

Figure 26 - Effective delamination extension to correct for rotation.

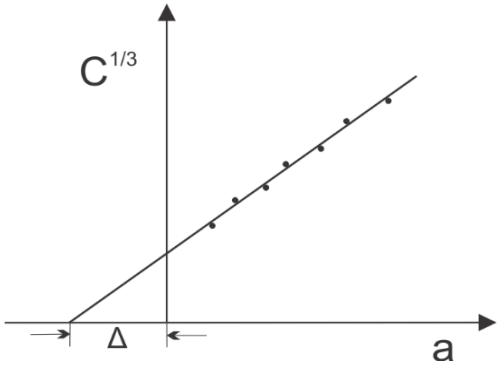

Source – Figure referenced from ASTM D5528-13(D5528-13, 2013)

The test method ends with a statistical analysis of the Mode I SERR values calculated for each specimen. The average value, standard deviation and coefficient of variation are calculated using the following equations:

$$\bar{x} = \frac{\left(\sum_{i=1}^{n} x_i\right)}{n} \tag{3.29}$$

$$S_{n-1} = \sqrt{\frac{\sum_{i=1}^{n} x_i^2 - n\bar{x}^2}{(n-1)}} \tag{3.30}$$

$$CV = \frac{100 \times S_{n-1}}{x} \tag{3.31}$$

Where,

$\bar{x}$ = Average value;

S_{n-1} = Standard deviation;

CV = Coefficient of variation;

n = Number of specimens; and

x_i = SERR values.

The standard deviation is a measure that is used to quantify the amount of variation or dispersion between the results obtained. If the data tends to be close to the mean, the standard deviation should be low. The coefficient of variation measures how much a calculated value differs from the data average. This value is expressed as a percentage.

3.2.2.2. End Notched Flexure Test

This test method is performed to obtain the strain energy released rate for mode II interlaminar fracture (G_{IIC}). The ASTM D7905 (2014) is employed to perform an ENF test using unidirectional continuous fiber-reinforced polymer matrix composites.

The specimen, containing a non-adhesive insert that serves as delamination initiator, is submitted to in-plane shear forces with controlled displacement, so the crack will propagates under sliding fracture mode. This type of loading is induced by performing a 3-points bending

employing an INSTRON universal testing machine with an adaptation of the crossheads to perform bending tests (fig. 27).

Figure 27 - ENF test.

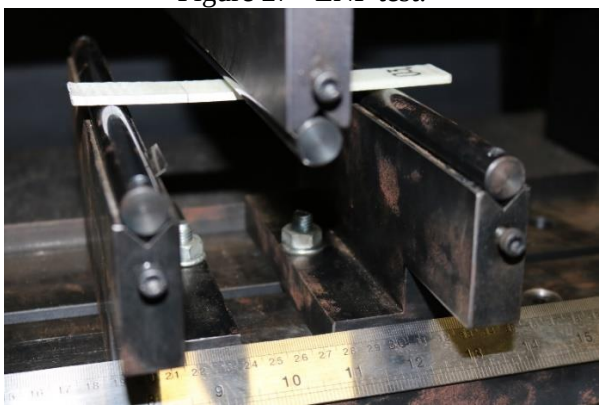

The delamination for this case has non-stable growth, thus, a special procedure is presented in this standard. The compliance calibration (CC) method is the only acceptable method to measure G_{IIC} for ENF interlaminar fracture test.

Due to the abrupt jump of delamination, while propagating, a visual recording is not necessary since the load-displacement data will give us the elementary values to calculate the parameters.

Once the specimens are manufactured and accurate dimensions are accomplished, the following procedure can be performed using at least five specimens:

(1) Calculate the average value of width and thickness of each specimen.

(2) The compliance calibration (CC) method demands to load the specimens using three different initial crack lengths. A coat of white paint is applied to improve the visual detection, mark the crack tip and the compliance calibration markings as sketched in fig. 28. The distances of the calibration markings are 20, 30 and 40 mm from the insert tip.

Figure 28 - Geometry of ENF specimen.

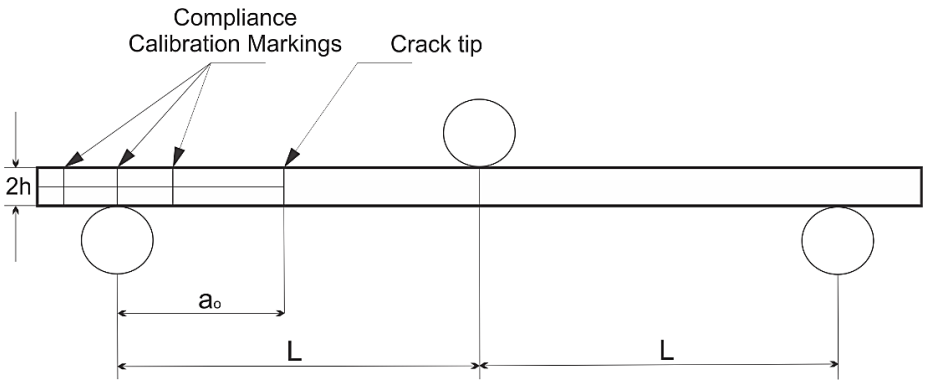

Where,

L = Specimen half-span;

h = Specimen half-thickness; and

a_o = Initial delamination length.

(3) Place the specimen over the supports as illustrated in fig. 28. The standard recommends a fixture geometry with a nominal specimen span length ($2L$) of 100 mm and a nominal half-span length (L) of 50 mm. Three loading procedures are performed to each specimen due to the three different initial delamination lengths considered. Thus, the specimen is firstly placed so that the initial delamination length corresponds to a_o=20 mm, then is re-positioned so a_o=40 mm and finally a_o=30 mm.

(4) Calculate the peak forces (P_j), which correspond to 50% of the expected critical force (P_c), for the CC tests with a_o=20 mm and a_o=40 mm using eq. 3.33. Load the specimen to the calculated peak force for each case, with a load rate of 0.5 mm/min and subsequently unload it. For the CC test with a_o=30 mm, load the specimen until delamination failure happens using the same loading rate.

$$P_C = \frac{4B}{3a_0}\sqrt{G_{IIC} E_{1f} h^3} \tag{3.32}$$

$$P_j = \frac{2B}{3a_0}\sqrt{G_{IIC} E_{1f} h^3} \tag{3.33}$$

Where,

B = Specimen width;

G_{IIC} = Initial estimated SERR value for Mode II; and

E_{1f} = Flexural Modulus;

The G_{IIC} value is a supposed value obtained from the literature or from previous tests of similar composite materials. The flexural modulus can be calculated from eq. 3.34; for the first test, this value can be assumed as being equal to the normal longitudinal modulus E_{11}.

$$E_{1f} = \frac{L^3}{4ABh^3} \tag{3.34}$$

Where,

A = CC coefficient.

The computing of the CC coefficient, *A*, is explained in further sections.

(5) In order to calculate the CC coefficients, the compliance versus crack length cubed curve needs to be plotted. Three compliances are obtained, which correspond to each of the loadings regarding the initial delamination length: two CC tests (a_o= 20 mm and a_o=40 mm) and from the full fracture test (a_o=30 mm). The compliance is obtained by performing a linear least squares regression analysis to calculate the slope of the displacement-force curve. Finally, the CC coefficients, *A* and *m*, correspond to the intercept and slope, respectively, from the regression analysis of the compliance versus crack length cubed curve (Eq. 3.35).

$$C = A + ma^3 \tag{3.35}$$

(6) The G_{IIC} values are to be obtained from the maximum force (P_{max}). The following equation is employed:

$$G_{IIC} = \frac{3mP_{\max}a_0^2}{2B} \tag{3.36}$$

Where,

m = CC coefficient; and

P_{max} = Maximum force from the force-displacement data.

We can generalize this equation in order to calculate the G_{II} value at any crack length (a):

$$G_{II} = \frac{3mPa^2}{2B}$$

Where,

P = Force at a specific crack length; and

a = Crack length.

(7) The test method finalizes with a statistical analysis as described in section 3.3.2.1.

3.2.2.3. Mixed-Mode Bending Test

Delamination within structural parts propagates under a combination of loadings. The mixed-mode test describes the determination of SERR of interlaminar fracture (G_c) at various Mode I and Mode II loading ratios. For continuous fiber-reinforced plastic composite material, the ASTM D6671 (2013) standard is employed.

The specimen is identical to the one used for DCB test described in section 3.3.2.1. To submit the specimen to both fracture modes, a Mixed-Mode Bending (MMB) apparatus, assembled to a universal testing machine INSTRON, is employed. This apparatus performs a 3-points bending at the same time that the edge of the specimen, with the delamination insert, is being separated apart by opening forces applied through piano hinges bonded on the surfaces (Fig. 29).

Figure 29 - Mixed-Mode Bending (MMB) test.

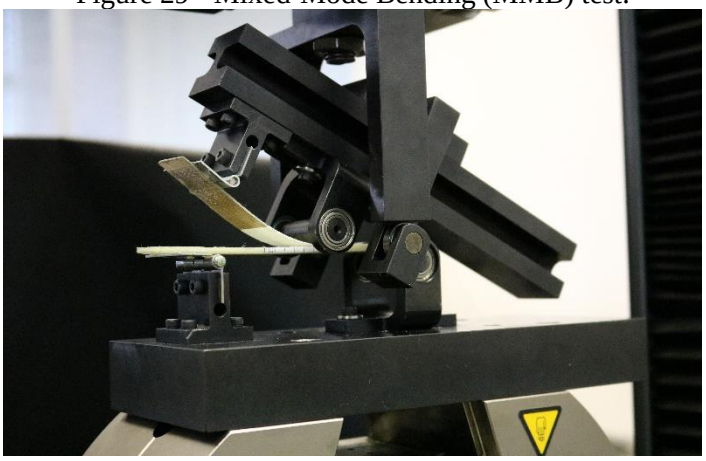

This method has a particularity; the ratios between Mode I and Mode II could be several. These ratios are defined by the percentage of Mode II SERR (G_{II}) in the total critical SERR (G_c), thus, different mode mixtures $\left(G_{II}/G_C\right)$ need to be established. For our case study, three mode mixtures were selected corresponding to 20, 50 and 80 %. These rates are achieved by modifying the lever position and therefore the loading distance, so the influence of mode I respect to mode II may vary.

For an MMB test, the recording of crack growth is required in order to calculate parameters to describe the delamination propagation. Since both fracture modes are present, some cases will have a stable behavior and other will present abrupt crack jumps with unstable behavior.

The following procedure was performed employing five correctly manufactured specimens per each of the three cases:

(1) Calculate the average dimension of the width and thickness of each specimen.

(2) Both edges of the specimen were painted with a white coat to improve the visual detection of a crack growth.

(3) The insert tip was marked with a vertical line. In addition, every 1 mm for the first 5 mm past the end of the insert tip was marked with a vertical line and every 5 mm further up to 25 mm were marked too.

(4) The length of the lever (c) is estimated in order to produce the desire mode mixture (G_{II}/G_c) by using the following equations:

$$c = \frac{12\beta^2 + 3\alpha + 8\beta\sqrt{3\alpha}}{36\beta^2 - 3\alpha} L \tag{3.37}$$

$$\alpha = \frac{1 - \frac{G_{II}}{G}}{\frac{G_{II}}{G}} \tag{3.38}$$

$$\beta = \frac{\alpha + \chi h}{a + 0.42\chi h} \tag{3.39}$$

$$\chi \equiv \sqrt{\frac{E_{11}}{11G_{13}}\left\{3 - 2\left(\frac{\Gamma}{1+\Gamma}\right)^2\right\}} \tag{3.40}$$

$$\Gamma \equiv 1.18\frac{\sqrt{E_{11}E_{22}}}{G_{13}} \tag{3.41}$$

Where,

c = Lever length of the MMB test apparatus;

β = Non-dimensional crack length correction for mode mixture;

α = Mode mixture transformation parameter for setting lever length;

χ = Crack length correction parameter; and

Γ = Transverse modulus correction parameter.

(5) Now, a calibration test must be performed. The MMB apparatus is used for loading a calibration specimen made of a homogenous material and with a shape of a rectangular bar. The compliance and the slope of the force-displacement curve obtained is calculated. For our

case study, a steel bar was employed and the following equations were used to calibrate the system:

$$C_{cal} = \frac{2L(c+L)^2}{E_{cal} b_{cal} t^3} \quad 3.42$$

$$C_{sys} = \frac{1}{m_{cal}} - C_{cal} \quad 3.43$$

Where,

C_{cal} = Compliance of the calibration specimen;

b_{cal} = Width of the calibration specimen;

E_{cal} = Elastic modulus of the calibration bar;

t = Thickness of the calibration specimen;

m_{cal} = Slope of the force-displacement curve of the calibration specimen; and

C_{sys} = Calibration of the system.

This calibration procedure must be performed for each set of lever length to be used.

(6) Once the calibration is done, the MMB specimens can be tested. Attach the piano hinges to the machine grips with bolts and place the specimen over the MMB apparatus supports. A half-span length of 50 mm is recommended by the standard. The final fixture is illustrated in fig. 30:

Figure 30 - MMB specimen and fixture.

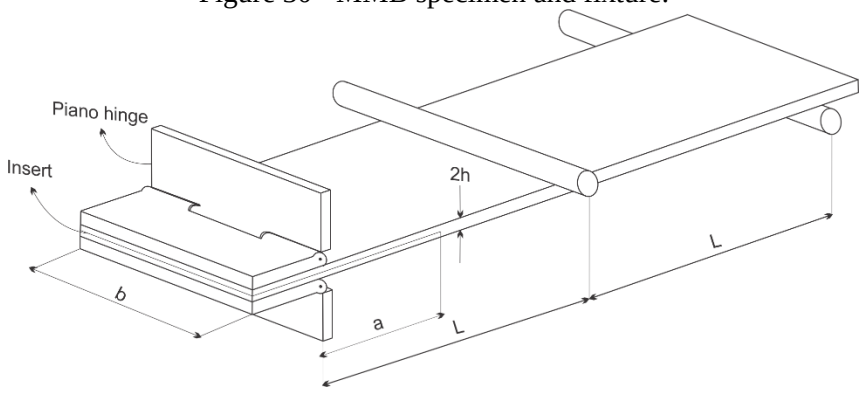

(7) A camera equipped with a magnifier lens is placed pointing to the insert tip in order to record the crack advance while loading the specimen and do the required annotations.

(8) Load the specimen at a constant displacement rate of 0.5 mm/min and record the force-displacement response. The first crack advance is market as the visual observation of delamination onset. While the crack reaches the marks describe in step (3), we should write down the corresponding force and displacement for each point of interest.

(9) When the crack has extended far enough, the specimen is unloaded and we proceed to the calculations.

(10) Before determining the SERR values, a bending modulus (E_{1f}) is required, which is a weak function of E_{11}, E_{22}, and G_{13}. Use the following equation:

$$E_{1f} = \frac{8(a_0 + \chi h)^3 (3c - L)^2 + \left[6(a_0 + 0.42\chi h)^3 + 4L^3\right](c + L)^2}{16L^2 bh^3 \left(\frac{1}{m} - C_{sys}\right)} \quad 3.44$$

Where,

E_{1f} = Bending modulus;

a_0 = Initial delamination length; and

m = Slope of the force-displacement curve.

(11) Finally, we can calculate the critical SERR for MMB fracture, the corresponding Mode I and Mode II value and the mode mixture rate:

$$G_C = G_{IC} + G_{IIC} \quad 3.45$$

$$G_{IC} = \frac{12P_{\max}^2 (3c - L)^2}{16b^2 h^3 L^2 E_{1f}} (a_0 + \chi h)^2 \quad 3.46$$

$$G_{IIC} = \frac{9P_{\max}^2 (3c + L)^2}{16b^2 h^3 L^2 E_{1f}} (a_0 + 0.42\chi h)^2 \quad 3.47$$

$$\frac{G_{II}}{G} = \frac{G_{II}}{G_I + G_{II}} \quad 3.48$$

Where,

P_{max} = Maximum load of the load-displacement curve.

And their respective general equations to calculate the SERR values at every propagation point market on the specimen.

$$G_C = G_I + G_{II}$$

$$G_I = \frac{12P^2(3c-L)^2}{16b^2h^3L^2E_{1f}}(a+\chi h)^2$$

$$G_{II} = \frac{9P^2(3c+L)^2}{16b^2h^3L^2E_{1f}}(a+0.42\chi h)^2$$

(12) The test method finalizes with a statistical analysis as described in section 3.3.2.1.

3.2.3. Nominal Stresses and Traction-Separation Law

Once the energy released by the crack growing is calculated at each desired distance, we need to determine the stress that triggers the release of energy at each delamination distance. These stresses are known as the *Nominal Stresses* and represent the maximum stress supported by the material before a significant degradation.

All the nominal stresses are then represented by a mathematical function that must respect the degradation behavior observed during experimental tests. This function is better known, within Fracture Mechanics, as a Traction-Separation law, which is used in Cohesive Zone modeling to rule whenever an element should totally fail or not.

Within this section, the procedure of calculating the nominal stresses is reviewed and explained. The formulation of the Traction-Separation law for delamination within glass/epoxy composite laminates is explained as well.

3.2.3.1. Nominal Stresses

One of the most famous developments in material science is the Energy-Balance approach introduced by Griffith (1921). He was an aeronautical engineer that studied fracture within brittle materials (most glasses), prior to 1920. He modified the Inglis solution (Inglis, 1913) to develop a fundamental approach for predicting fracture strengths, since the original Inglis' work has a mathematical difficulty by approaching the stress, at a crack tip, to infinity.

Griffith's approach begins with the definition of the strain energy per unit volume of a stressed material:

$$U^* = \frac{1}{V}\int f\,dx = \int \frac{f}{A}\frac{dx}{L} = \int \sigma d\varepsilon \qquad 3.49$$

Where,

U^* = Strain energy per unit volume;

V = Volume;

f = Force; and

A = Area.

If we assume the material as linear elastic, we know that $\sigma = E\varepsilon$, thus:

$$U^* = \frac{E\varepsilon^2}{2} = \frac{\sigma^2}{2E} \qquad 3.50$$

Where,

E = Elastic modulus;

ε = Strain; and

σ = Stress.

Griffith observed that when a crack grows, it generates two surfaces that are no longer supporting loads. In order to create these surfaces, strain energy must be released.

He explained, using an illustration, how this energy is calculated (Fig. 31). Regard two triangular regions, above and below the crack plane, of width a and height βa, totally unloaded. For a plane stress loading, $\beta=\pi$, the total strain energy U released is the energy per unit volume times the volume (unit thickness) of the two triangular regions:

$$U = -\frac{\sigma^2}{2E}\pi a^2 \qquad 3.51$$

Figure 31 - Triangular unloaded region.

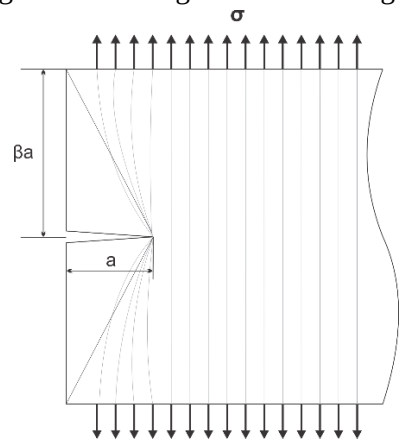

The negative sign is conventional since this energy is being ‘liberated’. Another energy involved in the process of crack propagation is the energy required to break the bonds to separate the surfaces, *S*, which is associated with a crack length. This bond energy is ‘absorbed’ by the material to complete the process; therefore, the sign is positive:

$$S = 2\gamma a \qquad 3.52$$

Where,

S = Surface energy with unit depth; and

γ = Surface energy.

Thus, the total energy involved in the process of crack growing is the sum of the energy required to create new surfaces (positive) plus the strain energy released by allowing the regions above and below the crack to become unloaded (negative). Fig. 32 shows the final fracture energy balance:

Figure 32 - Fracture energy balance.

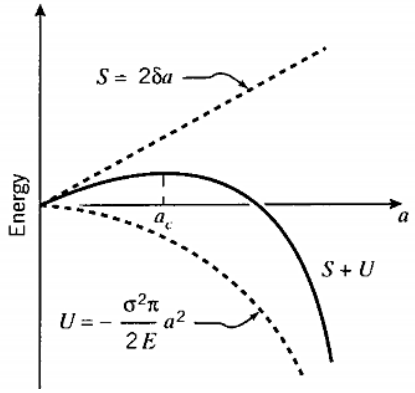

Source – Roylance D, (2001)

The quadratic dependence of the strain energy eventually dominates the function behavior. Note that there is a critical crack length from where the energy starts to decrease by letting the crack to grow longer and increasing the stress, thus, this critical crack length will give us the value of stress level at which the bonds are separated and allows to create complete unloaded surfaces. It is possible to find this critical crack length by calculating the limit of the function representing the fracture energy balance:

$$\frac{\partial(S+U)}{\partial a} = 2\gamma - \frac{\sigma_f^2}{E}\pi a = 0 \qquad 3.53$$

Then, isolating the critical stress σ_f:

$$\sigma_f = \sqrt{\frac{2E\gamma}{\pi a}} \qquad 3.54$$

This approach was developed for very brittle materials. When treating more ductile materials, as is the case of polymer composites, a correction is needed since considering a unique surface energy fail when estimating an accurate stress value.

Irwin (1958) and Orowan (1949), independently suggested that the strain energy released in ductile materials does not just correspond to the creation of new surfaces but by energy dissipation due to plastic flow in the material near to the crack tip, as well. As we mentioned in previous sections, this energy dissipated is known as the critical strain energy released rate (G_C) and introducing it in eq. 3.54, will give us the nominal stress of the fracture process:

$$\sigma_C = \sqrt{\frac{EG_C}{\pi a}} \qquad 3.55$$

Where,

σ_C = Nominal Stress.

3.2.3.2. Traction-Separation Law

The damage behavior of the cohesive zone can be completely represented by a Traction-Separation Law (TSL). Commonly, this law is governed by a function that describes the dependence of a traction T on a separation distance δ, as a function $T(\delta)$. By this, there are some statement to consider:

— There is a parameter that represents the maximum traction sustainable by an element. It is represented as T_C.

— There exist a maximum opening at which elements totally fail. It is represented as δ_0.

— The area under the TSL curve must be equal to the critical SERR at each mode. This demonstrated and explained further.

The shape of a TSL is governed by elementary functions that can be classified as Multi-linear, Polynomial, Trigonometric or Exponential (Fig. 33). All these functions must follow a qualitative process that is in agreement with the fracture rupture process; thus, it begins with a traction increasing until a maximum value where degradation is triggered, then the stress approach to zero while the separation is in progressive increase.

Figure 33 - Shapes of Traction-Separation Laws.

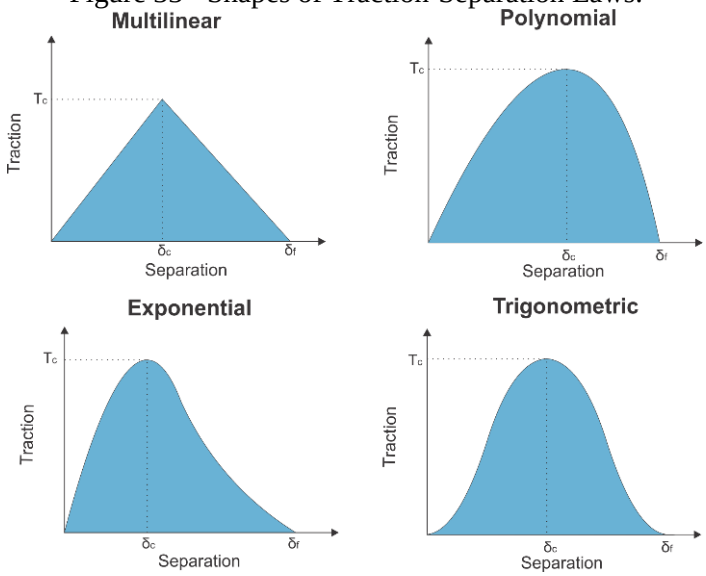

The specific shape of the TSL must be selected carefully by considering the type of material being studied. The linear-elastic response of the materials can be perfectly represented by a linear function, but the real challenge is to find a function that represents the progressive

degradation from the initial failure until the total collapse. This is commonly known as the "softening function" and the shape varies whether the material is brittle or ductile. A brittle failure supposes a quick degeneration of the stiffness with big crack jumps; while a crack within a ductile material has a progressive growth with the presence of some plasticity episodes at the crack tip that results in a progressive loss of the stiffness.

The three phases that constitute a conventional composite material have different plastic deformation, with the fibers been brittle inside a ductile matrix. It is widely accepted that polymeric based composites have a ductile behavior in the presence of plastic yielding. Specifically, when speaking about fracture, it is usually observed that the crack grows within the matrix with a progressive advance and the local crack tip fields affected by the fiber orientation. This behavior often requires a non-linear function of the TSL in order to well represent the degradation. Several studies have been performed, comparing different shapes for laminated composites (Yang & Cox, 2005), bonded joints (Sorensen, 2002) (R. Campilho, Banea, Neto, & da Silva, 2013), metallic foams (C. Chen, Fleck, & Lu, 2001), impacted cross-ply laminated composites (Aymerich, Dore, & Priolo, 2008), repaired FRPC (R. D. Campilho et al., 2008), etc.

Finally, after reviewing a few TSL shape comparisons for composite materials in the literature (Elices, Guinea, Gómez, & Planas, 2002; Scheider & Brocks, 2003), and after testing different functions, a cubic polynomial function (Fig. 34) was selected to represent our case study.

Figure 34 - Cubic Polynomial Function.

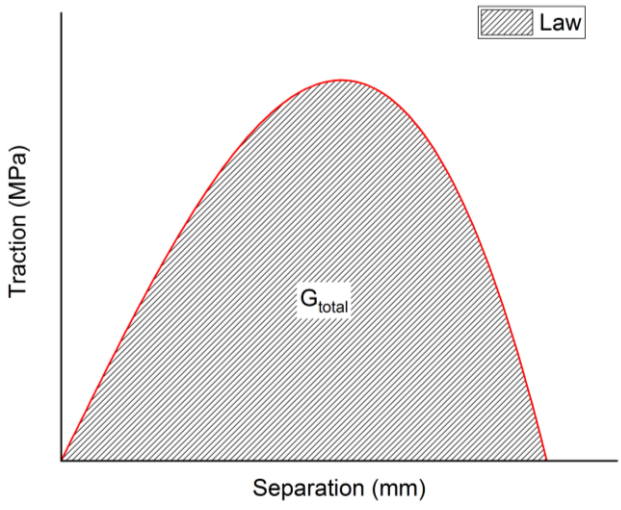

The general equations will be now described to completely formulate a cubic polynomial TSL and represent the interlaminar fracture failure of laminated composite materials. The function to generate a cubic polynomial shape is as follows:

$$T(\delta) = \varphi T_C \frac{\delta}{\delta_0}\left[1 - \left(\frac{\delta}{\delta_0}\right)^2\right] \tag{3.56}$$

Where,

$T(\delta)$ = Any traction or nominal stress at the curve depending on a separation δ;

φ = Adjustment coefficient;

T_C = Critical nominal stress;

δ = Separation; and

δ_0 = Ultimate separation.

As mentioned before, regardless of its shape, the area under the curve of Traction-Separation must be equal to the corresponding critical SERR; this characteristic is earned from Griffith's Theory. This leads us to find a value for δ_0 by satisfying the following condition:

$$\int_0^{\delta_0} T(\delta) d\delta = G_C \tag{3.57}$$

Thus,

$$\delta_0 = \frac{4G_C}{\varphi T_C} \tag{3.58}$$

The critical value of the separation, where the maximum nominal stress is located, can be found by setting the derivative of the function to zero:

$$\frac{dT(\delta)}{d\delta} = 0 \tag{3.59}$$

Thus,

$$\delta_C = \frac{\delta_0}{\sqrt{3}} \tag{3.60}$$

If we consider $T = T_C$, then $\delta = \delta_C$. Solving for eq. 3.56 will gives us a value for φ:

$$\varphi \approx 2.6 = \frac{13}{5} \tag{3.61}$$

Having calculated values of SERR and nominal stresses for any interlaminar fracture case within laminated composite materials and employing those general equations, a cohesive law can be established to predict delamination phenomenon. This procedure can be calibrated for different types of laminated composite materials with polymeric matrix and fiber reinforcement. Further sections employ the procedures detailed in this chapter to completely characterize the fracture behavior of glass/epoxy composites.

CHAPTER IV

4. Experimental Results

This chapter presents the results obtained from experimental tests and the formulation of a traction-separation law for interlaminar fracture. The procedures detailed in the previous chapter are carried out and all the calculation are shown here.

Different aspects and behaviors were observed during the tests and are discussed at each corresponding section. All the Fracture Mechanics parameters considered, like the strain energy released rates or the fracture strengths, are calculated and validated.

4.1. DCB Results

After following the procedures described in section 3.3.2.1, the DCB test was carried out successfully. The main challenge appeared during the manufacturing process when bonding the piano hinges to the specimens. A procedure for preparation of the surfaces for adhesive bonding was necessary, thus, the ASTM D2651 (2016) and ASTM D2093 (2017) were employed respectively for each material type. Despite this surface preparation, some adhesive bonds still failed during loading; but finally, we get four specimens successfully tested.

The Load-Displacement plot is shown in fig. 35 and tab. 5 resumes the values of the parameters used to calculate the Mode I SERR considering eq. 3.28 and shows the critical SERR calculated values for our case study:

Table 5 - DCB critical SERR results.

Specimen	Max. Load (N) P	Load Displacement (mm) δ	Width (mm) b	Delamination Length (mm) a	Rotation Correction (mm) Δ	Critical SERR (kJ/m^2) G_{IC}
01	41.0754	16.4543	24.9	50.35	1.2205	0.7895
02	39.0122	16.0983	24.8	49.93	0.8364	0.7482
03	38.7789	15.9163	25	49.55	0.859	0.7347
04	42.2532	16.5874	24.9	50.25	1.3833	0.8177

Figure 35 - Force-Displacement curve from DCB tests.

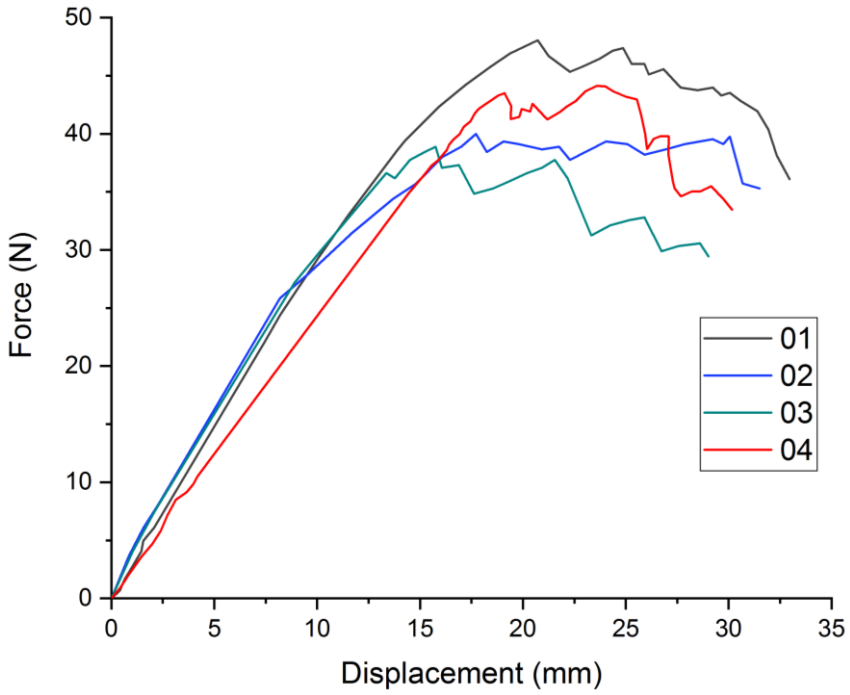

This outcomes in a mean average value for G_{IC} of 0.7725 kJ/m^2, which is accepted as a reasonably accurate value for a glass/epoxy laminated composite since is close to results found in the literature (Do not misunderstand this value with epoxy based adhesives). The result calculated has a good correlation with the work performed by Marat-Mendes and Freitas (2010), which used the virtual crack closure technique (VCCT) to calculate interlaminar fracture parameters of glass/epoxy composite with similar characteristics of our case study. The G_{IC} value estimated by them was 0.818 kJ/m^2 which comparison with our experimental result gives us a difference of 5.56%.

A statistical analysis was performed as well using eq. 3.30 and 3.31. The value of the CV shown is the average of all the specimens. It is shown in tab. 6:

Table 6 - DCB statistical analysis.

	Average Mean G_{IC} (kJ/m^2) $\bar{x}$	**Standard Deviation S_r**	**Coefficient of Variation % CV**
Mode I	0.7725	0.0381	4.93

Propagation values for SERRs were also calculated for a crack growth of 1, 2, 3, 4, 5, 10, 15 and 20 mm which is taken as an increase of delamination length and introduced in eq. 3.28 as

the value for *a*. The visual onset of delamination (VIS) is also registered and considered; tab. 7 shows all these values. It is important to mention that the critical value (CRI) was observed to lie between crack growths of 4 and 5 mm; this means that when a crack length of 5 mm is reached, the material degradation is triggered.

Table 7 - SERR at each propagation point.

Specimen	**Strain Energy Released Rates (kJ/m²)**								
	VIS	1	2	3	4	5	10	15	20
1	0,6015	0,6381	0,6777	0,7351	0,7569	0,7922	0,7995	0,8208	0,8421
2	0,5887	0,6206	0,6635	0,7054	0,7332	0,7634	0,7815	0,8056	0,8297
3	0,5709	0,6126	0,6693	0,7026	0,7569	0,7528	0,7677	0,7846	0,8175
4	0,6093	0,6550	0,6957	0,7423	0,7789	0,8212	0,8305	0,8367	0,8569
Average	0,5926	0,6315	0,6765	0,7221	0,7468	0,7824	0,7948	0,8119	0,8365

Mathematically, the values for SERR are directly proportional to the opening displacement and indirectly proportional to the crack length. The increment in opening displacement is relatively larger than the crack growth length, thus, the SERR value increases as the delamination propagates. Physically, we can interpret this increase as a more energy required to create new fracture surfaces as the delamination propagates. Fig. 36 illustrates the increment of G_I while the crack propagates:

Figure 36 - G_I vs *a*.

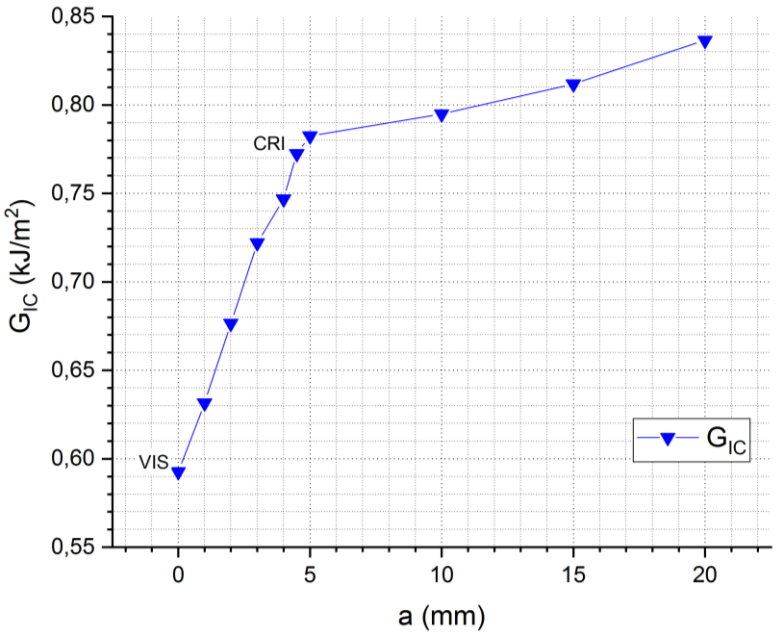

Moving forward with calculations, now it is possible to compute values of the nominal stresses (tab.8) by following the eq. 3.55. The value taken for E was the laminate property E_{33} since the crack is not penetrating the fibers but the matrix and the load is supported in this direction.

Table 8 - Mode I nominal stresses.

	σ_c	VIS	1	2	3	4	5	10	15	20
Mode I (MPa)	8.23	7.21	7.37	7.55	7.73	7.79	7.90	7.62	7.40	7.24

For critical fracture strength, a value of 8.23 MPa was obtained and compared with literature results observing a good correlation (Coelho, 2016).

With the SERRs and the nominal stresses calculated, we are able to formulate the TSL for Mode I interlaminar fracture following the procedure described in section 3.3.3.2. Tab. 9 shows the significant factors that compose this law and fig. 37 illustrate the shape of the TSL:

Table 9 - Mode I TSL parameters.

	Adjustment Coefficient φ	Ultimate Separation (mm) δ_0	Critical Separation (mm) δ_c	Critical Stress (MPa) σ_c	Area (kJ/m^2) G_{IC}
Mode I TSL	13/5	0.1444	0.0834	8.23	0.7725

Figure 37 - Mode I TSL.

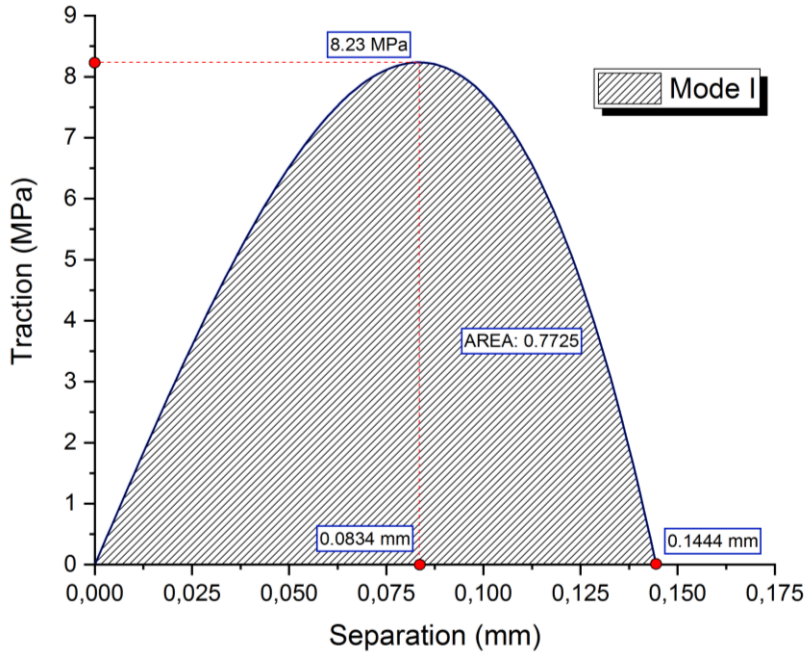

This TSL completely characterizes the Mode I fracture interlaminar behavior of glass/epoxy laminated composite materials.

4.2. ENF Results

The Mode II interlaminar fracture was determined by following procedures of section 3.3.2.2. During the tests, most of the specimens suffered intralaminar failure by matrix smashing. Finally, three specimens had an expected behavior and were considered for calculations. Fig. 38 shows the Load-Displacement data of the three specimens and the average. Tab. 10 shows the final value obtain.

Figure 38 - Force-Displacement curve from ENF tests.

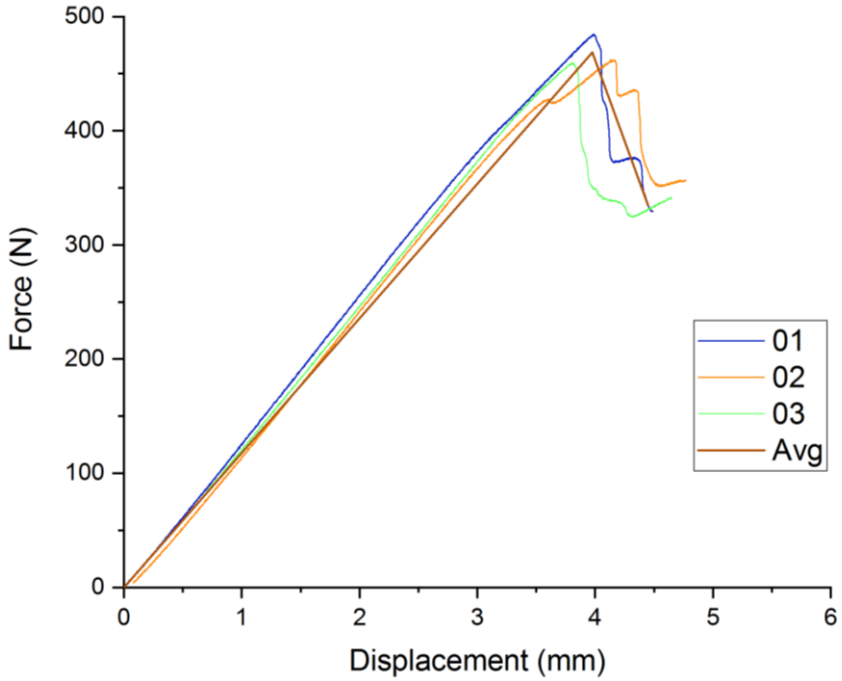

Table 10 - Mode II SERR.

Specimen	CC Slope m	Max. Load (N) P_{max}	Delamination Length (mm) a	Width (mm) B	Critical SERR (kJ/m²) G_{IIC}
01	6.40E^{-8}	484.71	30	25.2	0.8051
02	7.29E^{-8}	462.38	30	24.7	0.8518
03	7.60E^{-8}	459.62	30	24.9	0.8711

Thus, the average value calculated for G_{IIC} is 0.8427 kJ/m^2, which is an acceptable value since it has good correlation with literature results like the parameter calculated by Marat-Mendes and Freitas (2010) with the employment of VCCT that has a G_{IIC} value of 0.861 kJ//m^2; resulting in a difference of just 2.14% (Do not misunderstand this value with epoxy based adhesives).

The statistical analysis is shown in tab. 11:

Table 11 - ENF statistical analysis.

	Average Mean G_{IC} (kJ/m^2) $\bar{x}$	**Standard Deviation S_r**	**Coefficient of Variation % CV**
Mode II	0.8427	0.0339	4.02

During the ENF tests, it was observed that the crack growth behavior for this fracture mode has abrupt jumps; the first jump of the crack was about 20 mm and this happens since the plastic flow after crack propagation reaches a big area at the crack front. For this reason, detailed propagation values were not considered and only values for critical SERR and at 20 mm delamination length, were calculated. When the crack reaches this length, the material degradation is significant and catastrophic, for this reason, the test was considered as ended. Tab. 12 shows the SERRs calculated:

Table 12 - SERR for Mode II propagation.

Specimen	**Strain Energy Released Rates (kJ/m^2)**	
	Critical	**20 mm delamination**
01	0.8051	1.0414
02	0.8518	1.3473
03	0.8711	1.2143
Average	0.8427	1.2010

As expected, the SERR value for the delamination increment was higher than the critical value due to the large surfaces created during crack growth and due to the plastic flow.

Using eq. 3.55, the nominal stresses for Mode II fracture were estimated (Tab. 13). The value taken for E was the laminate property E_{33} since the crack is not penetrating the fibers but the matrix and the load is supported in this direction.

Table 13 - Nominal stresses for Mode II fracture.

	σ_c	20 mm
Mode II (MPa)	18.06	16.68

The critical value of fracture strength for Mode II calculated has good correlation with other results found in the literature (Coelho, 2016). Having calculated the SERR and nominal stresses, we proceed to formulate the TSL by employing the equations included in section 3.3.3.2. Tab. 14 shows the parameters calculated and fig. 39 illustrates the shape of the cohesive law:

Table 14 - Mode II TSL.

	Adjustment Coefficient φ	**Ultimate Separation (mm)** δ_0	**Critical Separation (mm)** δ_c	**Critical Stress (MPa)** σ_c	**Area (kJ/m²)** G_{IC}
Mode II TSL	13/5	0.0719	0.0415	18.06	0.8426

Figure 39 – Mode II TSL.

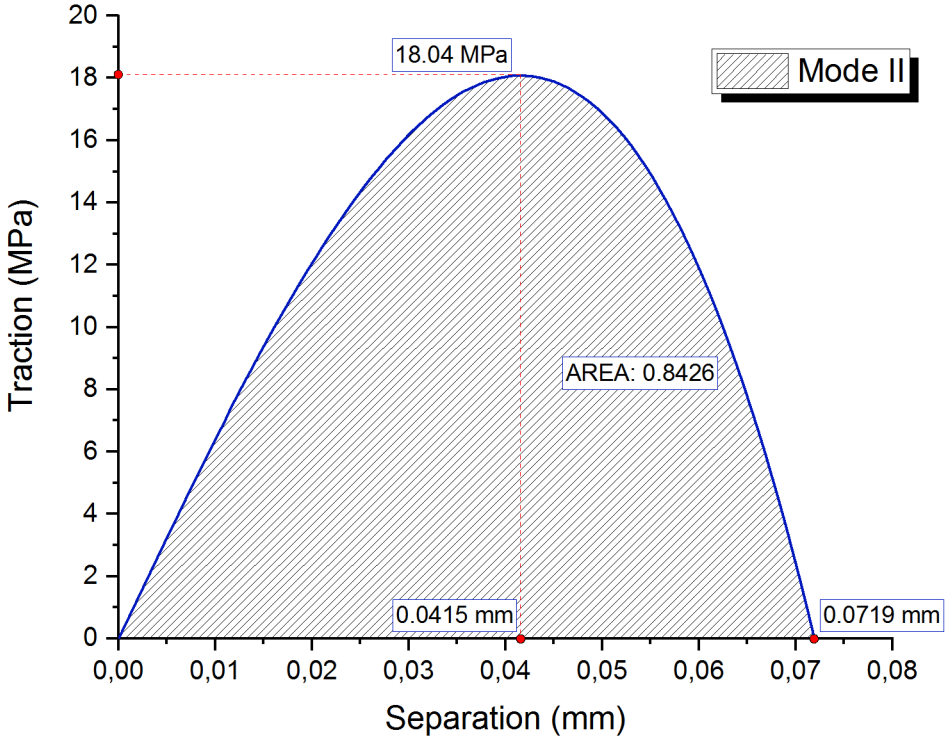

With this law, the behavior of Mode II interlaminar fracture is completely represented and can be used to predict progressive damage in glass/epoxy laminated composite materials.

4.3. MMB Results

Mixed-Mode test consists of three different cases regarding different mode mixture (G_{II}/G_C) as described in section 3.3.2.3. The lever length was calculated and adjusted for each case following eq. 3.37 – 3.41; lengths employed are shown in tab. 15. The mode mixture ratio considered were 20, 50 and 80% of Mode II; the peculiarities founded are described at each respective section, as well as all the parameter required to calculate the critical SERR, TSL and nominal stresses.

Table 15 - Lever lengths for MMB tests.

	$G_{II}/G_C = 20\%$	$G_{II}/G_C = 50\%$	$G_{II}/G_C = 80\%$
Transverse Modulus Correction Parameter (Γ)	2.76	2.76	2.76
Crack Length Correction Parameter (χ)	0.79	0.79	0.79
Correction for Mode Mixture (β)	1.032	1.033	1.030
Mode Mixture Transformation Parameter (α)	4	1	0.25
Lever Length (c) mm	100.93	42.59	27.49

4.3.1. $G_{II}/G_C = 20$ %

The test using this mode mixture was the one that presented more instability during loading. The propagation of the crack was slow and the opening displacement was high due to the dominant presence of Mode I. By limitations of the MMB apparatus, the crack could not grow until the 25 mm required, but a 10 mm of crack length were achieved. Three of five specimens were considered since two specimens presented undesired failure at the bond of the hinge with the laminate. Fig. 40 presents the load-displacement obtained and all the parameters calculated are shown in tab. 16.

Figure 40 - Force-displacement curves for MMB with G_{II}/G_C =20 %.

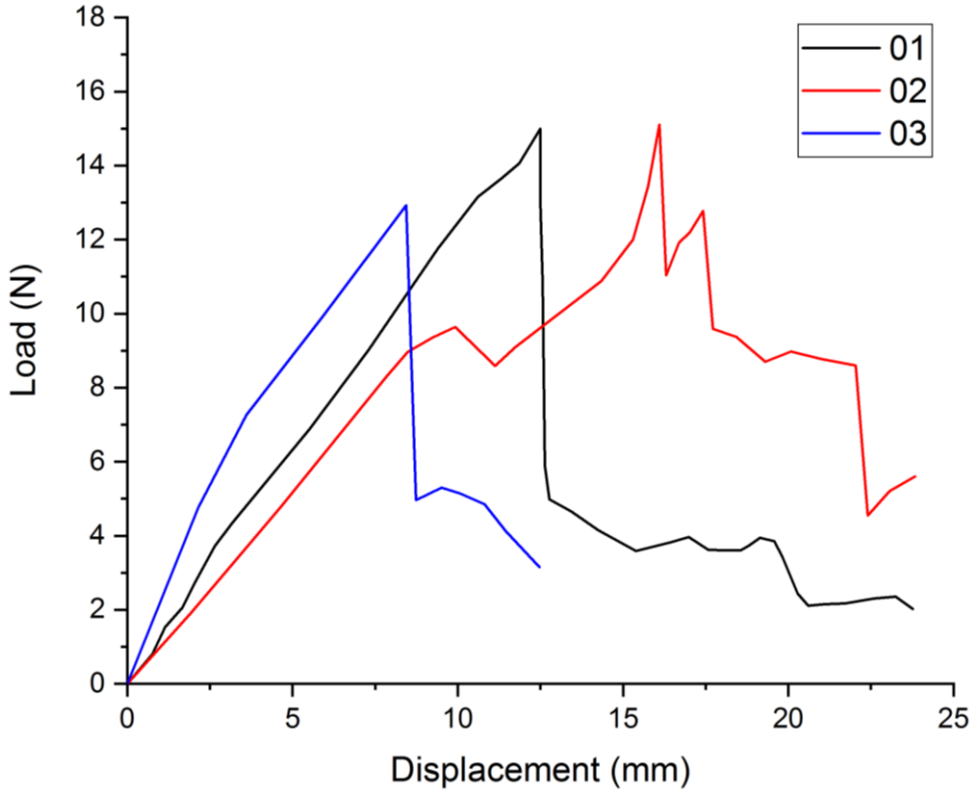

Table 16 - SERR values for Mixed-Mode fracture with G_{II}/G_C =20 %.

	01	02	03
m (N/mm)	1.29	1.01	0.88
C_{sys} (mm/N)	0.0057	0.0057	0.0057
E_{1f} (N/mm²)	6174.85	5660.29	4908.77
P (N)	16.09	15.81	14.07
b (mm)	24.87	25.15	25
h (mm)	1.73	1.69	1.71
a (mm)	25.6	27.45	28
G_I (kJ/m²)	0.187	0.234	0.217
G_{II} (kJ/m²)	0.047	0.059	0.055
G_C (kJ/m²)	0.234	0.292	0.271

The average value of the critical SERR at this mode mixture is 0.266 kJ/m^2. As expected, this value is lower than the SERR of the single Modes since a crack will easily propagate when submitted to multiple loadings. The statistical analysis is shown in tab. 17:

Table 17 - Statistical analysis for Mixed-Mode with G_{II}/G_C=20%.

	Average Mean G_C (kJ/m²) $\bar{x}$	**Standard Deviation** S_r	**Coefficient of Variation %** CV
Mixed-Mode $G_{II}/G_C = 20\%$	0.266	0.029	11.08

During the tests, a load instability was observed, this is a common characteristic of this mixed-mode. The limit of deflection of the MMB apparatus was reached before getting the standardized delamination propagation length of 25 mm, instead of that a 10 mm propagation was reached, which can be considered as enough since the load levels at this length were already low. Using eq. 3.55, nominal stresses for this mixed-mode were calculated and are shown in tab. 18:

Table 18 - Nominal stresses for Mixed-Mode with G_{II}/G_C=20%.

		σ_c	**VIS**	**1**	**2**	**3**	**4**	**5**	**10**
Mixed-Mode $G_{II}/G_C = 20\%$	**(MPa)**	6.56	2.79	3.41	4.27	4.98	4.94	3.04	1.85

This is the maximum critical nominal stress value found for our Mixed-Mode case. A TSL can now be formulated with the parameters calculated. Tab. 19 shows the TSL parameters and fig. 41 illustrates the TSL shape:

Table 19 - TSL parameters for Mixed-Mode with G_{II}/G_C=20%.

	Adjustment Coefficient φ	**Ultimate Separation (mm)** δ_0	**Critical Separation (mm)** δ_c	**Critical Stress (MPa)** σ_c	**Area (kJ/m²)** G_{IC}
Mixed-Mode $G_{II}/G_C = 20\%$	13/5	0.0625	0.0361	6.56	0.266

This law represents the Mixed-Mode interlaminar fracture behavior with G_{II}/G_C=20% and can be used to estimate the damage degradation in glass/epoxy laminated composite materials.

Figure 41 – TSL for MMB with G_{II}/G_c=20%.

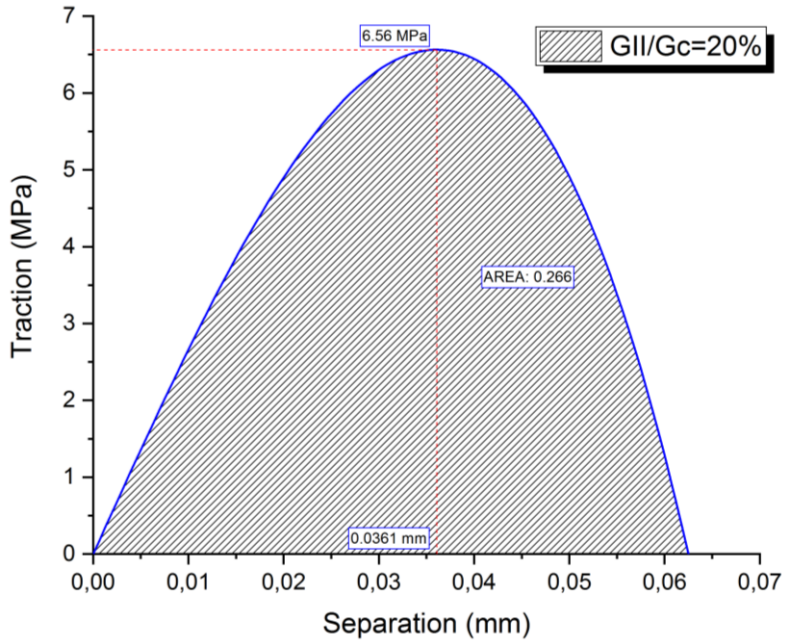

4.3.2. $G_{II}/G_C = 50$ %

Three specimens were tested for this mode, presenting no irregularities. A more stable crack propagation was observed if compared with the previous MMB tests. Fig. 42 presents the load-displacement curve obtained and all the parameters calculated are shown in tab. 20

Figure 42 - Force-Displacement curves for MMB with G_{II}/G_C = 50%.

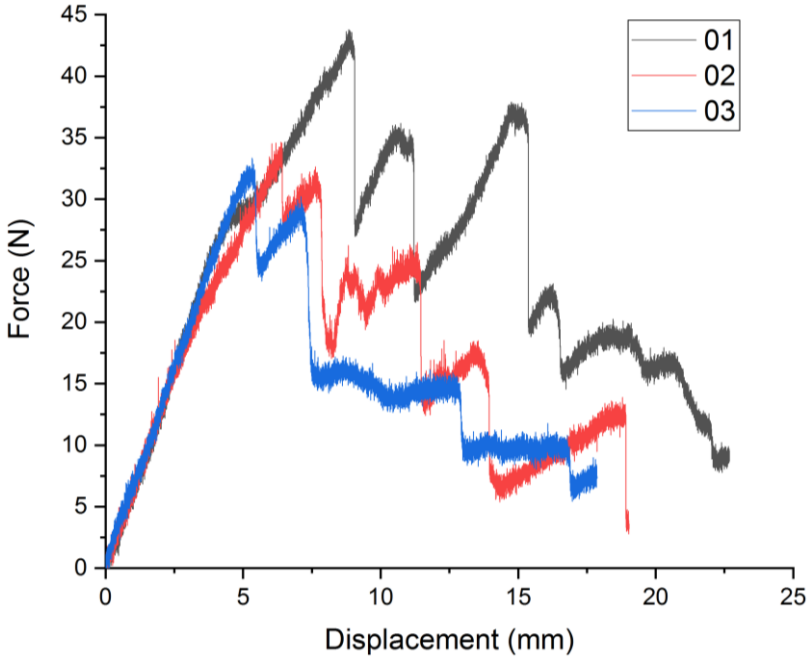

Table 20 - Critical SERR values for MMB with G_{II}/G_C=50%.

	01	02	03
m (N/mm)	6.95	6.11	6.50
C_{sys} (mm/N)	0.0011	0.0011	0.0011
E_{1f} (N/mm^2)	6252.28	5463.75	6236.38
P (N)	43.78	34.63	33.33
b (mm)	25	24.87	24.98
h (mm)	1.92	1.94	1.84
a (mm)	26	26.6	24.4
G_I (kJ/m^2)	0.096	0.070	0.056
G_{II} (kJ/m^2)	0.096	0.071	0.055
G_C (kJ/m^2)	0.192	0.141	0.111

The mean value of the critical SERR for this mode is 0.148 kJ/m^2. Observe that G_I and G_{II} have quite the same values since each of them represents a 50% of the total critical SERR. The statistical analysis of the results is shown in tab. 21:

Table 21 - Statistical analysis for MMB with G_{II}/G_C=50%.

	Average Mean G_{IC} (kJ/m^2) $\bar{x}$	**Standard Deviation S_r**	**Coefficient of Variation % CV**
Mixed-Mode $G_{II}/G_C = 50\%$	0.148	0.041	27,62

A 25 mm delamination length was reached without inconvenient. Eq. 3.55 assisted the calculations of the nominal stresses (in MPa) for this mode and are shown in tab. 22:

Table 22 - Nominal stresses for MMB with G_{II}/G_C=50%.

	σ_c	VIS	1	2	3	4	5	10	15	20	25
Mixed-Mode $G_{II}/G_C = 50\%$	5.01	3.72	4.15	4.39	4.88	4.99	3.67	2.76	2.15	2.04	1.60

These stresses are represented by a TSL (Fig. 43) with parameters enlisted in tab. 23:

Table 23 - TSL parameters for MMB with G_{II}/G_C=50%.

	Adjustment Coefficient φ	Ultimate Separation (mm) δ_0	Critical Separation (mm) δ_c	Critical Stress (MPa) σ_c	Area (kJ/m²) G_{IC}
Mixed-Mode $G_{II}/G_C = 50\%$	13/5	0.0452	0.0261	5.01	0.148

Figure 43 - TSL for MMB with G_{II}/G_C=50%.

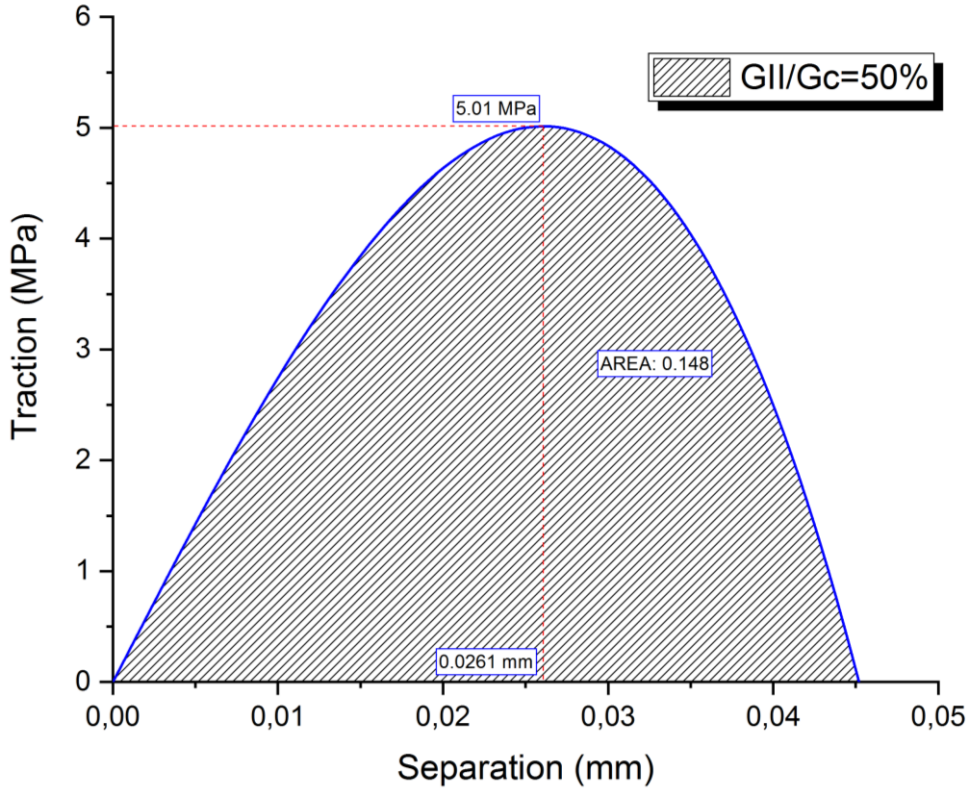

This TSL fully represents the material degradation of glass fiber laminated composite material under mixed-mode fracture with G_{II}/G_C=50%.

4.3.3. $G_{II}/G_C = 80\ \%$

This is the last mode mixture considered during MMB tests, which represents an 80% of dominant Mode II fracture over a presence of 20% of Mode I fracture. For this mode, was observed a low resistance to fracture with a stable crack growth. The energy dissipated was the

lower between the three MMB cases studied, this means that the energy required to fracture at this mode is short. Fig. 44 presents the load-displacement curve obtained for three specimens, and all the parameters calculated are shown in tab. 24. Specimen 03 shows a lower maximum load provoked by a larger insert length, this characteristic was a manufacturing error. Despite this, the SERR value obtained was accurate.

Figure 44 - Force-Displacement curve for MMB with G_{II}/G_C = 80%.

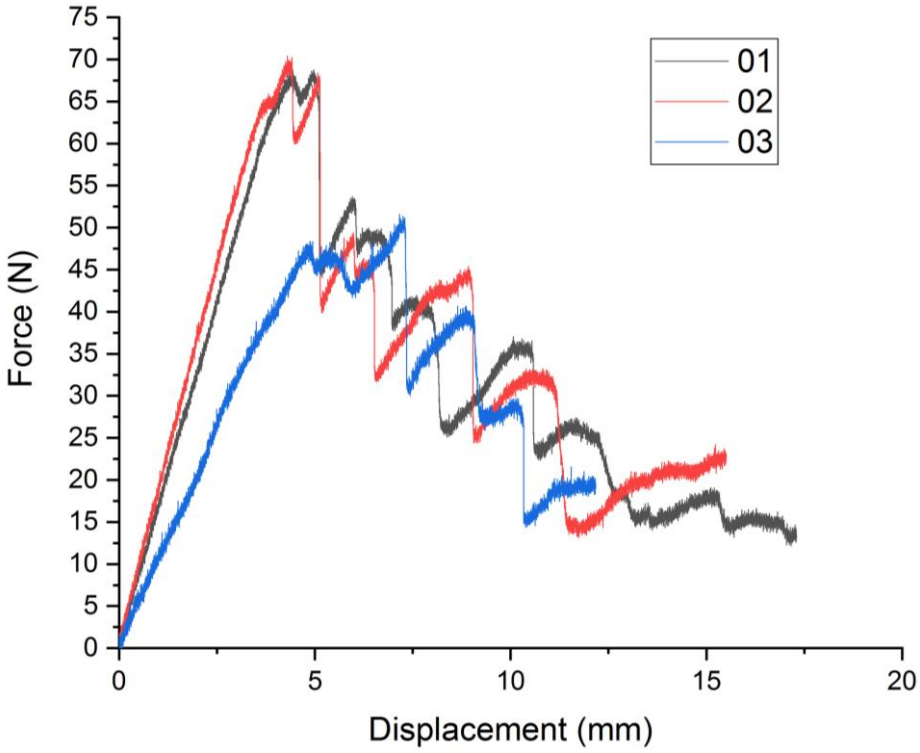

Table 24 - Critical SERR values for MMB with G_{II}/G_C = 80%.

	01	**02**	**03**
m (N/mm)	16.31	17.98	10.63
C_{sys} (mm/N)	0.00085	0.00085	0.00085
E_{1f} (N/mm^2)	11947.65	12753.29	8864.31
P (N)	62.59	53.74	36.47
b (mm)	25.27	23.9	24.78
h (mm)	1.7	1.73	1.68
a (mm)	22.9	20.5	26
G_I (kJ/m^2)	0.023	0.02	0.022
G_{II} (kJ/m^2)	0.094	0.080	0.087
G_C (kJ/m^2)	0.117	0.100	0.109

As expected, the value of the critical SERR for this mode was the lower. We obtained a mean value for G_C of 0.109 kJ/m^2. The statistical analysis is presented in tab. 25:

Table 25 - Statistical analysis for MMB with G_{II}/G_C = 80%.

	Average Mean G_{IC} (kJ/m^2) $\bar{x}$	**Standard Deviation S_r**	**Coefficient of Variation % CV**
Mixed-Mode $G_{II}/G_C = 80\%$	0.109	0.009	8.17

The 25 mm delamination length required was easily reached and the crack growth was observed as stable. Tab. 26 shows the nominal stresses calculated by employing eq. 3.55:

Table 26 - Nominal stresses for MMB with G_{II}/G_C = 80%.

	σ_c	**VIS**	**1**	**2**	**3**	**4**	**5**	**10**	**15**	**20**	**25**
Mixed-Mode $G_{II}/G_C = 80\%$	4.54	3.52	4.26	4.44	4.50	4.53	3.14	2.94	2.47	2.24	1.30

As the SERR value is the lower, the value of the critical nominal stress for this mixed-mode was expected to be the lower as well. Tab. 27 resumes the parameters to construct a TSL (Fig. 45) that fully represent the material degradation due to delamination propagation for this mode.

Table 27 – TSL parameters for MMB with G_{II}/G_C = 80%.

	Adjustment Coefficient φ	**Ultimate Separation (mm) δ_0**	**Critical Separation (mm) δ_c**	**Critical Stress (MPa) σ_c**	**Area (kJ/m^2) G_{IC}**
Mixed-Mode $G_{II}/G_C = 80\%$	13/5	0.0369	0.0213	4.54	0.109

Figure 45 - TSL for MMB with G_{II}/G_C=80%.

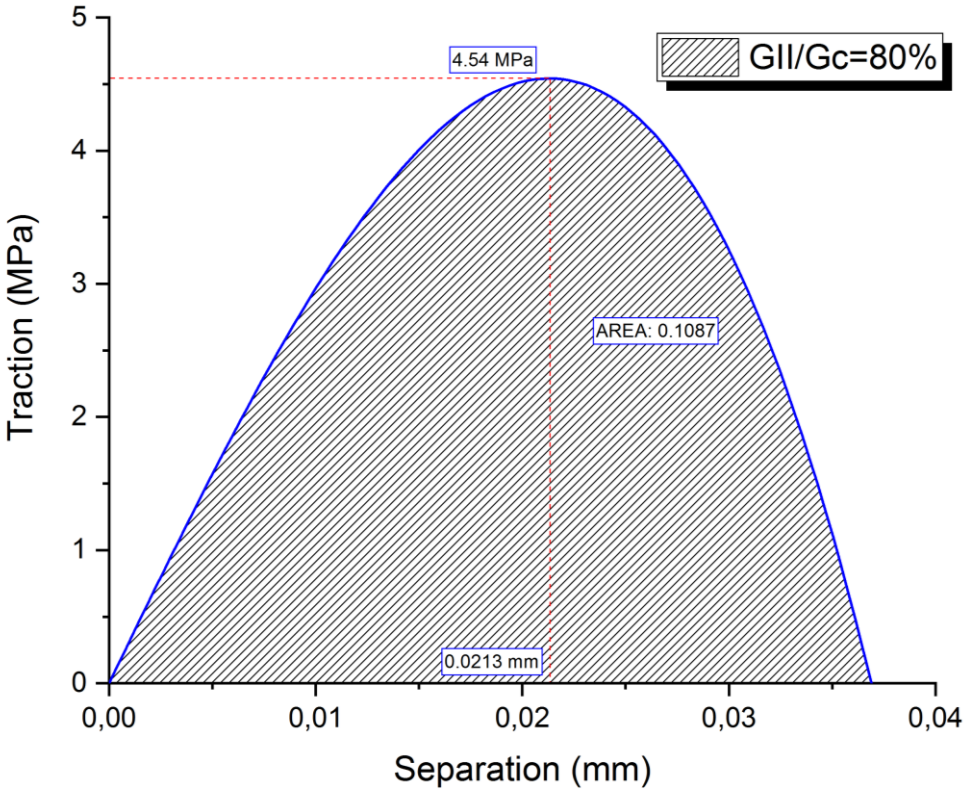

4.4. Conclusions of Experimental Results

The progressive interlaminar failure of glass-fiber/epoxy laminated composite material was investigated by using experimental techniques. Two principal fracture modes (I and II) and three Mixed-Modes between them, were reproduced in the laboratory by means of destructive testing like DCB, ENF and MMB tests. SERRs for each mode and for their respective propagation were calculated with accuracy validated with literature results. Following the procedures, the nominal stresses were determined as well and the values found have good correlation with other similar works available in the literature. These parameters are necessary to characterize a Traction-Separation Law which can be employed as a law for cohesive method simulations or damage material model formulations. Fig. 46 resumes the five TSLs calculated and showed along this chapter.

Figure 46 - TSLs for all the fracture modes.

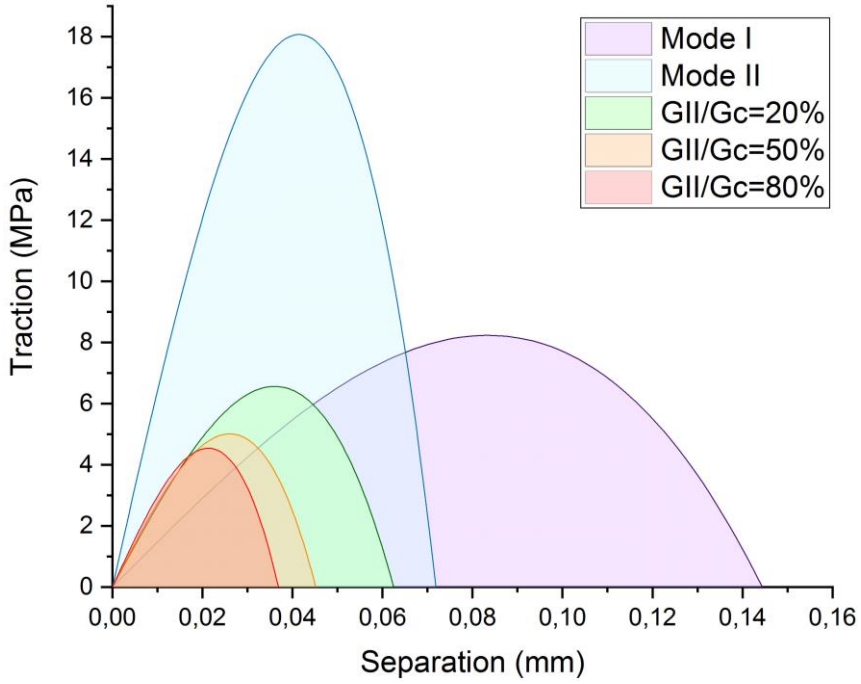

Note the similarity of the three MMB TSLs, this characteristic will be considered when calculating the damage variable and during the damage model implementation.

The tests were carried out almost without inconvenience, the main problem appeared at the hinge bond since the adhesive failed in many specimens during the testing. At DCB tests, some of the specimens present a run-arrest extension of the crack with abruptly delamination front jumps, this is an indication of a problem with the insert like a large neat resin pocket as sketched in fig. 47:

Figure 47 - Resin rich zone.

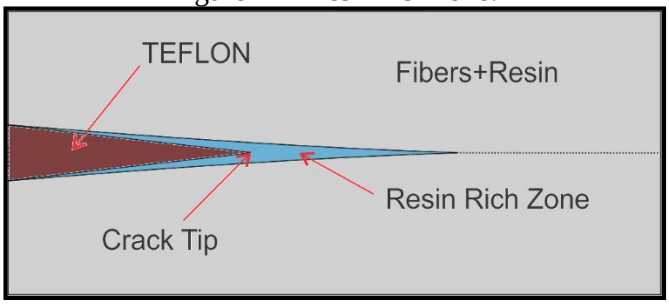

These irregularities were solved at the laboratory so the tests were successfully performed. With the complete characterization of fracture reached, an interlaminar damage model was formulated and is shown in the next chapter.

CHAPTER V

5. Delamination Propagation Model

Assisted by Continuum Damage Mechanics (CDM), this chapter presents a delamination propagation model in order to estimate the damage provoked by interlaminar fracture. First sections give a theoretical review of damage interpretation and the chapter ends with the calculation of damage variables for our case study and their implementation via UMAT.

5.1. Mechanical Interpretation of Damage: Theoretical Review

To understand how a damage variable could be conceived, the most basic visualization is to consider a representative volume element (RVE) of a damaged body in a point *P* on a normal plane *r*, located over the abscissa *x* along the *r* direction as seen in Fig. 48 (J. Lemaitre, 1984). Suppose that δS is the area of the intersection between the plane and the RVE, and δS_{Dx} is the effective area of the intersection between all the microcracks and microcavities over δS.

Figure 48 - Representative Volume Element (RVE).

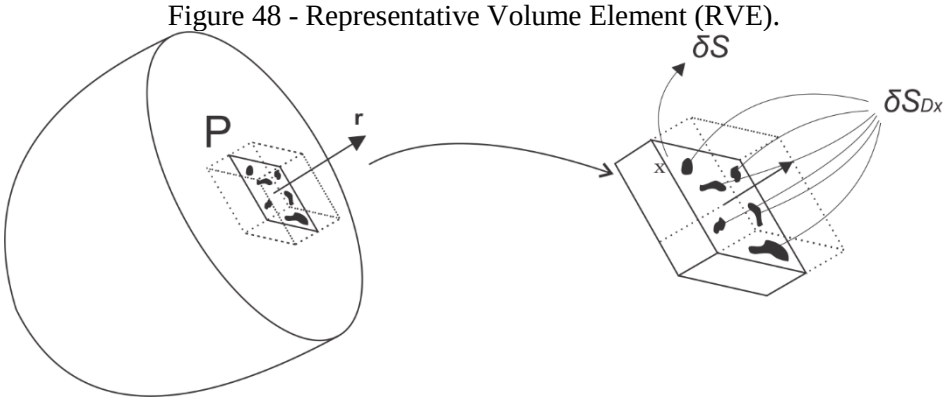

The damage variable value at the point *P* in the *r* direction and over the *x* abscissa is given by:

$$D(P,r,x) = \frac{\delta S_{Dx}}{\delta S} = \frac{S_D}{S} \qquad 5.1$$

This variable is continuous over the representative volume and has values between 0 and 1:

$$0 \leq D \leq 1 \tag{5.2}$$

Where,

D=0 for undamaged material, and

D=1 for totally damaged material.

This non-dimensional scalar variable can be used within constitutive equations to degrade the material properties. If we want to calculate an effective tension $\bar{\sigma}$, for example, we understand tension σ as a force F acting over a surface S:

$$\sigma = \frac{F}{S} \tag{5.3}$$

However, this surface S is affected by some damage forms represented by the surface S_D that does not support any load, so the real surface supporting the force F is actually the subtraction $S - S_D$. Thus, the effective stress is given by:

$$\bar{\sigma} = \frac{F}{S - S_D} \tag{5.4}$$

Recalling eq. 5.1 $D = \frac{S_D}{S}$ and introducing it in equation 5.4, we finally obtain an expression for $\bar{\sigma}$ related to the damage variable D:

$$\bar{\sigma} = \frac{F}{S\left(1 - \frac{S_D}{S}\right)} = \frac{F}{S(1-D)} = \frac{\sigma}{(1-D)} \tag{5.5}$$

There exist different methods to measure damage according to the variation due to degradation of some physical properties like Young's module, ultrasound waves propagation, micro-hardening, density, electric resistance, cyclic plastic response and slow tertiary creep. Each of these methods has limitations for different kinds of materials and fracture mechanism involved.

Within composites, the damage is observed slightly different. At the microscale, damage could be the concentration of micro-stresses at the proximities of defects or interfaces and rupture of the bonds; this is commonly observed in most of the materials at this scale. At the

mesoscale of a representative volume, this could be understood as the growth and nucleation of microcracks and microvoids until the onset of a crack. Finally, at the macroscale the damage mechanism is represented by propagation of the crack mentioned, this supposes an energy *consumption* known in FM as the SERR.

5.1.1. Basis for Damage Models

When defining a damage model, we first must accept that the non-linear behavior and internal changes of the material are associated with the damage process. Whenever dealing with composite materials, the model has to take into account three important aspects (Chow & Wang, 1987):

- Initial anisotropy.
- The nature of the damage growth, always affected by a specific direction.
- The unilateral character of damage which is related to the fact that this damage, while it is irreversible, it could be active or inactive regarding the load conditions (J.-L. Chaboche, 1992).

Particularly, for laminated composite materials, the nature of the damage is extremely complex with a mixture of progressive propagation and abrupt brittle damage as observed during testing. There is no a single, but many damage mechanisms involved. These materials are highly anisotropic and, develop strong unilateral behavior mostly affected by the presence of microcracks and whether they are open or closed.

To reach an accurate simulation of the material behavior, several investigations at each of the three scales have been performed. The real challenge is to derive an appropriate damage model compatible with all the information coming from the micro, meso and macro scale. But this is conceived through the study of the phenomenon at each scale and by formulating failure criteria, afterward, a homologation of the theories needs to be performed so the models can establish a relationship between each of them and work together (Fish & Yu, 2001). This aspect forces the researchers to develop mathematical models with a high complexity that usually represent a huge computational effort and cost. When more phenomena are considered, the number of parameters increases and, in consequence, the correct selection for damage variables becomes a hard task. This results in a difficulty when comparing the predicted anisotropy induced by damage, between a numerical model and experimental observations.

So far, we can note the relevance of choosing the proper damage variable and the structure of the model; these models can have a micromechanical and/or phenomenological nature. A micromechanical model seeks to describe the meso and macro failure behavior from observations at the microscale, so it considers elementary constitutive equations for displacement, crack growth and fracture known at meso or macro scale. After a good mathematical description of the micromechanics of discontinuities, developing a micromechanical model may focus in finding an accurate homogenization of the microstructural defects field, so it is possible to have a 1:1 scale between a discontinuous field at an inhomogeneous microscale and a continuous effective field at a homogeneous mesoscale.

A phenomenological model, in contrast, disregards the micro-details of the material and models the damage indirectly by introducing internal variables; this action must ensure the invariant and fulfillment of the thermodynamic laws. A series of tridimensional experiment with different load cases must be carried out in order to compute the appropriate parameters. It uses a non-local scheme, which consists in introducing non-local terms within the constitutive equations to take into account the heterogeneous substructure of the material like plastic displacement or microcrack interaction. The procedure usually lies on including non-local terms by the employment of an integral equation or by a gradient equation. Integral equations may be hard to linearize, which is computationally inefficient; but the employment of gradient represents a useful alternative since in this method, the finite element equations remain local and which means that the linearization is easily accomplished. Theories in gradient at a macroscale are a good tool to treat problems of localization due to plasticity and damage.

5.1.2. Basis for Damage Variables

The potentiality of a damage model to predict a failure behavior is strongly related to the particular choice of the damage variable. We can find in the literature innumerable approaches to phenomenologically describe the damage and to derive the damage variables (Ju, 1990), (Burr, Hild, & Leckie, 1995). Normally, scalar damage variables have been widely employed in isotropic damage models for quasi-brittle anisotropic materials, using damage vectors, second-order damage tensors, and fourth-order damage tensors.

Damage in anisotropic materials, like composites, are influenced by directions in the same manner as their mechanical properties. So, it is recommended to employ not one but many

damage variable as needed in order to conserve the characteristics of damage mechanism. The vectorial representation is attractive since is possible to capture the microcrack orientations and damaged surfaces and it is an extension of Kachanov's scalar model. It uses two scalar variables, one associated with the energy contained at a volumetric deformation and the other associated with the distortion energy. However, until a certain point, it shows indifference to the shape of microcracks and tensor operation problems related to the transformation of stresses.

Second-order damage tensor is the most employed to represent the anisotropy induced by damage, but only for original isotropic materials. It is accepted for an anisotropic theory since it allows capturing the surfaces and orientation of the microcracks; however, it is unable to capture the whole anisotropy.

Moreover, fourth-order tensors are the best to represent a general anisotropy. It was firstly used by Chaboche (1988) and can be naturally applied using the effective stress concept and the infinitesimal strain theory. In this case, the damage variable (which is a fourth-order tensor) plays the role of a damage effect tensor. Theories that are more current employ the elastic stiffness tensor or the flexibility tensor, both fourth-order tensors, directly as state variable associated with damage.

5.1.3. Different Damage Interpretations

Damage models must begin from a hypothesis that describes the transformation provoked by damage. Usually, this hypothesis considers a fictitious undamaged space that can be obtained from real stress or strain state through a transformation. The stress at an undamaged fictitious space is known as *effective stress*. There exist several hypotheses to define the transformations between the real damage space and the undamaged fictitious space.

a) Effective stress concept and principle of strain equivalence:

Within CDM, the damage process can be modeled by introducing an internal variable that could be a scalar or tensor quantity. Since it has been demonstrated that fourth-order tensors are suitable for anisotropic nature, we will employ a fourth-order tensor $M = M_{ijkl}$ that characterizes a damaged state and transform a nominal stress tensor σ_{ij} into an effective stress tensor $\bar{\sigma}_{ij}$:

$$\bar{\sigma}_{ij} = M^{-1}_{ijkl}\sigma_{kl} \qquad 5.6$$

The simplest case was shown in equation 5.5:

$$\bar{\sigma}_{ij} = \frac{1}{1-d}\sigma_{ij}$$

The principle of strain equivalence was originally introduced by Lemaitre (1978) and explain that the strain associated with a damaged state under the applied load is equivalent to the strain associated with an undamaged state under the effective stress.

These both theories are related by constitutive equations based on strain. This principle has been widely employed and, despite the good result that has been reached, there exists a theoretical limitation that is the presence of non-symmetric tensors for stiffness and flexibility. This leads to an energy not conserved during loading and unloading.

b) Effective strain concept and hypothesis of stress equivalence

Effective strain, like in the case of the stress, can be also derived and it is expressed as follows:

$$\bar{\varepsilon}_{ij} = M_{ijkl}\varepsilon_{kl} \qquad 5.7$$

And the simplest case:

$$\bar{\varepsilon}_{ij} = (1-d)\varepsilon_{ij} \qquad 5.8$$

Where ε_{ij} is the strain tensor and $\bar{\varepsilon}_{ij}$ is the tensor of effective strain. From similar concepts of the principle of strain equivalence, Simo and Ju (1987) proposed a hypothesis for stress equivalence where they defined that the stress associated to a damage state under an applied strain is equivalent to a stress associated with an undamaged state under an effective strain.

As in the previous case, both theories can be related to the employment of constitutive equation based on stress. Once again, there exists a theoretical issue that leads to non-symmetric tensors for stiffness and flexibility.

c) The principle of energy equivalence

The philosophy applied to previous principles is preserved. The following statement is considered: The strain energy associated with a damaged state under an applied load is equivalent to the strain energy associated with the fictitious undamaged state under an applied effective stress (Krajcinovic & Fonseka, 1981).

By this hypothesis, neither the effective stress nor the effective strain agrees with their nominal values. Supposing that the relation between nominal and effective quantities are linear, they must be given by the same fourth-order tensor as follows:

$$\sigma_{ij} = \bar{M}_{ijkl}\bar{\sigma}_{kl} \ \wedge \ \bar{\varepsilon}_{ij} = \bar{M}_{ijkl}\varepsilon_{kl} \tag{5.9}$$

Or the inverse,

$$\bar{\sigma}_{ij} = M_{ijkl}\sigma_{kl} \ \wedge \ \varepsilon_{ij} = M_{ijkl}\bar{\varepsilon}_{kl} \tag{5.10}$$

Thus, the nominal and effective elastic energy density must coincide:

$$\sigma_{ij}\varepsilon_{ij} = \bar{M}_{ijkl}\bar{\sigma}_{kl}M_{ijrs}\bar{\varepsilon}_{rs} = \bar{\sigma}_{ij}\bar{\varepsilon}_{ij} \tag{5.11}$$

Which demand that the tensors M_{ijkl} and $\bar{M}_{ijkl}$ must be inverse one from another.

Connecting the relations between nominal and effective stress and strain; it is possible to obtain the secant tensor for stiffness and flexibility:

$$C_{ijkl} = \bar{M}_{ijpq}\overset{\circ}{C}_{pqrs}\bar{M}_{klrs} \ \wedge \ E_{ijkl} = M_{pqij}\overset{\circ}{E}_{pqrs}M_{rskl} \tag{5.12}$$

Where, $\overset{\circ}{C}_{pqrs}$ and $\overset{\circ}{E}_{pqrs}$ are the undamaged stiffness and flexibility tensors. Beside the previous principles, this principle presents symmetric tensors for stiffness and flexibility (Carol, Rizzi, & Willam, 2001).

d) Kinematic Relations

With basis on formulations of the Finite Strain Theory, damage can be mathematically interpreted as a kinematic transformation between two spaces. A fictitious undamaged space is supposed, which is obtained from a real damaged space by subtracting the damage. At this fictitious undamaged space, the material acts like it was a virgin material (Voyiadjis & Deliktas, 2000).

It is accepted that there exists a bi-univocal relation (F_{ik}) between this two spaces that allows the transformation of a variable from the fictitious undamaged space to the real damaged space; this relation can be expressed as follows:

$$\sigma_{ij} = F_{ik}F_{jl}^{T}\bar{\sigma}_{kl} = M_{ijkl}\bar{\sigma}_{kl} \quad 5.13$$

$$\varepsilon_{ij} = F_{ik}^{-T}F_{jl}^{-1}\bar{\varepsilon}_{kl} = M_{ijkl}^{-1}\bar{\varepsilon}_{kl} \quad 5.14$$

It is possible to note that transformations at the strain field result from the theory of conjugated stress through the constitutive law of the material. The inverse transformation of the spaces is shown below:

$$\bar{\sigma}_{ij} = F_{ki}^{-1}F_{lj}^{-T}\sigma_{kl} = F_{ik}^{-T}F_{jl}^{-1}\sigma_{kl} = M_{ijkl}^{-1}\sigma_{kl} \quad 5.15$$

$$\bar{\varepsilon}_{ij} = F_{ki}^{T}F_{lj}\varepsilon_{kl} = F_{ik}F_{jl}^{T}\varepsilon_{kl} = M_{ijkl}\varepsilon_{kl} \quad 5.16$$

At the fictitious undamaged space, there exists an isotropically constitutive equation corresponding to the virgin material:

$$\bar{\sigma}_{ij} = \bar{C}_{ijkl}\bar{\varepsilon}_{kl} \quad 5.17$$

Where,

$\bar{C}_{ijkl} = C_{ijkl}^{\circ}$, is the elastic constitutive tensor of the virgin material.

Replacing within eq. 5.7 all the inverse equations, we can obtain the constitutive equation of the real space:

$$F_{ri}^{-1}F_{sj}^{-T}\sigma_{rs} = \bar{C}_{ijkl}F_{tk}^{T}F_{ul}\varepsilon_{tu} \quad 5.18$$

$$\sigma_{rs} = \left(F_{ir}F_{js}^{T}\bar{C}_{ijkl}F_{tk}^{T}F_{ul}\right)\varepsilon_{tu} = C_{rstu}\varepsilon_{tu}$$

Here, the secant constitutive tensor in the damaged space is expressed as:

$$C_{ijrs} = M_{ijkl}\bar{C}_{klmn}M_{mnrs} = F_{ik}F_{jl}^{T}\bar{C}_{klmn}F_{mr}F_{ns}^{T} \quad 5.19$$

And the strain energy results:

$$W = \frac{1}{2}\sigma_{ij}\varepsilon_{ij} = \frac{1}{2}M_{ijkl}\bar{\sigma}_{kl}M_{ijrs}^{-1}\bar{\varepsilon}_{rs} = \frac{1}{2}I_{klrs}\bar{\sigma}_{kl}\bar{\varepsilon}_{rs} = \frac{1}{2}\bar{\sigma}_{kl}\bar{\varepsilon}_{kl} = \bar{W} \quad 5.20$$

As expected, the energy is an invariant of the changes in space. The tensor F_{ij} links the two spaces described, like the strain gradient tensor (Badreddine, Saanouni, & Nguyen, 2015).

From the theories and principles reviewed above, the principle of energy equivalence is the most employed by researchers for cases where the material degradation is related to plastic deformations as it happens with composite materials. This principle is also useful when defining damage at a macroscale since the damage is intrinsic in a variable defined by elastic potential and a definition of a superficial density of defects and a physic interpretation of damaged is not required anymore.

5.2. Calculation of Damage Variables

The main mechanism while fracturing a material is the energy dissipation to create newly fractured surfaces. Thus, the damage variables considered within this model must relate the SERRs calculated for delamination propagation. The concept of a Traction-Separation Law comes from the Cohesive Zone Model (CZM) approach, so our damage model is based on the same approach.

As reviewed in section 3.3.3.2, the area under the curve of TSL represents the characteristic critical SERR value of the material being considered. From CDM, a damage variable is defined as the ratio between a damaged state and an undamaged state associated with local discretization. For our case study, the undamaged state (G_c) is taken as the total area under the TSL curve or as the total critical SERR; and the damaged state (G_D) is represented by the area between the curve and a line traced from the origin to a point at the curve as illustrated in fig. 49. The employment of this damage variable has evidence in the literature (Turon et al., 2010).

Figure 49 - Definition of the damaged and undamaged area.

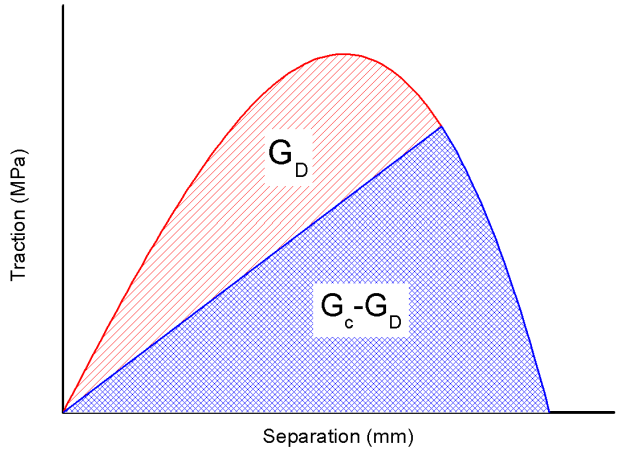

Thus, eq. 5.21 gives the determination of the damage variable:

$$d = \frac{Area_{Damaged}}{Area_{Undamaged}} = \frac{G_D}{G_C} \qquad 5.21$$

With this definition, we can proceed with the calculations of damage variables for our case study. For each fracture mode considered, a damage variable is calculated for the critical value and for each value at the propagation of the delamination.

During the tests, it was observed that a significant degradation occurs when the crack has propagated more than 4 mm, this is when the crack reached the critical crack length at the critical traction value. A degradation may also occur at each 5 mm of crack growth measured from the insert front. Taking these details into account, we define a damage variable for the critical point and at each 5 mm point of delamination advance.

Table 28 - Damage Variables.

		CRI	5 mm	10 mm	15 mm	20 mm	25 mm
Mode I		0.1098	0.1975	0.2359	0.2797	0.2956	-
Mode II		0.1010	-	-	-	0.2488	-
Mixed-Mode	$\boldsymbol{G_{II}/G_C = 20\%}$	0.1162	0.6236	0.7783	-	-	-
	$\boldsymbol{G_{II}/G_C = 50\%}$	0.1148	0.4296	0.5718	0.6551	0.6848	0.7472
	$\boldsymbol{G_{II}/G_C = 80\%}$	0.1108	0.4487	0.4712	0.5699	0.6247	0.7790

For Mode II, the delamination advance is so abrupt that the crack may grow 20 mm from a single jump. Therefore, a damage variable was calculated only for the critical value and for a crack length of 20 mm as seen in tab. 28. For the mixed-mode with 20% presence of Mode II, crack propagation is so injurious that a 5 mm grow may degrade the material for more than 60% of its initial strength.

5.3. Implementation via UMAT (User Material Sub-routine)

The damage model proposed, is written as a User Material sub-routine (UMAT) using FORTRAN language and implemented to the FE analysis. This sub-routine is an *ABAQUS*^{TM}

tool that allows the users to put their own failure criteria into effect while performing FE analyses.

During an analysis, the behavior of the composite ply is evaluated by the UMAT in each Gauss point of the model's elements and simulated by calculating the stresses and the Jacobian matrix ($\partial\sigma/\partial\varepsilon$) in function of the strains at each step. The calculated stress state is evaluated and if there exists a stress value that exceeds a critical nominal stress, the degradation is triggered and the damage variables updated. At the next step, the stress tensor is updated using the constitutive relations in eq. 5.22 – 5.24.

Observations during experimental tests revealed that, for laminated composites, the crack must move along a path between two plies where the presence of the resin phase is dominant. This approach is observed in the literature (Donadon & Lauda, 2015). This allows us to define the stiffness matrix for the interlaminar damage mode as being isotropic:

$$D_{ijkl} = 2\mu^{*}\varepsilon_{ij} + \lambda^{*}\delta_{ij}\varepsilon_{kl} \tag{5.22}$$

Where,

$$\mu^{*} = \frac{E^{*}}{2(1+\upsilon)} \tag{5.23}$$

And,

$$\lambda^{*} = \frac{E^{*}\upsilon}{(1+\upsilon)(1-2\upsilon)} \tag{5.24}$$

Within these equations, υ represent the Poisson's ration and the damage variable d_3 is contained in E^{*} as follows:

$$E^{*} = E(1-d_3) \tag{5.25}$$

Where E represents the Young's Modulus.

The damage variables introduced in the whole model are the maximum calculated values along the load history analyses in order to avoid material self-healing.

The damage variable follows a single path defined by the quadratic fit of the critical damage variable values of the three fracture modes vs the percent of mode II present during the fracture process as shown in fig. 50. The same approach was considered for the critical nominal stresses as seen in fig. 51:

Figure 50 - Quadratic fit for critical damage variable vs percent of Mode II.

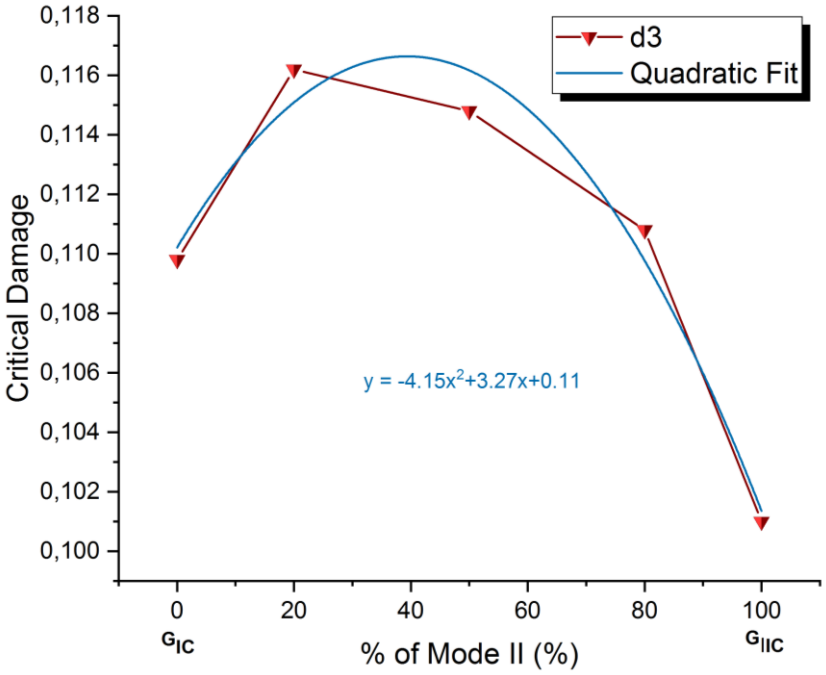

Figure 51 - Quadratic fit for critical nominal stresses vs percent of Mode II.

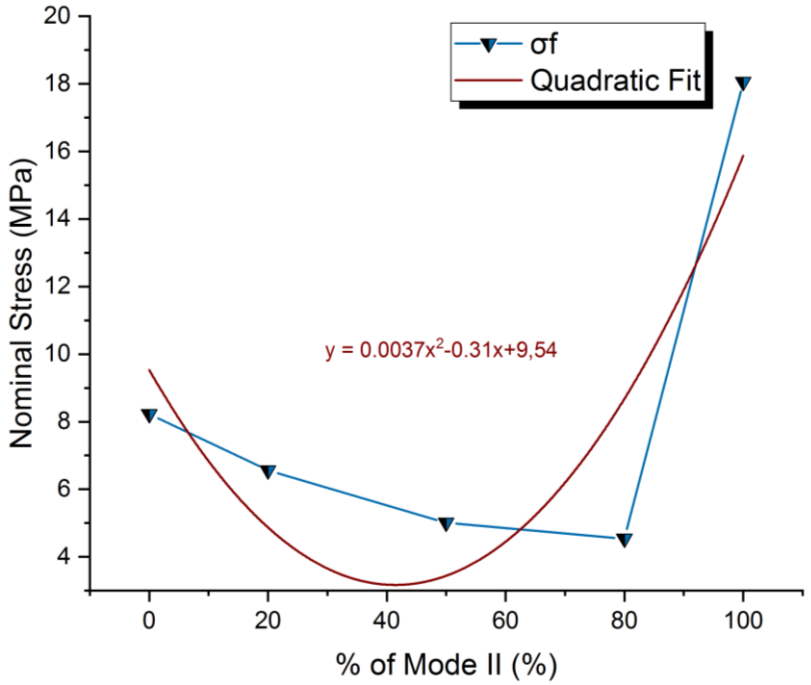

In both figures, the x-axis represents the amount of Mode II present during the fracture evaluation. The 0 value represent pure Mode I, the 100 value represent pure Mode II of interlaminar fracture and in between are the MMB values. The characteristic function for the fit of the damage variable and the nominal stresses are given in eq. 5.26 and 5.27 respectively:

$$y = -4.15x^2 + 3.27x + 0.11 \tag{5.26}$$

$$y = 0.0037x^2 - 0.31x + 9.54 \tag{5.27}$$

Equation 5.27 is used as the failure criterion to determine when the damage should evolve and the damage variable will be activated following eq. 5.26.

CHAPTER VI

6. Numerical Results

Experimental tests were carried out in order to obtain material parameters; new TSLs were formulated from these parameters and a damage variable was obtained for each case considered. A numerical model for interlaminar failure was developed and within this chapter, the performance of the model is exhibited.

Two application results are shown, one considering glass-fiber laminate under DCB loading and another simulating bending behavior of a carbon/epoxy composite. Both cases are compared with experimental results.

6.1. Glass-fiber/epoxy laminate under Mode I fracture

In this first example, the experimental test shown in section 3.2.2.1. was reproduced using the commercial finite element software, Abaqus, compiled with the interlaminar model implemented as a UMAT.

6.1.1. Mode I Fracture: Numerical Simulation

The model was designed following the dimensions specified in the standard test method, described in tab. 4. Fig. 52 shows a 3D solid deformable part with a mesh containing 28644 C3D20 elements. An isotropic zone is modeled where the crack is supposed to propagate (between plies and in-front of the crack tip) using the epoxy properties listed in tab. 2. This resin path parallel to the crack plane is an approach present in the literature (Donadon & Lauda, 2015).

Figure 52 - DCB simulation using Abaqus.

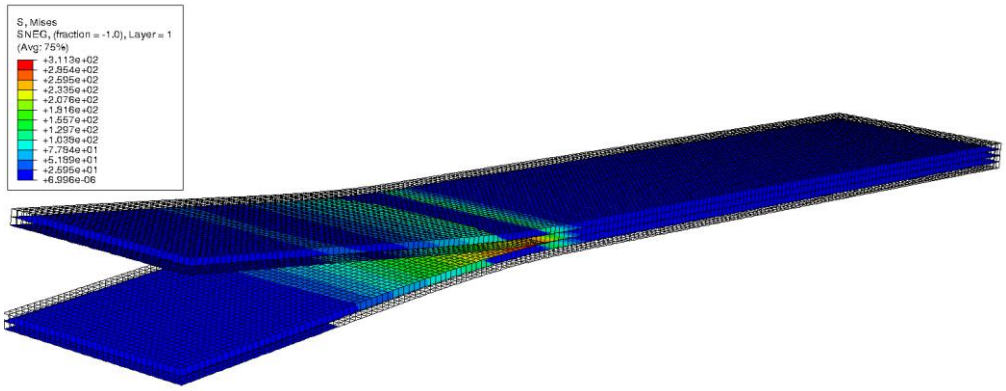

For sake of comparison, the same simulation was carried out employing cohesive elements between the top and bottom laminate from the crack plane. The model presents almost none convergence problem and a promissory result discussed in the further section.

6.1.2. Mode I Fracture: Numerical Results

The first result discussed is the cohesive model. It was found that it predicts a more rigid response, thus, the maximum load value is higher and the load-displacement value is lower when compared to experimental results.

In the case of the UMAT result, the predictions were more accurate with an error less than 10%. Fig. 53 and tab. 29 resumes the values obtained:

Figure 53 - Load-Displacement response for experimental and numerical Mode I fracture.

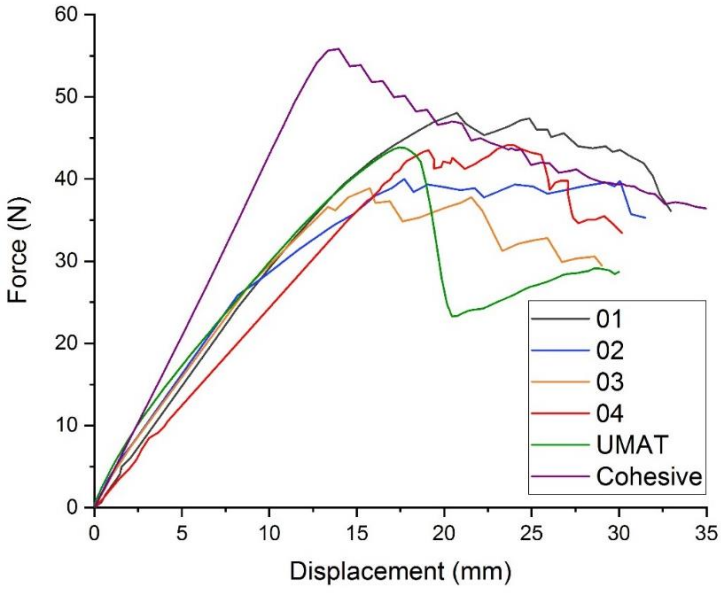

Table 29 - Maximum Load and Load Displacement values of experimental, cohesive elements and model proposed.

	Average Experimental	Cohesive Elements	UMAT	%Error CZM	%Error UMAT
Maximum Load (N)	40.28	55.84	43.86	38.6	8.89
Load Displacement (mm)	16.26	13.97	17.45	14.1	7.32

A material regeneration is observed during the simulation employing the UMAT, this characteristic is possible since the stress tensor is evaluated, at each interaction, to check if the failure criterion is being fulfilled and the stiffness matrix is updated.

6.1.3. Conclusions for Glass-Fiber/Epoxy Application

In this first application of the numerical model developed, we obtain a more favorable result if we make a comparison with traditional progressive failure simulation methods like Cohesive Zone Model (CZM). The model matched the experimental results with at least 90% of accuracy and even exhibit a material regeneration episode which is typically observed in DCB tests due to plastic flow deformation. Other fracture cases need to be explored to consolidate the potentiality of the model when predicting glass-fiber/epoxy laminate degradation due to delamination fracture.

6.2.Carbon/Epoxy Composite

The formulation of the TSLs, the definition, and implementation of the damage variables were applied for a case involving carbon/epoxy composite laminate under 3-points bending. This study was successfully performed, which resulted in a publication of a journal article and is partially presented in this chapter.

An intralaminar damage model (Ribeiro et al., 2012) was used in complement to the interlaminar model to capture damage within the lamina. A description of this model is presented in the next section.

6.2.1. Intralaminar model

Ribeiro, Tita and Vandepitte (2012) proposed an intra-laminar failure model regarding composite lamina under plane stress and considering uniform damage through the thickness. The model has three damage variables, each of them related to fiber failure, matrix failure, and shear stress failure under tensile or compression, respectively.

Fiber failure is considered linear elastic with a brittle fracture. In this direction, the model considers that matrix failure does not imply a degradation of the E_{11} property since the whole load is supported by the fibers. For this type of failure, an internal damage variable d_1 was assigned.

Matrix failure is exclusively controlled by transverse stress (σ_{22}) and shear stress (τ_{12}). In this direction, the non-linear behavior is observed due to inelastic strains (Puck & Schürmann, 2004). A corresponding damage variable was assigned for each stress: d_2 for transverse loading and d_6 for shear loading. The hypothesis of effective stress was employed to link damage variables to the stresses:

$$\begin{Bmatrix} \dot{\sigma}_{11} \\ \dot{\sigma}_{22} \\ \dot{\sigma}_{12} \end{Bmatrix} = \begin{bmatrix} \frac{1}{1-d_1} & 0 & 0 \\ 0 & \frac{1}{1-d_2} & 0 \\ 0 & 0 & \frac{1}{1-d_6} \end{bmatrix} \begin{Bmatrix} \sigma_{11} \\ \sigma_{22} \\ \tau_{12} \end{Bmatrix} \tag{6.1}$$

Table 30 resumes the complete damage model and a full description can be found in Ref. (Ribeiro et al., 2012). The model has shown good potentiality when predicting progressive failure when loading has predominating in-plane stresses. Some application can be found in literature like a 3-points bending simulation of flat filament wound laminates (Ribeiro, Vandepitte, & Tita, 2013), optimization of composite stacking sequence(José Humberto S Almeida Jr, Ribeiro, Tita, & Amico, 2017b), hydrostatic external pressure of composite tubes (Jose Humberto S Almeida Jr, Ribeiro, Tita, & Amico, 2016) and radial compression (José Humberto S Almeida Jr, Ribeiro, Tita, & Amico, 2017a).

Table 30 - Ribeiro's intra-laminar failure model.

Failure Criteria	Mode of Failure	Degradation Law
$\frac{\sigma_{11}}{X_T} \leq 1$	Fiber tensile	$E_{11} = 0$
$\frac{\lvert\sigma_{11}\rvert}{X_{C_0}} \leq 1$	Fiber compression	$E_{11} = \frac{X_{C_0}}{\lvert\varepsilon_{11}\rvert}(1 - f(\varepsilon_{11})) + f(\varepsilon_{11})E_{11_0}$
$f \geq 0$	Matrix tensile	$d_2 = A(\theta)Y_2 + B(\theta)$
$f \geq 0$	Matrix compression	$E_{22} = \frac{\sigma_{22_y}}{\lvert\varepsilon_{22}\rvert}(1 - f(\varepsilon_{22})) + f(\varepsilon_{22})E_{22_0}$
$f \geq 0$	Shear	$d_6 = C(\theta)Y_6 + D(\theta)$

Where f is defined in eq. 6.2 and $f(\varepsilon_{11})$ is obtained from the fitting of stress-strain data of specimens under compressive loads.

$$f = \sqrt{\sigma_{22}^2 + \tau_{12}^2} - \left(-S_{12_y} + \frac{2S_{12_y}}{1 + \left(\lvert\sigma_{22}\rvert / \sigma_{22_0}\right)^3} \right) \tag{6.2}$$

Despite the good predictions achieved by employing this model, a reinforcement is required in order to improve the model predictions for cases when out-of-plane shear stresses are predominant.

6.2.2. Interlaminar damage model

A new damage variable is defined as d_3 and is totally related to delamination phenomenon. It will affect the out-of-plane stress state of the material stiffness matrix. The value of this variable depends on the mode of fracture being considered. Tab. 31 present the critical values for Mode I (D5528-13, 2013), Mode II (D7905M-14, 2014) and Mixed-Mode (Pereira & de Morais, 2008) of carbon-epoxy material. For Mixed-Mode three different mode mixtures (G_{II}/G_C) were considered.

Table 31 - Critical values of SERR for carbon-epoxy.

	Mode I	Mode II	Mixed-Mode		
			G_{II}/G_C= 20%	G_{II}/G_C = 50%	G_{II}/G_C= 80 %
Carbon-Epoxy (kJ/m^2)	1.439	2.11	0.28	0.43	0.62

Using these values, five TSL can be generated by following the procedure described in section 3.2.3.2. The maximum traction or critical nominal stress for each fracture mode is estimated with eq. (3.55) and shown in tab. 32. From the plots, the damage variables are calculated by employing eq. (5.21):

Table 32 - Nominal stresses and critical damage variable value.

	Mode I	Mode II	Mixed-Mode		
			G_{II}/G_C= 20%	G_{II}/G_C = 50%	G_{II}/G_C= 80 %
Nominal Stress (MPa)	35.81	55.98	6.26	7.76	9.32
Damage Variable (d_3)	0.87	0.91	0.89	0.89	0.89

The interlaminar failure within carbon fiber composites has a brittle behavior, thus, the damage variables have almost the same critical value. A quadratic least squares regression was performed using the values of damage variables for each fracture mode considered; this generates a single path for the variable evolution during simulations. The next section gives details about model implementation via User Material subroutine.

6.2.3. UMAT Implementation

The full model implementation considers two tridimensional user materials, one for intralaminar damage and another for delamination. The intralaminar damage model will degrade in-plane elastic properties only; on the other hand, the interlaminar model will degrade stiffness parameters.

The stiffness matrix for intralaminar damage model is considered as orthotropic:

$$D=\begin{bmatrix} \frac{(1-\upsilon_{23}\upsilon_{32})}{E_{22}E_{33}\Delta(1-d_2)} & \frac{(\upsilon_{21}+\upsilon_{23}\upsilon_{31})}{E_{22}E_{33}\Delta(1-d_2)} & \frac{(\upsilon_{31}+\upsilon_{21}\upsilon_{32})}{E_{22}E_{33}\Delta(1-d_2)} & 0 & 0 & 0 \\ \frac{(\upsilon_{21}+\upsilon_{23}\upsilon_{31})}{E_{22}E_{33}\Delta(1-d_2)} & \frac{(1-\upsilon_{13}\upsilon_{31})}{E_{11}E_{33}\Delta(1-d_1)} & \frac{(\upsilon_{32}+\upsilon_{31}\upsilon_{32})}{E_{11}E_{33}\Delta(1-d_1)} & 0 & 0 & 0 \\ \frac{(\upsilon_{31}+\upsilon_{21}\upsilon_{32})}{E_{22}E_{33}\Delta(1-d_2)} & \frac{(\upsilon_{32}+\upsilon_{31}\upsilon_{32})}{E_{11}E_{33}\Delta(1-d_1)} & \frac{(1-\upsilon_{21}\upsilon_{12})}{E_{22}E_{11}\Delta_3} & 0 & 0 & 0 \\ 0 & 0 & 0 & G_{12}(1-d_6) & 0 & 0 \\ 0 & 0 & 0 & 0 & G_{13} & 0 \\ 0 & 0 & 0 & 0 & 0 & G_{23} \end{bmatrix} \quad 6.3$$

Where,

$$\Delta=\frac{(1-\upsilon_{12}\upsilon_{21}-\upsilon_{23}\upsilon_{32}-2\upsilon_{12}\upsilon_{13}\upsilon_{21})}{E_{11}E_{22}E_{33}(1-d_1)(1-d_2)}$$

And,

$$\Delta_3=\frac{(1-\upsilon_{12}\upsilon_{21}-\upsilon_{23}\upsilon_{32}-2\upsilon_{12}\upsilon_{13}\upsilon_{21})}{E_{11}E_{22}E_{33}}$$

The stiffness matrix for interlaminar damage model is considered as isotropic. We identify an intermediate ply, representing an epoxy region, between fiber laminates (Donadon & Lauda, 2015), therefore, we consider this zone as an isotropic material. This approach is true for certain manufacturing process since the thickness of the intermediate ply (resin domain) may vary.

$$D_{ijkl}=2\mu^{*}\varepsilon_{ij}+\lambda^{*}\delta_{ij}\varepsilon_{kk} \quad 6.4$$

Where,

$$\mu^{*}=\frac{E^{*}}{2(1+\upsilon)}$$

And,

$$\lambda^{*}=\frac{E^{*}\upsilon}{(1+\upsilon)(1-2\upsilon)}$$

Where υ is the Poisson's ratio and $E^{*}=E(1-d_3)$ with E being Young's modulus.

The damage variables introduced in the whole model are the maximum calculated values along the load history analyses in order to avoid material self-healing.

6.2.4. Experimental testing and numerical simulation

Experimental test

A 3-points bending test was carried out employing five specimens manufactured using an infusion process of pre-impregnated carbon fibers. The specimen geometry and stacking sequence are given in tab. 33, and tab. 34 shows the mechanical properties of the material considered:

Table 33 - Specimen geometry and stacking sequence.

	Length (mm)	**Width (mm)**	**Thickness (mm)**	**Stacking Sequence**
Carbon/epoxy	70	10	3	$[0°]_8$

Table 34 - Material mechanical properties.

	E_{11} (GPa)	**E_{22} (GPa)**	**ν_{12}**	**G_{12} (GPa)**	**G_{23} (GPa)**
Carbon/epoxy	140	11	0.3	4.5	2.2

These properties were calculated at the laboratory of the Group of Aeronautical Structures (GEA from Portuguese) of the University of São Paulo localized in São Carlos City, excepting the value for out-of-plane shear modulus at the 2-3 plane (G_{23}), which correspond to 20% of E_2 (Pandit et al., 2010).

The test was performed employing an INSTRON universal testing machine adapted for 3-points bending with dimensions illustrated in fig. 54. The test was displacement-controlled with a displacement rate of 0.5 mm/min.

Figure 54 - 3-points bending setup.

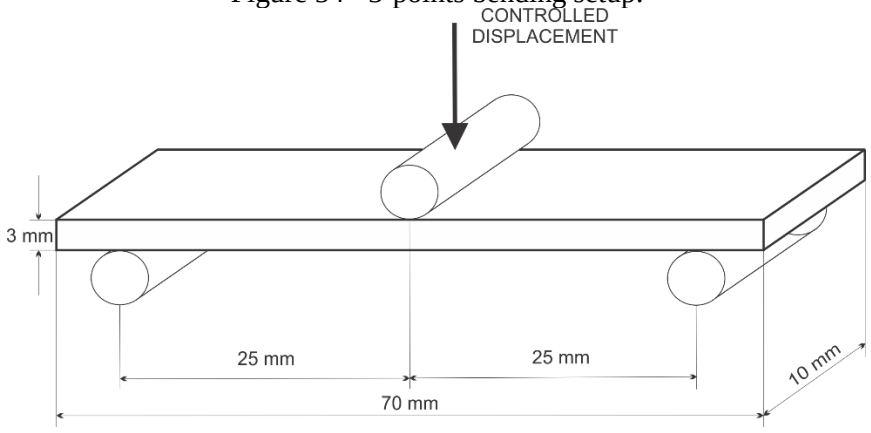

Numerical Simulation

Commercial FE software ABAQUS™ was employed to simulate the 3-points bending test following the same specifications previously detailed. A 3D solid deformable part was modeled with the same geometry and material properties. The mesh had 53200 quadratic hexahedral elements of type C3D20, which are general purpose quadratic brick element with three integration points through the thickness, excellent for linear elastic calculations.

Figure 55 - Numerical Simulation of 3-points Bending Tests for Carbon/epoxy.

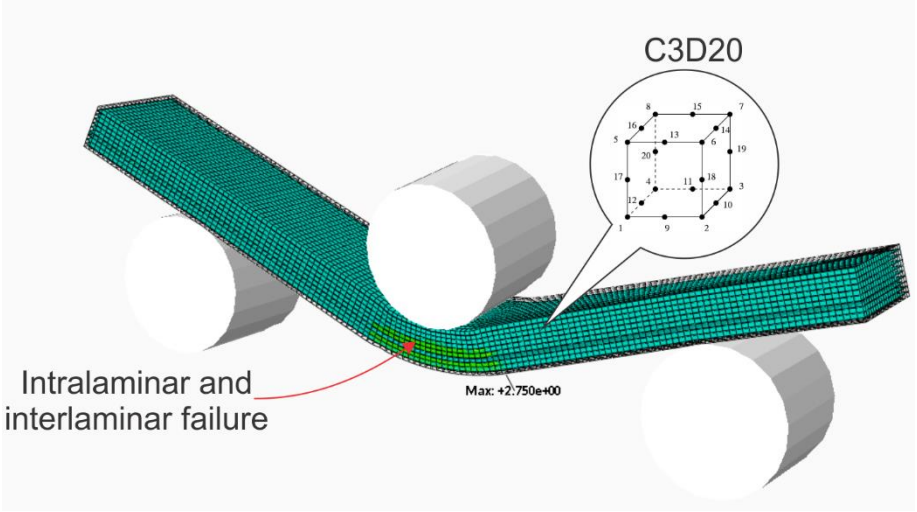

The laminate stacking sequence was modeled by creating partitions for each ply and for each interface between the plies (see Fig. 56). Two different materials were defined for the lamina and for the interface between lamina, respectively, following the approaches described in section 6.2.3.

Figure 56 - Laminate Design on Abaqus.

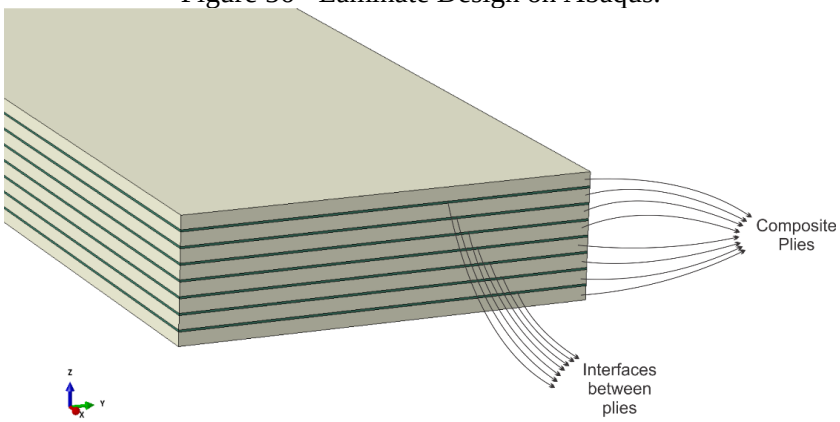

The failure criteria were implemented in the UMAT subroutine using FORTRAN language in order to capture both intra and inter laminar failure while running the simulation.

The model presents almost none convergence problem and a promissory result discussed in the further section.

6.2.5. Results and Discussion

The numerical simulation, working together with the UMAT, was capable to reproduce the maximum load and respectively load displacement. Tab. 35 resumes the maximum load and the respective displacement of each specimen tested and from the simulation as well. Fig. 57 shows the load-displacement curve obtained.

Figure 57 - Load-Displacement response for Carbon/epoxy laminate under flexure.

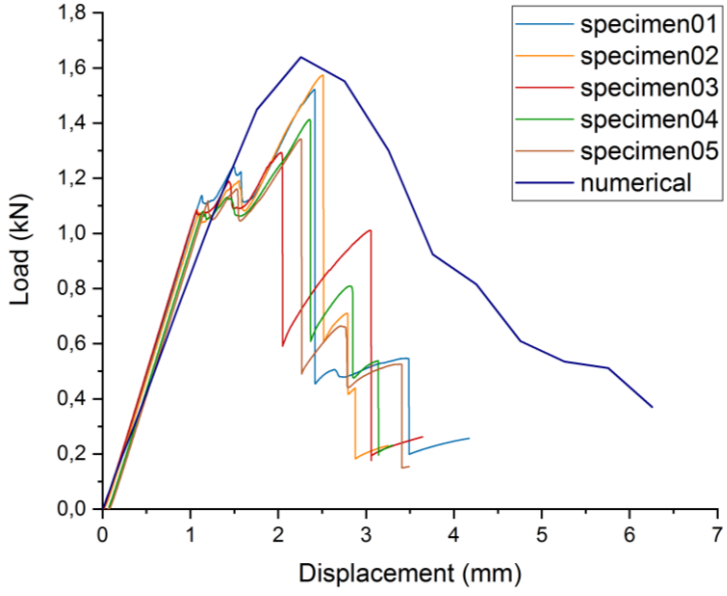

Table 35 - Maximum load and respective displacement. Experimental and numerical.

	01	02	03	04	05	mean	num	error
Maximum Load (kN)	1.52	1.57	1.29	1.41	1.34	1,43	1.64	13%
Load Displacement (mm)	2.41	2.51	2.03	2.36	2.26	2.31	2.26	2.4%

As seen in Fig. 57, the model was capable to capture degradation due to inter-laminar failure. The evolution of the delamination damage variable (d_3), along with the simulation, was captured for the nearest interface ply to the loading roller and is shown in fig. 58.

Figure 58 - Evolution of the delamination damage variable (d3).

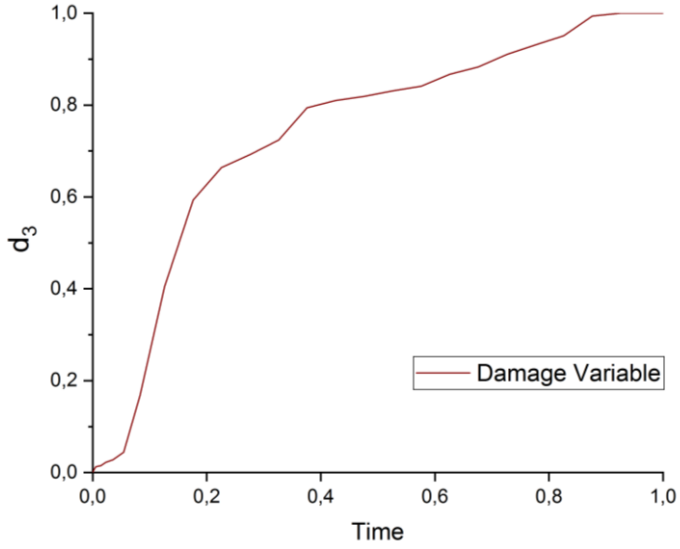

The results of maximum load and respective load displacement are acceptable. At the end of the first portion of the curve, before the maximum load, all the experimental specimens present a yield zone affected by matrix crushing (very common during 3-points bending test), which the model could not represent. This matrix effect needs to be studied and characterized in order to be incorporated within the damage model.

6.2.6. Conclusions for Carbon/Epoxy Application

A delamination propagation model was applied for a carbon/epoxy failure and showed a good prediction of inter-laminar degradation. It works well in complement with the Ribeiro's intra-laminar model to capture degradation of composite materials. The implementation of the

model, using FORTRAN UMAT subroutine, is simple and demand low computational cost. The accuracy of the result can be considered as acceptable.

The model was able to capture delamination propagation and material degradation due to interlaminar failure. We can conclude that the proposed model has a strong potentiality to simulate and prevent delamination effects within composite structures.

Some discrepancies were observed in the results due to the incapability of the model to capture matrix crushing which is present in bending loadings. Additional studies are needed to account for this effect and may be proposed in further investigations.

CHAPTER VII

7. Conclusions and further works

This research project aims the characterization of interlaminar failure by means of delamination propagation in fiber reinforced composite laminates. Experimental tests were carried out to find fracture parameters with the purpose of formulating degradation laws. This dissertation grants a procedure to develop a damage material model from fracture parameters, which is a significant tool for structural engineers. A plain solution for delamination degradation was conceived, nevertheless, many of the conclusion give suggestions for further investigations that will enrich the damage model proposed.

7.1. Conclusions

The problem of describing the propagation of delamination was analyzed and guidelines to treat this phenomenon were established. Five fracture tests were realized by means of DCB, ENF and three MMB cases; for these fracture modes, SERR were accurately calculated. The computing of these fracture toughness parameters becomes the first contribution of this research project and reinforced the results found by other researchers and present in literature. Despite some difficulties presented during testing, the test methods recommended by ASTM International organization are adequate for fracture characterization within composite laminates.

During the tests, long plastic processes were observed related to fracture mechanism and this influenced the TSL shape selection. The TSLs presented, in this dissertation, have a cubic polynomial function which resulted in a suitable function to represent degradation due to delamination since it has a softening region. The TSLs were formulated regarding the SERR values experimentally calculated.

From the five TSLs, damage variables were estimated. The definition of the damage variables is related to energy dissipation, this is, the damaged and undamaged states were related to areas under the TSL curves which represent an amount of energy released during

fracture. This choice was necessary in order to maintain the philosophy of performing the model formulations with base in energy release mechanism. As presented in previous sections, the damage variable values obtained, present a true interpretation of the degradation observed during the tests.

Once the damage model was fully formulated, it was implemented via UMAT Abaqus subroutine. The implementation was simple and it was demonstrated, through an FE analysis, that it is capable to perform good predictions of material degradation due to delamination propagation. As seen in the journal article, the model was checked to simulate delamination within carbon/epoxy laminates. The TSLs were suited for this material and a simulation of 3-points bending was carried out. The degradation of the material due to delamination was accurately estimated and described, despite the inconvenient with the intralaminar model predictions. This showed a model limitation and dependency on other damage criteria since the present model does not possess a criterion for damage initiation or delamination onset.

Finally, we conclude that this contribution, put together with a damage initiation model, is a powerful tool for structural engineers to predict the damage onset and propagation within the fiber reinforced laminated composites.

7.2. Further Works

A solution for delamination propagation is presented, however, for a complete characterization of the delamination phenomenon, a delamination onset criterion must be conceived. The contemplation of this criterion was out of the scope of the present research project but we believe that is significant in order to develop a delamination model that attend and describe all the mechanisms involved with this phenomenon.

The model proposed must be evaluated in order to explore its potentialities and limitations, this is achieved by employing the model for simulating cases involving different composite laminated materials with alternate stacking sequences, fiber orientations and loading conditions from the cases already considered within this research.

The employment of every other TSL function may be an interesting research subject to observe the influence of the functions on the degradation response of the model. Even when a literature review of TSL functions was performed to choose the actual function, we encourage future researchers and students to explore different approaches.

CHAPTER VIII

8. Publications

— David Aveiga and Marcelo L. Ribeiro, "A Delamination Propagation Model for Fiber Reinforced Laminated Composite Materials," Mathematical Problems in Engineering, vol. 2018, Article ID 1861268, 9 pages, 2018. https://doi.org/10.1155/2018/1861268.

— Aveiga D, Ribeiro M L. DETERMINATION OF COHESIVE PARAMETERS FOR MODE I AND MODE II FRACTURE ANALYSES OF E-GLASS/EPOXY COMPOSITES. Meeting on Aeronautical Composite Materials and Structure – MACMS 2017, São Carlos, SP, Brazil. https://goo.gl/VnNWJu

— Aveiga D, Ribeiro M L, Tita Volnei. A finite element damage model to predict failure behavior of composite sandwich structures. Brazilian Conference on Composite Materials, 2016, Gramado, RS, Brazil. Third Brazilian Conference on Composite Materials, 3BCCM, v. 3. https://goo.gl/LTZNUi

— Vilar M, Aveiga D, Ferreira G, Ribeiro M L. CARBON-FIBRE/EPOXY LAMINATED PLATE: EVALUATION OF RESIDUAL FLEXURAL PROPERTIES AFTER LOW-VELOCITY IMPACT DAMAGE. 1° Simpósio de Pós-Graduação em Engenharia Mecânica – SIMPGEM 2016, São Carlos, SP, Brazil. https://goo.gl/Ah5WnC

— Prado J, Aveiga D, Ribeiro M L, Leonel E, Ferreira A, Tita V. FAILURE ANALYSIS OF AN AL 2024-T3 PLATE USING FRACTURE MECHANICS. Meeting on Aeronautical Composite Materials and Structures – MACMS 2017, São Carlos, SP, Brazil. https://goo.gl/i16dQ8

CHAPTER IX

9. References

Allix, O., & Ladeveze, P. (1992). INTERLAMINAR INTERFACE MODELING FOR THE PREDICTION OF DELAMINATION. *Composite Structures, 22*(4), 235-242.

Almeida Jr, J. H. S., Ribeiro, M. L., Tita, V., & Amico, S. C. (2016). Damage and failure in carbon/epoxy filament wound composite tubes under external pressure: Experimental and numerical approaches. *Materials & Design, 96*, 431-438.

Almeida Jr, J. H. S., Ribeiro, M. L., Tita, V., & Amico, S. C. (2017a). Damage modeling for carbon fiber/epoxy filament wound composite tubes under radial compression. *Composite Structures, 160*, 204-210.

Almeida Jr, J. H. S., Ribeiro, M. L., Tita, V., & Amico, S. C. (2017b). Stacking sequence optimization in composite tubes under internal pressure based on genetic algorithm accounting for progressive damage. *Composite Structures, 178*, 20-26.

Aymerich, F., Dore, F., & Priolo, P. (2008). Prediction of impact-induced delamination in cross-ply composite laminates using cohesive interface elements. *Composites Science and Technology, 68*(12), 2383-2390.

Badreddine, H., Saanouni, K., & Nguyen, T. D. (2015). Damage anisotropy and its effect on the plastic anisotropy evolution under finite strains. *International Journal of Solids and Structures, 63*, 11-31.

Barenblatt, G. I. (1962). The mathematical theory of equilibrium cracks in brittle fracture. *Advances in applied mechanics, 7*, 55-129.

Bernadette, P. T. B.-V. (2002). Composites Review. Retrieved from https://authors.library.caltech.edu/5456/1/hrst.mit.edu/hrs/materials/public/composites/Composites_Overview.htm

Besson, J. (2010). Continuum Models of Ductile Fracture: A Review. *International Journal of Damage Mechanics, 19*(1), 3-52.

Bordeu, F., Boucard, P.-A., & Lubineau, G. (2010). A mesoscale model for damage, cracking and delamination prediction in composite materials. *Science and Engineering of Composite Materials, 17*(4), 271-282.

Boyle, M. A., Martin, C. J., & Neuner, J. D. (2001). Epoxy Resins. *Composites Compendium, OH: ASM Handbook Volume 21, Composites (ASM International), 21*, 12.

Burr, A., Hild, F., & Leckie, F. A. (1995). MICROMECHANICS AND CONTINUUM DAMAGE MECHANICS. *Archive of Applied Mechanics, 65*(7), 437-456.

Camanho, P. P., Davila, C. G., & de Moura, M. F. (2003). Numerical simulation of mixed-mode progressive delamination in composite materials. *Journal of Composite Materials, 37*(16), 1415-1438.

Campilho, R., Banea, M. D., Neto, J., & da Silva, L. F. M. (2013). Modelling adhesive joints with cohesive zone models: effect of the cohesive law shape of the adhesive layer. *International Journal of Adhesion and Adhesives, 44*, 48-56.

Campilho, R. D., De Moura, M., & Domingues, J. (2008). Using a cohesive damage model to predict the tensile behaviour of CFRP single-strap repairs. *International Journal of Solids and Structures, 45*(5), 1497-1512.

Carol, I., Rizzi, E., & Willam, K. (2001). On the formulation of anisotropic elastic degradation. I. Theory based on a pseudo-logarithmic damage tensor rate. *International Journal of Solids and Structures, 38*(4), 491-518.

Chaboche, J.-L. (1992). Damage induced anisotropy: on the difficulties associated with the active/passive unilateral condition. *International Journal of Damage Mechanics, 1*(2), 148-171.

Chaboche, J. L. (1988). CONTINUUM DAMAGE MECHANICS .1. GENERAL CONCEPTS. *Journal of Applied Mechanics-Transactions of the Asme, 55*(1), 59-64.

Chaboche, J. L., Lesne, P. M., & Maire, J. F. (1995). Continuum Damage Mechanics, Anisotropy and Damage Deactivation for Brittle Materials Like Concrete and Ceramic Composites. *International Journal of Damage Mechanics, 4*(1), 5-22.

Chen, C., Fleck, N. A., & Lu, T. J. (2001). The mode I crack growth resistance of metallic foams. *Journal of the Mechanics and Physics of Solids, 49*(2), 231-259.

Chen, C., Kolednik, O., Scheider, I., Siegmund, T., Tatschl, A., & Fischer, F. (2003). On the determination of the cohesive zone parameters for the modeling of micro-ductile crack growth in thick specimens. *International journal of fracture, 120*(3), 517-536.

Chow, C., & Wang, J. (1987). An anisotropic theory of elasticity for continuum damage mechanics. *International Journal of Fracture, 33*(1), 3-16.

Coelho, A. M. G. (2016). Finite Element Guidelines for Simulation of Delamination Dominated Failures in Composite Materials Validated by Case Studies. *Archives of Computational Methods in Engineering, 23*(2), 363-388.

Cornec, A., Scheider, I., & Schwalbe, K.-H. (2003). On the practical application of the cohesive model. *Engineering fracture mechanics, 70*(14), 1963-1987.

Crisfield, M. A., Jelenic, G., Mi, Y., Zhong, H. G., & Fan, Z. (1997). Some aspects of the non-linear finite element method. *Finite Elements in Analysis and Design, 27*(1), 19-40.

D2093-03, A. (2017). Standard Practice for Preparation of Surfaces of Plastics Prior to Adhesive Bonding. West Conshohocken, PA: ASTM International.

D2651-01, A. (2016). Standard Guide for Preparation of Metal Surfaces for Adhesive Bonding. West Conshohocken, PA: ASTM International.

D5528-13, A. (2013). Standard Test Method for Mode I Interlaminar Fracture Toughness of Unidirectional Fiber-Reinforced Polymer Matrix Composites, *ASTM International*. West Conshohocken, PA.

D6671M-13e1, A. D. (2013). Standard Test Method for Mixed Mode I-Mode II Interlaminar Fracture Toughness of Unidirectional Fiber Reinforced Polymer Matrix Composites. West Conshohocken, PA: ASTM International.

D7905M-14, D. (2014). Standard Test Method for Mode II Interlaminar Fracture Toughness of Undirectional Fiber-reinforced Polymer Matrix Composites. West Conshohocken, PA: ASTM International.

Davidson, B. D., Hu, H., & Schapery, R. A. (1995). An Analytical Crack-Tip Element for Layered Elastic Structures. *Journal of Applied Mechanics, 62*(2), 294-305.

Davies, G. A. O., Hitchings, D., & Ankersen, J. (2006). Predicting delamination and debonding in modern aerospace composite structures. *Composites Science and Technology, 66*(6), 846-854.

Donadon, M. V., Iannucci, L., Falzon, B. G., Hodgkinson, J. M., & de Almeida, S. F. M. (2008). A progressive failure model for composite laminates subjected to low velocity impact damage. *Computers & Structures, 86*(11-12), 1232-1252.

Donadon, M. V., & Lauda, D. P. (2015). A damage model for the prediction of static and fatigue-driven delamination in composite laminates. *Journal of Composite Materials, 49*(16), 1995-2007.

Elder, D. J., Thomson, R. S., Nguyen, M. Q., & Scott, M. L. (2004). Review of delamination predictive methods for low speed impact of composite laminates. *Composite Structures, 66*(1), 677-683.

Elices, M., Guinea, G. V., Gómez, J., & Planas, J. (2002). The cohesive zone model: advantages, limitations and challenges. *Engineering Fracture Mechanics, 69*(2), 137-163.

Evans, A. G., & Zok, F. W. (1994). THE PHYSICS AND MECHANICS OF FIBER-REINFORCED BRITTLE-MATRIX COMPOSITES. *Journal of Materials Science, 29*(15), 3857-3896.

Fish, J., & Yu, Q. (2001). Multiscale damage modelling for composite materials: theory and computational framework. *International Journal for Numerical Methods in Engineering, 52*(1-2), 161-191.

Flatscher, T., & Pettermann, H. (2011). A constitutive model for fiber-reinforced polymer plies accounting for plasticity and brittle damage including softening–implementation for implicit FEM. *Composite Structures, 93*(9), 2241-2249.

Fleming, J. R., & Suh, N. P. (1977). Mechanics of crack propagation in delamination wear. *Wear, 44*(1), 39-56.

Garg, A. C. (1988). DELAMINATION - A DAMAGE MODE IN COMPOSITE STRUCTURES. *Engineering Fracture Mechanics, 29*(5), 557-584.

Geers, M. G. D., Kouznetsova, V. G., & Brekelmans, W. A. M. (2010). Multi-scale computational homogenization: Trends and challenges. *Journal of Computational and Applied Mathematics, 234*(7), 2175-2182.

Green, A. P. (1954). On the use of hodographs in problems of plane plastic strain. *Journal of the Mechanics and Physics of Solids, 2*(2), 73-80.

Griffith, A. A. (1921). The phenomena of rupture and flow in solids. *Philosophical transactions of the royal society of london. Series A, containing papers of a mathematical or physical character, 221*, 163-198.

Guédra-Degeorges, D. (2006). Recent advances to assess mono- and multi-delaminations behaviour of aerospace composites. *Composites Science and Technology, 66*(6), 796-806.

Hashemi, S., Kinloch, A., & Williams, G. (1991). *Mixed-mode fracture in fiber-polymer composite laminates*.

Hashin, Z. (1983). ANALYSIS OF COMPOSITE-MATERIALS - A SURVEY. [Review]. *Journal of Applied Mechanics-Transactions of the Asme, 50*(3), 481-505.

Herakovich, C. (1989). Edge effects and delamination failures. *The Journal of Strain Analysis for Engineering Design, 24*(4), 245-252.

Iannucci, L., & Willows, M. L. (2006). An energy based damage mechanics approach to modelling impact onto woven composite materials - Part I: Numerical models. *Composites Part a-Applied Science and Manufacturing, 37*(11), 2041-2056.

Inglis, C. E. (1913). Stresses in a plate due to the presence of cracks and sharp corners. *Transactions of the institute of naval architects, 55*(219-241), 193-198.

Irwin, G. R. (1958). Fracture. In S. Flügge (Ed.), *Elasticity and Plasticity / Elastizität und Plastizität* (pp. 551-590). Berlin, Heidelberg: Springer Berlin Heidelberg.

Jahanmir, S., & Suh, N. (1977). Mechanics of subsurface void nucleation in delamination wear. *wear, 44*(1), 17-38.

Johnson, A. F., Pickett, A. K., & Rozycki, P. (2001). Computational methods for predicting impact damage in composite structures. *Composites Science and Technology, 61*(15), 2183-2192.

Johnson, P., & Chang, F. K. (2001). Characterization of matrix crack-induced laminate failure - Part I: Experiments. [Article]. *Journal of Composite Materials, 35*(22), 2009-2035.

Ju, J. (1990). Isotropic and anisotropic damage variables in continuum damage mechanics. *Journal of Engineering Mechanics, 116*(12), 2764-2770.

Kachanov, L. M. (1958). Time of the rupture process under creep conditions. *Izv. Akad. Nauk. {S.S.R.} Otd. Tech. Nauk., 8*, 26-31.

Kashtalyan, M., & Soutis, C. (2000). The effect of delaminations induced by transverse cracks and splits on stiffness properties of composite laminates. *Composites Part A: Applied Science and Manufacturing, 31*(2), 107-119.

Kashtalyan, M., & Soutis, C. (2005). Analysis of composite laminates with intra- and interlaminar damage. *Progress in Aerospace Sciences, 41*(2), 152-173.

Kaufmann, M. (2008). *Cost/weight optimization of aircraft structures*. KTH.

Kenane, M., & Benzeggagh, M. (1997). Mixed-mode delamination fracture toughness of unidirectional glass/epoxy composites under fatigue loading. *Composites Science and Technology, 57*(5), 597-605.

Krajcinovic, D., & Fonseka, G. (1981). The continuous damage theory of brittle materials. *J. appl. Mech, 48*(4), 809-824.

Krueger, R., Cvitkovich, M. K., O'Brien, T. K., & Minguet, P. J. (2000). Testing and analysis of composite skin/stringer debonding under multi-axial loading. *Journal of composite Materials, 34*(15), 1263-1300.

Krueger, R., & O'Brien, T. K. (2001). A shell/3D modeling technique for the analysis of delaminated composite laminates. [Article]. *Composites Part a-Applied Science and Manufacturing, 32*(1), 25-44.

Ladeveze, P., & Ledantec, E. (1992). DAMAGE MODELING OF THE ELEMENTARY PLY FOR LAMINATED COMPOSITES. *Composites Science and Technology, 43*(3), 257-267.

Lasn, K., Echtermeyer, A. T., Klauson, A., Chati, F., & Decultot, D. (2015). An experimental study on the effects of matrix cracking to the stiffness of glass/epoxy cross plied laminates. [Article]. *Composites Part B-Engineering, 80*, 260-268.

Lee, M. J., Cho, T. M., Kim, W. S., Lee, B. C., & Lee, J. J. (2010). Determination of cohesive parameters for a mixed-mode cohesive zone model. *International Journal of Adhesion and Adhesives, 30*(5), 322-328.

Lemaitre, J. (1984). HOW TO USE DAMAGE MECHANICS. *Nuclear Engineering and Design, 80*(2), 233-245.

Lemaitre, J., & CHABOCHE, J.-L. (1978). Aspect phénoménologique de la rupture par endommagement. *J Méc Appl, 2*(3).

Lim, S. G., & Hong, C. S. (1989). Prediction of Transverse Cracking and Stiffness Reduction in Cross-Ply Laminated Composites. *Journal of Composite Materials, 23*(7), 695-713.

Lubineau, G., & Ladevèze, P. (2008). Construction of a micromechanics-based intralaminar mesomodel, and illustrations in ABAQUS/Standard. *Computational Materials Science, 43*(1), 137-145.

Maimi, P., Camanho, P. P., Mayugo, J. A., & Davila, C. G. (2007). A continuum damage model for composite laminates: Part II - Computational implementation and validation. *Mechanics of Materials, 39*(10), 909-919.

Marat-Mendes, R. M., & Freitas, M. M. (2010). Failure criteria for mixed mode delamination in glass fibre epoxy composites. *Composite Structures, 92*(9), 2292-2298.

Merwin, J., & Johnson, K. (1963). An analysis of plastic deformation in rolling contact. *Proceedings of the Institution of Mechanical Engineers, 177*(1), 676-690.

Nairn, J. A., & Hu, S. (1992). THE INITIATION AND GROWTH OF DELAMINATIONS INDUCED BY MATRIX MICROCRACKS IN LAMINATED COMPOSITES. *International Journal of Fracture, 57*(1), 1-24.

Nak-Ho, S., & Suh, N. P. (1979). Effect of fiber orientation on friction and wear of fiber reinforced polymeric composites. *Wear, 53*(1), 129-141.

Noijen, S., vd Sluis, O., Timmermans, P., & Zhang, G. (2010). *Meso-scale analysis of interface roughness effect on delamination of polymer/metal interfaces.* Paper presented at the 18th European Conference on Fracture, Proceedings 2010.

Orifici, A. C., Herszberg, I., & Thomson, R. S. (2008). Review of methodologies for composite material modelling incorporating failure. *Composite Structures, 86*(1), 194-210.

Orowan, E. (1949). Fracture and strength of solids. *Reports on progress in physics, 12*(1), 185.

P. Suh, N. (1973). The delamination theory of wear. *Wear, 25*(1), 111-124.

Pamies-Teixeira, J. J., Saka, N., & Suh, N. P. (1977). Wear of copper-based solid solutions. *Wear, 44*(1), 65-75.

Pandit, M., Sheikh, A., & Singh, B. (2010). Analysis of laminated sandwich plates based on an improved higher order zigzag theory. *Journal of Sandwich Structures & Materials, 12*(3), 307-326.

Pavan, R., Oliveira, B., Maghous, S., & Creus, G. (2010). A model for anisotropic viscoelastic damage in composites. *Composite Structures, 92*(5), 1223-1228.

Pereira, A. B., & de Morais, A. B. (2008). Mixed mode I+II interlaminar fracture of carbon/epoxy laminates. *Composites Part A: Applied Science and Manufacturing, 39*(2), 322-333.

Point, N., & Sacco, E. (1996). A delamination model for laminated composites. *International Journal of Solids and Structures, 33*(4), 483-509.

Puck, A., & Schürmann, H. (2004). Failure analysis of FRP laminates by means of physically based phenomenological models *Failure Criteria in Fibre-Reinforced-Polymer Composites* (pp. 832-876): Elsevier.

R., R. J. (1992). *An Evaluation of Mixed-Mode Delamination Failure Criteria*: NASA Langley Technical Report Server.

Raju, I. S., & Shivakumar, K. N. (1990). An equivalent domain integral method in the two-dimensional analysis of mixed mode crack problems. *Engineering Fracture Mechanics, 37*(4), 707-725.

Reeder, J. R. (1993). A bilinear failure criterion for mixed-mode delamination *Eleventh Volume: Composite Materials—Testing and Design*: ASTM International.

Ribeiro, M. L., Tita, V., & Vandepitte, D. (2012). A new damage model for composite laminates. *Composite Structures, 94*(2), 635-642.

Ribeiro, M. L., Vandepitte, D., & Tita, V. (2013). Damage model and progressive failure analyses for filament wound composite laminates. *Applied Composite Materials, 20*(5), 975-992.

Rodrigue, J. P. (2012). The Geography of Global Supply Chains: Evidence from Third-Party Logistics. *Journal of Supply Chain Management, 48*(3), 15-23.

Samuels, L. E. (1971). *Metallographic polishing by mechanical methods*: American Elsevier Pub. Co.

Scheider, I., & Brocks, W. (2003). *The effect of the traction separation law on the results of cohesive zone crack propagation analyses.* Paper presented at the Key Engineering Materials.

Schmauder, S. (2002). Computational mechanics. *Annual Review of Materials Research, 32*, 437-465.

Schuecker, C., & Pettermann, H. E. (2008). Fiber reinforced laminates: Progressive damage modeling based on failure mechanisms. *Archives of Computational Methods in Engineering, 15*(2), 163-184.

Shi, Y., Swait, T., & Soutis, C. (2012). Modelling damage evolution in composite laminates subjected to low velocity impact. *Composite Structures, 94*(9), 2902-2913.

Simo, J. C., & Ju, J. W. (1987). Strain- and stress-based continuum damage models—I. Formulation. *International Journal of Solids and Structures, 23*(7), 821-840.

Singh, C. V., & Talreja, R. (2010). Evolution of ply cracks in multidirectional composite laminates. [Article]. *International Journal of Solids and Structures, 47*(10), 1338-1349.

Sorensen, B. F. (2002). Cohesive law and notch sensitivity of adhesive joints. *Acta Materialia, 50*(5), 1053-1061.

Soutis, C. (2005). Fibre reinforced composites in aircraft construction. [Review]. *Progress in Aerospace Sciences, 41*(2), 143-151.

Suh, N. P. (1977). An overview of the delamination theory of wear. *Wear, 44*(1), 1-16.

Suh, N. P., Saka, N., & Jahanmir, S. (1977). Implications of the delamination theory on wear minimization. *Wear, 44*(1), 127-134.

Tabor, D. (1974). Friction, Adhesion and Boundary Lubrication of Polymers. In L.-H. Lee (Ed.), *Advances in Polymer Friction and Wear* (pp. 5-30). Boston, MA: Springer US.

Talreja, R. (1985). A CONTINUUM-MECHANICS CHARACTERIZATION OF DAMAGE IN COMPOSITE-MATERIALS. *Proceedings of the Royal Society of London Series a-Mathematical Physical and Engineering Sciences, 399*(1817), 195-216.

Tita, V., de Carvalho, J., & Vandepitte, D. (2008). Failure analysis of low velocity impact on thin composite laminates: Experimental and numerical approaches. *Composite Structures, 83*(4), 413-428.

Turon, A., Camanho, P. P., Costa, J., & Renart, J. (2010). Accurate simulation of delamination growth under mixed-mode loading using cohesive elements: Definition of interlaminar strengths and elastic stiffness. *Composite Structures, 92*(8), 1857-1864.

Turon, A., Costa, J., Camanho, P. P., & Davila, C. G. (2007). Simulation of delamination in composites under high-cycle fatigue. *Composites Part a-Applied Science and Manufacturing, 38*(11), 2270-2282.

van Dijck, J. A. B. (1977). The direct observation in the transmission electron microscope of the heavily deformed surface layer of a copper pin after dry sliding against a steel ring. *Wear, 42*(1), 109-117.

Varna, J., & Berglund, L. (1991). Multiple Transverse Cracking and Stiffness Reduction in Cross-Ply Laminates.

Varna, J., Joffe, R., Akshantala, N. V., & Talreja, R. (1999). Damage in composite laminates with off-axis plies. *Composites Science and Technology, 59*(14), 2139-2147.

Voyiadjis, G. Z., & Deliktas, B. (2000). A coupled anisotropic damage model for the inelastic response of composite materials. *Computer methods in applied mechanics and engineering, 183*(3), 159-199.

Wallenberger, F. T., Watson, J. C., & Li, H. (2001). Glass fibers. *Materials Park, OH: ASM International, 2001.*, 27-34.

Weitsman, Y. J. (2006). Anomalous fluid sorption in polymeric composites and its relation to fluid-induced damage. *Composites Part a-Applied Science and Manufacturing, 37*(4), 617-623.

Williams, K. V., Vaziri, R., & Poursartip, A. (2003). A physically based continuum damage mechanics model for thin laminated composite structures. [Article]. *International Journal of Solids and Structures, 40*(9), 2267-2300.

Wosu, S. N., Hui, D., & Daniel, L. (2012). Hygrothermal effects on the dynamic compressive properties of graphite/epoxy composite material. *Composites Part B-Engineering, 43*(3), 841-855.

Wu, E. M.-c., & Reuter, R. C. (1965). *Crack extension in fiberglass reinforced plastics*. Urbana.

Yang, Q. D., & Cox, B. (2005). Cohesive models for damage evolution in laminated composites. *International Journal of Fracture, 133*(2), 107-137.

Zerbst, U., Heinimann, M., Donne, C. D., & Steglich, D. (2009). Fracture and damage mechanics modelling of thin-walled structures - An overview. *Engineering Fracture Mechanics, 76*(1), 5-43.

Zhang, W., & Cai, Y. (2010). *Continuum damage mechanics and numerical applications*: Springer Science & Business Media.

Zhu, T.-L. (1993). A reliability-based safety factor for aircraft composite structures. *Computers & Structures, 48*(4), 745-748.

Zou, Z., Reid, S. R., & Li, S. (2003). A continuum damage model for delaminations in laminated composites. *Journal of the Mechanics and Physics of Solids, 51*(2), 333-356.